inquiro

Founded and staffed by undergraduate students at the University of Alabama at Birmingham, *Inquiro* is an annual research journal produced as an outlet for the publication of undergraduate scientific research. UAB is an excellent undergraduate research university, and with the addition of a journal such as *Inquiro* in which to publish their findings, the package is complete. Any undergraduate student at UAB, as well as any student participating in a summer program at the university, is eligible to submit research. The rights to every paper published in *Inquiro* are retained by the author, leaving each individual free to submit to and publish in a larger national journal or magazine. Students are invited to submit research papers, short reports derived from posters or research narratives throughout the year.

inquiro staff

UAB THE UNIVERSITY OF ALABAMA AT BIRMINGHAM

letter from the editor

"Research is to see what everybody else has seen, and to think what nobody else has thought." These are the words of Albert Szent-Györgi, a Hungarian physiologist who received the Nobel Prize for discovering vitamin C and for elucidating oxidative processes key to the citric acid cycle. Researchers have made immense progress since his time. Today, much of his work is fundamental knowledge for students of biology and chemistry, including the authors published in this journal, many of whom wish to forge their own legacies in science. The essence of this quote is the importance of creativity; however, the capacity for innovation in science is not inherent, but is crafted by one's education and experiences.

My own path to the decision to become a scientist has been a journey in itself. When I began college, I chose to major in chemistry and knew I had an interest in medicine, but was unsure how it would manifest in my career. Four years later, I look forward to pursuing a Ph.D. in biophysics so that I can contribute to the world of biomedical research. My experiences as a UAB student have prepared me for this future in a multitude of ways, from hands-on lab experience to many other aspects of my chosen profession, including teaching, presenting, writing, collaborating, and—through *Inquiro*—publishing. Sharing the same opportunities with other students who may not yet know where they belong is a personal passion of mine and is what has made my years spent working on *Inquiro* so rewarding.

Chapin entered UAB with the intention of pursuing a biomedical engineering degree; but, after exposure to the challenges and rewards of scientific research and the incredible devotion of those engaged in it, he realized that his passion lay in gaining understanding at the theoretical level. Chapin's interest in research has been sustained and refined by the many opportunities offered by this university to gain practical skills critical to a scientific career. Together, we view *Inquiro* as another tool available for UAB students to learn and practice the nuanced art of scientific discovery and communication.

During our tenure as editors, Chapin and I have worked to manage *Inquiro* more efficiently than ever before and to give our editorial board the opportunity to become more involved in the publication process. We created committees for the board members: the Website Committee, to oversee and update our website; the Publicity Committee, to promote our presence on campus; the Article and Interview Committee, for those with an interest in scientific journalism to help edit and select our science news pieces; and the Faculty Review Committee, who helped us find faculty members and post-doctoral fellows with the expertise to review the submissions we received.

In addition to the committees, we streamlined our submission and review processes by moving them entirely online, which could not have been possible without the help of Nick Bieser, UAB's Coordinator for Undergraduate Research. Lastly, we wrote specific guidelines for authors to abide by when preparing their manuscripts, with the goal of standardizing our papers and exposing students to the rigorous standards they must meet when submitting to professional journals.

Implementing all of these changes while simultaneously producing Volume VII has not been without its challenges, but Chapin and I welcomed the opportunity to help *Inquiro* grow and flourish. As UAB adapts to the current national climate of budgetary restrictions and increased pressure to justify all research endeavors, so must *Inquiro* adapt to UAB. Volume VII boasts research papers from various areas of academia, including biology, neurobiology, inorganic chemistry, mathematics,

physics, forensics, and psychology. We continued to attempt to publish material that will be interesting and comprehensible to readers with a general science background. On page 38, you will find an excellent biology paper with important implications for the treatment of Alzheimer's disease. One of our short reports (page 19) describes an interesting application of mathematics to solve problems in medical imaging. In science news, Sadhvi and Harsh share their passion for medical research in their articles on progress toward HIV and tuberculosis treatments (pages 6 and 9, respectively).

Inquiro would not exist without continued support and guidance from UAB faculty and administrators. We extend our utmost gratitude to each of our reviewers who volunteer their time to maintain the high quality of the journal. We would also like to especially thank Mike Sloane for his ongoing mentorship and for helping us present Inquiro at the 2013 National Collegiate Honors Council Conference as a model to students and faculty from several other universities who wish to found their own undergraduate research journals. Special thanks to Nick Bieser, with whom we hope to continue to partner as he unites various aspects of undergraduate research at UAB. Finally, we sincerely thank Julio Rivera, Robert Palazzo, and Suzanne Austin for recognizing the importance of Inquiro and supporting its continued publication.

While it cannot cover everything, Chapin and I hope that this edition of Inquiro conveys some of the scope and magnitude of the research in which UAB undergraduates are involved and serves as a harbinger for the great work many of them will surely go on to accomplish. To mentors and supporters, we ask that you continue to encourage these students and foster in them a passion for research. And to students, as you go forward in your educations and careers, often observing what others have seen, use the foundation you build at UAB to think what no one else has thought.

Miranda Collier, Chief Editor 2013-2014

inquiro

table of contents

The "pause" in global climate change, and what we can learn from it

John Decker

Recently, media outlets, politicians, and critics of mainstream climate science have stirred up controversy over the unexpectedly slow rise of global mean surface air temperature in the most recent 15-year period for which data are available, from 1998 to 2012. Though it is only one of many findings detailed in the 2013 report by Working Group I of the Intergovernmental Panel on Climate Change (IPCC), and the vast majority of those findings indicate that the danger of climate change has worsened or remained the same relative to previous assessments (IPCC 2013), this "pause" was highlighted in 41% of all mainstream media coverage of that report in the United States (Greenberg, Robbins & Theel 2013) and contributed to an increase in popular denial of climate change (cf. Bojanowski, Stampf & Traufetter 2013; Rose 2013; Ridley 2013; Lloyd 2013; Lewis 2013).

It is true that the trend of warming for this period, about 0.044 °C per decade (Met Office 2013), has been significantly lower than the 0.10-0.35 °C per decade predicted in 1990 by the IPPC for the period from 1990-2030 (IPCC 1990). However, two questions remain about these data. First, do they affect the need for action on climate change or the validity of climate science? Second, how can climate scientists learn from them to improve both their understanding of natural short-term climate variability and their ability to communicate their science effectively to policymakers and the public?

To the first of these questions, the answer according to 97% of the world's active climate scientists is a resounding "no" (Cook et al. 2013). The most obvious fault in the logic of extrapolating a 15-year period of slower warming to long-term climate changes is that 15 years is not enough time to average out the noise of short-term fluctuations that are significant on annual or semi-decadal scales but do not affect long term trends (IPCC 2013). Of particular significance as contributors to this noise are El Niño and La Niña events, which are periods of warming and cooling of the Pacific Ocean, respectively. Short periods that begin and end in abnormal years yield abnormal trends, and it is significant that the year 1998 included one of the most intense El Niño events of the 20th century and that the following 15 years have been dominated by strong La Niñas and weak El Niños (Held 2013). Indeed, other 15-year periods since 1990 have shown rates of warming that are actually in the high range of the IPCC estimates. For example, the rate of warming between 1992-2006 was approximately 0.28 °C per decade (Met Office 2013). From 1987 to 2012, the rate has been well

within predictions at about 0.15 °C per decade (Met Office 2013). Finally, the 2013 IPCC report indicated that it is likely that the 30-year period from 1983-2012 was the warmest 30-year period of the last 1400 years (IPCC 2013). Saying that trends from 1992-2006 show that the long-term climate change situation is even worse than the IPCC expected, or that 1998-2012 shows that climate change has paused, reflects cherry-picking of data and poor understanding of climate science.

Even if the decadal rate of increase in global mean surface air temperature in the most recent 15-year period actually did reflect trends over a longer term, global mean surface air temperature would remain only one of many indicators of anthropogenic global climate change. In its 2013 report, the IPCC also expressed confidence (IPCC 2013) in significant trends of change in the following: sea level; ocean acidity; regional extremes of temperatures and precipitation; temperatures in the tropospheric and stratospheric layers of the atmosphere (which are warming and cooling, respectively); rates of ice loss in ice sheets in the Arctic, the Antarctic, and Greenland, as well as from glaciers; and thawing of global permafrost (soil frozen for more than two consecutive years), which currently contains roughly half of all organic materials in all soils around the world and is likely to release vast amounts of methane as it thaws (Zimov, Schuur & Chapin III 2006). The IPCC report also stated with high confidence that the oceans have absorbed more than 90% of the global energy surplus accumulated from 1971-2010, with much of the rest contributing to ice melt and stratospheric warming (IPCC 2013). Such a distribution of energy further diminishes the logic of placing great weight on short-term trends in decadal rates of warming of surface air, because warming of surface air as a whole has accounted for only a very small fraction of the planet's energy surplus in the last several decades.

Despite its unsuitability as a predictor of long-term trends in global climate change and the validity of the science as a whole, the recent 15-year slowdown in surface warming does have something positive to offer scientists: a chance to learn more about the natural variability of the Earth's climate, separate from the external factors known as "forcing" agents—chief among them, greenhouse gases and variations in solar activity. A better understanding of the climate's natural variability will aid climate science and the public in at least three ways. First, it will improve estimates of climate sensitivity (a measure of how strongly the climate responds to forcing agents), resulting in less variability among the

Image source: Druckenmiller 2008.

projections of future conditions produced by different climate models. Second, it will increase public and political trust in climate science, both by tightening the spread of projections and by reducing the appearance of contradiction between short-term climate fluctuations and long-term projections. Finally, it may allow better prediction of seasonal and regional changes in climate, which could help in preparing specific populations for extreme events such as floods, droughts, and heat waves. These changes, along with more accessible and more frequent communication of results by the IPCC, will help to reduce climate denial and increase humankind's willingness and ability to take action against climate change.

References

1. Bojanowski, A., Stampf, O. & Traufetter, G. (2013, September 23). Warming plateau? climatologists face inconvenient truth. Der Spiegel, (39).

2. Cook, J., et al. (2013). Quantifying the consensus on anthropogenic global warming in the scientific literature. Environ. Res. Lett., 8(2), doi: doi:10.1088/1748-9326/8/2/024024

3. Druckenmiller, M. (Photographer). (2008, June 5). Walk on water [Web Photo].

4. Greenberg, M., Robbins, D., & Theel, S. (2013, October 10). Study: Media sowed doubt in coverage of un climate report.

5. Held, I. M. (2013, September 19). Climate science: The cause of the pause. Nature, (501), 318–319.

6. IPCC Working Group I. Intergovernmental Panel on Climate Change, (1990). Scientific assessment of climate change. Summary for policymakers.

7. Lewis, M. (2013, September 26). Models of misinformation -- climate reports melt under scrutiny.

8. Lloyd, G. (2013, September 16). Doubts over ipcc's global warming rates. The Australian.

9. Met Office, United Kingdom. (2013, August 14). Global surface temperature.

10. Ridley, M. (2013, September 17). Dialing back the alarm on climate change. The Wall Street Journal.

11. Rose, D. (2013, September 14). World's top climate scientists confess: Global warming is just quarter what we thought - and computers got the effects of greenhouse gases wrong. The Daily Mail.

12. Twelfth Session of Working Group I. Intergovernmental Panel on Climate Change, (2013). Climate change 2013: The physical science basis. Summary for policymakers. Cambridge University Press.

13. Zimov, S. A., Schuur, E. A. G., & Chapin III, F. S. (2006). Permafrost and the global carbon budget. Science, 312(16), 1612-1613. doi: 10.1126/science.1128908

The SAV001-H vaccine: A new hope for HIV patients
Sadhvi Batra

Since the human immunodeficiency virus (HIV) was identified in 1983, it has generated fear, discrimination, and major changes to public health policy. Among the scientific community, it has also generated a great deal of curiosity because of its unique pattern of progression. Patients often spend years without any symptoms and then begin to suffer from a variety of diseases that are generally easily combatted by healthier immune systems. These patients are almost certain to die in the absence of antiretroviral drugs. Unfortunately, by the time the effort to change the effects of HIV began, there seemed to be little chance of finding patient zero (in epidemiology, the first recorded case of a condition).

Following the advancement of genetic tests, a possible candidate for patient zero was soon revealed in Gaetan Dugas, a Canadian flight attendant who acquired the virus in Africa and introduced it to Western society. It was later found that Dugas was not actually patient zero, and that the most likely origin of the disease was a chimpanzee (Abumrad n.d.). Scientists have since concluded that the virus probably made its way to humans in the late 19th century during the colonization of Africa. According to the Bushmeat theory, a hunter was most likely bitten or cut while "hunting or preparing" a chimp or a monkey (Rope 2004).

HIV infects host cells such as a CD4+ lymphocyte. CD4 receptors and co-receptors on the surface of CD4+ lymphocytes interact with glycoproteins on the viral envelope of HIV. When the glycoproteins of HIV bind to the CD4 receptors, the membranes of the virus and the lymphocyte fuse, allowing the nucleocapsid to enter the host cell and release two single-stranded RNA molecules and three replication enzymes. One of these enzymes, reverse transcriptase, starts to transcribe viral RNA into an RNA-DNA double helix. The RNA is then broken down and the DNA strand undergoes polymerization to complete the DNA helix. This virally derived DNA is then transported to the cell's nucleus and integrated into the host cell's DNA.

When the host cell becomes activated, its DNA undergoes transcription. The mRNA that results is then translated and the viral proteins are synthesized. Proteases cleave long viral amino acid sequences into smaller proteins. The small proteins, along with core replicating enzymes, come together to form a capsid, which eventually leaves the host cell enveloped in the host cell's proteins. The virus then goes on to infect other immune cells (Rajadurai n.d.).

Image source: Kaiser 2012.

From understanding transmission to developing effective treatments, the scientific and medical communities have been pushing to find a cure for this ever-changing virus. Drugs have come to target HIV replication in order to decrease the viral load in an infected individual, which also leads to a decrease in the rate of transmission. Among all advancements in HIV treatment, one stands alone in its potential towards finding a cure: the recently tested SAV001-H vaccine.

At Western University, Canada's Schulich School of Medicine and Dentistry, Dr. Chil-Yong Yang and his team developed the vaccine in collaboration with a biotech company (Mullins 2013). According to Dr. Yang, the SAV001-H vaccine—based on a genetically modified virus, which has been killed—is the only HIV vaccine that is in clinical trials. During phase I of its trials, it showed no adverse side effects. The randomized, observer-blind placebo-controlled study began in March 2012 and finished in August 2013 (HIV Vaccine 2013). It was important that this study was randomized and observer-blind in order to make sure that all participants received treatment without biases or judgment as well as to ensure generalizability among the participants. It was placebo-controlled so that investigators could ensure that patients in the experimental group were indeed showing improvement in comparison to those who were not on the actual vaccine, but believed otherwise.

Investigators studied the effects of the vaccine when it was administered directly into a muscle in HIV-infected,

asymptomatic men and women between 18-50 years of age. Participants were randomly assigned to one of two study groups, placebo or HIV-1 vaccine, and the investigators asked that any adverse side effects be recorded in a diary over a seven-day period. Afterwards, the volunteers were analyzed for chemicals in the body which were "indicative of HIV activity by principal investigators" (HIV Vaccine 2013). The investigators did not observe any serious side effects. HIV-1 antibody detections were performed and the investigators found that the increased antibodies "were maintained during the 52 week study period" (HIV Vaccine 2013). These findings and the lack of adverse side effects in phase I of the clinical trials provide investigators and HIV victims with a new sense of hope for a cure. Given the safety of the vaccine as found by phase I, findings predict high success rates in phase II of the trial, which will look at side effects and safety of the vaccine in a larger study group.

The US Centers for Disease Control and Prevention (CDC) has estimated that since June 1981, "1.7 million [people] in the U.S…have been infected with HIV, including over 619,000 who have already died and approximately 1.2 million adults and adolescents who were living with HIV infection at the end of 2008, the most recent year for which national prevalence estimates are available" (Mahon n.d.). Though it is only in its initial stages, the SAV001 vaccine seems to be a very promising hallmark in the history of HIV. If it lives up to the same success in phase II and phase III of the clinical trials,

then the scientific and medical communities will have to deal with concerns that will arise from implementing the vaccine. These concerns include and are not limited to patenting of the vaccine by pharmaceuticals, implications for marketing it internationally, and screening for those who would be good candidates for the vaccine. More so, since the trials were performed using asymptomatic patients, further research is required to determine the vaccine's efficacy for people who are at-risk or symptomatic. Nonetheless, the SAV001-H vaccine seems to be a groundbreaking step towards a feasible treatment for one of the most pressing concerns in modern healthcare.

References

1. Abumrad, J. (Performer) (n.d.). Patient zero. Radiolab . [Audio podcast].

2. HIV vaccine produces no adverse effects in trials. (2013, September 03). Western News.

3. Kaiser, T. (2012, November 07). Phase I of HIV prevention vaccine clinical trials looks promising. DailyTech.

4. Mahon, N. (n.d.). HIV in the United States: A Glance. Aids.gov.

5. Mullins, D. (2013, September 6). Hiv vaccine completes first round of trials with no side effects. Aljazeera America.

6. Rajadurai, A. R. (Producer) (n.d.). Hiv replication [Web].

7. Rope, K. (2004). Film raises ire over hiv origins. Retrieved from Wired News website.

science news

Undergraduate student helps create eco-friendly nanobattery
Amy Stewart

One of the challenges green energy technologies face is their high cost compared to current non-renewable, "dirty" energy sources. However, researchers Liangbing Hu and Teng Li at the University of Maryland, with the help of undergraduate student Nicholas Weadock, may have found a solution. They developed a unique sodium-ion nanobattery, both cheap and environmentally friendly, that is composed of a sliver of wood coated with tin.

Until recently, sodium-ion batteries were not feasible. Because of sodiation – a phenomenon in which sodium ions cause the anode, the negative terminal, of the battery to expand and then contract during a charge/discharge cycle – sodium-ion batteries have very short lives, usually lasting only 20 cycles before the anode is destroyed (Borghino 2013). Hu, Li, and Weadock managed to make their sodium-ion battery last for 400 cycles, thanks to the innovative idea of using wood fibers instead of the usual metallic substrates (Hu et al. 2013).

There are two characteristics of wood that make it an optimal substrate. First, unlike inflexible and brittle metal substrates,

wood is able to "wrinkle" itself, alleviating the stresses associated with sodiation and giving the battery a longer lifetime than its predecessors. According to Li, "Pushing sodium ions through tin anodes often weakens the tin's connection to its base material. But the wood fibers are soft enough to serve as a mechanical buffer, and thus can accommodate tin's changes. This is the key to our long-lasting sodium-ion batteries" (Borghino 2013). Second, wood is very porous and naturally absorbs water and ions. Since sodium is a large ion, it diffuses very slowly through conventional materials. However, due to wood's high capacity for electrolyte absorption, sodium easily diffuses through cell walls of wood fiber (Hu et al. 2013).

Both components of the nanobattery, wood and sodium, are cheap, especially when compared to the materials used to manufactor common batteries such as lithium batteries, which are found in many electronic devices. Wood and sodium are also more widely available and more eco-friendly than the metals and other components of common batteries. Though

sodium is not as efficient as lithium at storing energy and will most likely never be used in electronic devices, sodium-ion batteries do have the potential to be used in large-scale energy storage facilities, like wind farms or solar energy installations (Hu et al. 2013).

What makes this revolutionary battery even more intriguing is the fact that an undergraduate student helped design it. Nicholas Weadock joined Hu's lab as an undergraduate engineering major at the University of Maryland. "In the very beginning," says Hu, "he was helping students, my Ph.D. students actually, correct some English grammar. During the process ... he asked a lot of interesting, very insightful questions, not only about the language, but about the science behind it" (Palca 2013). Because of Weadock's inquisitiveness,

he not only co-authored a paper in *Nano Letters*, he also made an important contribution to green energy technology.

References

1. Borghino, D. (2013, July 6). Wood nanobattery could be green option for large-scale energy storage. Retrieved October 13, 2013.

2. Hongli Zhu, Zheng Jia, Yuchen Chen, Nicholas Weadock, Jiayu Wan, Oeyvind Vaaland, Xiaogang Han, Teng Li, Liangbing Hu. Tin Anode for Sodium-Ion Batteries Using Natural Wood Fiber as a Mechanical Buffer and Electrolyte Reservoir. Nano Letters, 2013; : 130618094632004 DOI: 10.1021/nl400998t

3. Palca, J. (2013, July 17). All charged up: engineers create a battery made of wood. Retrieved October 13, 2013.
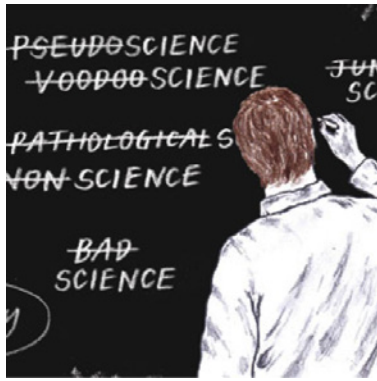
science news

Science vs. pseudoscience
Grace Nix

Science is defined by Merriam-Webster as "…study of the natural world based on facts learned through experiments and observation." Science is now more present in the layman's life than it used to be due to science-based media like the Discovery Channel and National Geographic productions. However, with the spread of science to the general populace by present-day media, another field has emerged: pseudoscience.

The difficulty with the emergence of pseudoscience is distinguishing between it and legitimate science as it is defined above (Science 2011). For example, many instances in history have arisen where theories were proposed before definitive evidence had been discovered. In 1915, Alfred Wegener suggested the controversial idea of continental drift. While Wegner's idea was largely rejected during his lifetime, a few decades later scientific research concerning plate tectonics began to support his hypothesis that continents had in fact shifted. In this instance, prior to tectonophysics, continental drift could have been coined pseudoscience (USGS 2011), highlighting the important and not quite straightforward matter of how to discriminate between the two.

The difficulty with the emergence of pseudoscience is distinguishing between it and legitimate science as it is defined above (Science 2011). For example, many instances in history have arisen where theories were proposed before definitive evidence had been discovered. In 1915, Alfred Wegener suggested the controversial idea of continental drift.

While Wegner's idea was largely rejected during his lifetime, a few decades later scientific research concerning plate tectonics began to support his hypothesis that continents had in fact shifted. In this instance, prior to tectonophysics, continental drift could have been coined pseudoscience (USGS 2011), highlighting the important and not quite straightforward matter of how to discriminate between the two. To try and differentiate between pseudoscience and real science, potential theories should be evaluated based on their relevance to society and their ability to be falsified. Two examples that can demonstrate this technique are the theory of Bigfoot's existence and the proposed correlation between vaccines and autism (Shermer 2011). Bigfoot is a "large, hairy, bipedal non-human primate," according to The Bigfoot Field Research Organization (BFRO). The BFRO website features various videos of moving anomalies in bushes and photographs of oversized primate-characterized feet ("Bigfoot field researcher's"). This evidence is not sufficient to put Bigfoot in the category of "real science." DNA-containing or fossil evidence have yet to be found and taken to laboratories for extensive testing; chasing such evidence has little relevance to society. Finding evidence for Bigfoot would probably not change worldviews or contribute to current medical knowledge, thus Bigfoot research could be classified as less or nonrelevant to society compared to other research (Shermer 2011).

What about a claim that is relevant? Bigfoot chasers can be looked over, but someone proposing that a common

What is pseudoscience? Image source: Shermer 2011.

practice could induce a neurodevelopmental disorder in infants is not taken near as lightly, and it should not be. In 1988, Andrew Wakefield published a paper in Lancet that claimed a link between gastrointestinal disorders and autism and the MMR vaccine. The paper's claims spread through media like a wildfire, and many support groups formed. Wakefield's trials were repeated, but other researchers could not replicate the evidence; thus Wakefield's paper was eventually retracted from the Lancet. Most evidence suggests there was a financial motive for Wakefield's conclusions in his paper (Godlee, Smith & Marcovitch 2011).

According to the Center for Disease Control there was a higher outbreak of measles in the United States in 2008 than in any other year besides 1997. Most of those with the infection reportedly had not been vaccinated. Larger outbreaks of measles have been observed in recent years in other countries as well, and are thought to be due in part to the MMR-Autism scare (Jasek 20ll). Despite numerous peer-reviewed studies published in scientific journals that falsify the correlation between the MMR vaccine and autism, some parents still believe having their child vaccinated will

predispose them to developing Autism (Gerber & Offit 2008). The ramifications of this are heavy; none of the diseases that MMR helps prevent in children, and therefore in the general population, should be taken lightly.

While some pseudoscience, such as the pursuit of Bigfoot, cannot make a clear contribution to current scientific research done across different laboratories and institutions, it at least does not seem to have a detrimental effect toward society. On the other hand, pseudoscience such as believing there is a link between the MMR vaccine and autism when peer-reviewed evidence says otherwise does incur substantial costs on society. Therefore, the discrimination between science "based on facts learned through experiments and observations" and pseudoscience can be an important one to make.

References

1. Bigfoot field researcher's organization. (n.d.). http://www.bfro.net/.

2. Gerber, J., & Offit, P. (2008). Vaccines and autism: A tale of shifting hypotheses. Clinical Infectious Diseases,8(4), 456-461. doi: 10.1086/596476

3. Godlee, F., Smith, J., & Marcovitch, H. (2011). Wakefield's article linking mmr vaccine and autism was fraudulent. BMJ.

4. Jasek, M. (2011, January 06). Healthwatch: Disputed autism study sparks debate about vaccines.

5. Science. (2011). In Merriam-Webster.com. Retrieved May 8, 2011.

6. Shermer, M. (2011, September 11). What is pseudoscience?. Scientific American.

7. USGS, (2011). Historical perspective on plate tectonics. Retrieved from http://www.usgs.gov/

science news

The last stand: A synthetic compound treatment for tuberculosis
Harsh Shah

As medicine evolved through the twentieth century, many discoveries and breakthroughs prolonged human life. Human ingenuity and the scientific method have conquered smallpox and polio; however, the antibiotic resistance of tuberculosis has baffled scientists for years. Tuberculosis is an airborne, infectious disease that typically infects the lungs and causes chronic cough, blood-tinged sputum, fever, night sweats, and weight loss. Infections are usually latent, meaning that those infected display no symptoms but can still spread the disease to others. However, an active infection will result in a 50% mortality rate if the tuberculosis is left untreated. The incidence and mortality rate due to a tuberculosis infection is greater in developing

nation compared to developed nations, with over 95% of cases and deaths occurring in developing countries (World Health Organization 2013).

Tuberculosis is caused by various strains of mycobacteria; however, the most common strain that causes tuberculosis is rightfully named *Mycobacterium tuberculosis*. It is an aerobic, non-motile, rod-shaped bacterium, which can only live in humans and has not been found to be present in other animals. The infectious agent of tuberculosis is lethal; when left untreated, *M. tuberculosis* divides every 16 to 20 hours. Also, Gram staining tests reveal that the bacterium is Gram negative, indicating that the cell wall has a high concentration of lipids. The high lipid content of the outer membrane

has evolved as a mechanism against selection pressures; organisms without this protective lipid coat are killed off by antibiotics, leaving the surviving bacteria resistant to many antibiotic treatments (Gupta 1998).

Currently, two popular treatments for tuberculosis are the drugs Isoniazid and Rifampin. Though the exact mechanism for Isoniazid is unknown, it is thought that the drug disrupts the production of mycolic acid, which is an important component of the bacteria's cell wall (Johnsson et al. 1995). Without a sufficient amount of mycolic acid incorporated into the cell wall, the bacteria's primary defense against antibiotics becomes compromised. Unlike Isoniazid, Rifampin affects the transcription process of the bacterial genome. The treatment inhibits an enzyme called DNA-dependent RNA polymerase, thereby halting the initiation of RNA synthesis and subsequently protein production (Baysarowich et al. 2008). Both Isoniazid and Rifampin are capable of stopping the proliferation of *M. tuberculosis*, but the bacterium has the ability to become resistant to these drugs and any drug cocktail used against them.

The discovery of Q203 may decrease the prevalence drug-resistant bacteria. Unlike its predecessors, Q203 is a synthetic compound that may resist the ability of the tuberculosis bacterium to create a drug-resistant strand. The discovery of Q203 is attributed to a team led by Kevin Pethe at the Pasteur Institute of Korea. Dr. Pethe and his team spent five years screening 121,156 compounds until they had narrowed the field of drugs to 106 active compounds using the parameter of at least a 70% inhibition in the growth of the bacteria (Pethe et al. 2013). From the 106 compounds, the team decided to focus their search on two imidazopyridine amide (IPA) compounds, which disturb the growth of bacteria by inhibiting the synthesis of ATP, the unit of cellular energy (Johnston 2013). Also, the IPA compounds were of interest to Dr. Pethe because the mechanism of the IPA compounds was different than the mechanisms of Isoniazid and Rifampin, to which *M. tuberculosis* has become resistant. The Q203 compound is a derivative of the IPA compound isolated from the screening group.

Q203 was administered to normal mice at a dose of 1,000 mg per kilogram for two weeks and no toxicity was observed. Also, a dose of 10 mg per kilogram of Q203 was administered to normal rats during a 20 day trial (Pethe et al. 2013). As with the mice experiments, no toxicity was observed in the rats. After the toxicity of Q203 was determined, the compound was administered to tuberculosis-infected mouse models. The Q203 treatment – 10 mg per kilogram – promoted a bacterial load reduction of more than 90%, which is comparable to the bacterial load reduction seen with Isoniazid (Pethe et al. 2013). The bacterial load concentration was measured for four

Scanning electron micrograph of Mycobacterium tuberculosis. Image source: Johnson 2013.

subsequent weeks and was reduced by 99.9%. Therefore, at the end of a four week treatment period, the tuberculosis bacterial concentration was non-existent. Even though the bacterial load concentration decreased markedly within a month, Q203 acted slower than Isoniazid (Pethe et al. 2013).

The success of Q203 in the four-week mouse model treatments has Dr. Pethe pushing the candidate drug into phase I clinical trials. The phase I clinical trials will help to assess the safety and tolerability of Q203 in a small group of human volunteers. Though the outlook for the candidate drug to become a potential treatment for tuberculosis seems positive, Dr. Pethe is cautious, since only 5% of drugs that enter phase I trials ultimately become marketed pharmaceuticals (Johnston 2013). The promise of Q203 is not only of another tuberculosis treatment that physicians can add to the drug cocktail menu, but rather a novel approach to combating an evasive bacteria that is capable of becoming resistant to previous organic treatments.

References

1. Baysarowich J, Koteva K, Hughes DW, Ejim L, Griffiths E, Zhang K, Junop M, Wright GD (2008). Rifamycin antibiotic resistance by ADP-ribosylation: Structure and diversity of Arr. Proceeding of the National Academy of Sciences of the United States of America, 105(12), 4886-4891.

2. Gupta RS (December 1998). "Protein phylogenies and signature sequences: A reappraisal of evolutionary relationships among archaebacteria, eubacteria, and eukaryotes". Microbiol. Mol. Biol. Rev. 62 (4): 1435–91

3. Johnston, R. (2013, August 05). Synthetic molecule chokes TB growth. Nature News.

4. Johnsson, K., King, D., & Schultz , P. (1995). Studies on the mechanism of action of isoniazid and ethionamide in the chemotherapy of tuberculosis. Journal of the American Chemical Society, 117, 5009-5010.

5. Pethe, K., Bifani, P., Jang, J., Kang, S, et al. (2013). Discovery Q203, a potent clinical candidate for the treatment of tuberculosis. Nature Medicine, 19(9), 1157 - 1160.

6. World Health Organization. (2013, October). Tuberculosis.

From lab to life-saving: UAB's Center for Clinical and Translational Science brings together researchers and physicians

Catherine Ritchey

Imagine you have a brilliant idea for a new research project that could change the world. You have found a new fuel source for airplanes that you believe will reduce the cost of flying and the resulting pollution, but you do not know which type of grant best fits your research. You have a promising new approach to curing cancer, but you need help narrowing the scope of your proposal to secure funding. You want to explore a new design for army uniforms that will better protect our soldiers, but you need an interdisciplinary partner to aid in your research. If only there was someone on UAB's campus who could help you take your idea from the bench to the bedside.

It turns out that there is! UAB's Center for Clinical and Translational Science (CCTS) exists for exactly this reason. The CCTS's main purpose, according to Dr. Kent Keyser, UAB's Assistant Vice President for Research, is to help "facilitate research from the lab bench to clinical trials, from clinical trials to clinical practice, and from clinical practice to public policy." The CCTS is funded by the National Institutes of Health (NIH) and the National Center for the Advancement of Translation Science (NCATS) in an effort to aid UAB researchers in their endeavors.

To maximize the benefit to researchers, the CCTS has multiple avenues for assistance. For example, the Phase 1 Clinical Trials Facility, located in UAB's Jefferson Tower, houses the Pilot Grant Program. This program allows investigators to apply for grants up to $60,000 per applicant per year. Jefferson Tower also houses Bioinformatics, Biostatistics, and Epidemiology Assistance, which help researchers from any field and phase of research apply for grants.

In addition to the Phase 1 Facility, CCTS is known for its Nascent Project Panels, Panels Done Quickly (PDQs), and Translation Investigator Exchange Service (TIES). These three programs pride themselves on in-depth assistance and feedback to researchers applying for funding or looking for ways to improve their research. Nascent Project Panels are monthly panels in which researchers present in front of a committee of experts in different fields in order to get feedback on proposals or to discuss their grant options. The Nascent Panels were highly successful, but because they are time-consuming, the CCTS decided to implement the PDQ and TIES programs to increase the turn-around time for helping researchers.

PDQs solve the problem of turn-around time and help narrow the scope of a research project. They are groups of three to five investigators who provide feedback in five to seven days. Feedback includes various application developments such as honing the hypothesis or developing stronger specific aims. PDQs provide rapid verbal and written feedback that helps researchers tailor their proposals and grant applications to exactly what NIH or NSF review boards are looking for. The investigators that make up both the PDQs and Nascent Project Panels have often served on review boards, so their insight is unparalleled for researchers looking for help with applications.

Finally, the TIES program is the match-maker of the group. TIES is meant to match investigators and researchers to the collaborations that best fit their needs. The CCTS hopes that these collaborations will lead to interdisciplinary research which has greater chance in securing funds and awards. For example, the army uniforms you have in mind could become a reality when the TIES program matches you with a researcher on campus who knows how to manipulate the materials you want to use so that they are safe for their intended application. These programs are all designed to best aid researchers in taking their ideas from the lab bench to the market. They can assist in project design; proposal development; research implementation; data interpretation; assistance with abstracts, posters, or articles; revision of applications in response to grant reviews; or even career development discussions.

Still wondering how the CCTS can help you take your ideas to the next level? Look at these people CCTS has already helped!

Dr. David Buys is an Instructor in the Division of Gerontology, Geriatrics, and Palliative Care at UAB. He recently completed postdoctoral training in Health Services and Outcomes Research through UAB's Center for Outcomes and Effectiveness Research and Education. Dr. Buys proposed a Career Development Award to the National Institute on Aging, and although his grant has not yet been funded, he credits CCTS for helping him immensely thus far. Dr. Buys participated in a Nascent Project Panel, which gave him much-needed feedback that he was able to incorporate extensively into his project. Dr. Buys' research involves neighborhood effects—the impact on health-related outcomes of the area in which one lives—for older adults. The last twenty years have seen an increased interest in neighborhood effects on health, including ways that social context influences cardiovascular health, depression, and other outcomes.

Dr. Buys is extending this research to the elderly, using two prominent, longitudinal studies including significant samples of older adults. The Jackson Heart Study and the Health and Retirement Study evaluate both functional capacity and health services utilization of people as they age. The CCTS Nascent Panels helped him formulate his original grant submission, and now he is looking to them for help in altering the grant for a resubmission based on the reviews. The CCTS is helping Dr. Buys translate his idea to research reality.

David Hilton, Ph.D., and Robin Collingwood, M.D., used the PDQs to develop their project involving laser sectioning of stented arterial tissue. This laser research will decrease the time it takes to test new drug-eluted stents, arterial stents that releases chemicals to prevent the formation of new blockages. Current methods involve curing artery segments in plastic and slicing the segment into numerous pieces, of which only a few can actually be tested. This process is highly inefficient and they are looking at ways to use optical techniques to improve efficiency. Dr. Hilton says the PDQ helped them narrow their specific aims to properly appeal to the NIH review panels, where the overall success rate of proposals is very low. An organization like CCTS is a great asset since it can connect researchers with different experiences together. In this case, it helped match the physics of laser science to the medical needs of pharmacology to create a collaborative effort. The research involved in this new approach has the potential to significantly increase drug testing and the efficacy of stents, and it would not have been possible without the aid of CCTS.

Dr. Karen Gamble benefitted from two different CCTS programs: the Nascent Project Panels and TIES. Dr. Gamble is an Assistant Professor in Psychiatry and Behavioral Neurobiology. The CCTS helped her specifically with a project that has the potential to improve the cardiometabolic health of shift workers through studies of how sleep and meal timing strategies can influence metabolic rhythms and even lead to a pre-diabetic state. Dr. Gamble asserts, "The CCTS Nascent Projects Panel was very useful for my upcoming R01 grant submission. Recommendations included justification of the sample population and study design. The panel was very diverse and is a good representation of the diversity of the future study section that may review my grant." The

Nascent Panel in which Dr. Gamble participated also lead to a TIES match-up, as it promoted new collaborations that helped to develop her research. Dr. Gamble has teamed up with Dr. Patricia Patrician in the School of Nursing (SON) to conduct a pilot study investigating alertness and cognitive function in shift workers (recently funded to Dr. Patrician as a SON Dean's Award). With the help of CCTS, Dr. Gamble was awarded a Pilot Grant, a grant to attain preliminary data for a bigger project, in 2012. She recently submitted an NIH R01 application (an application to fund a larger research project) using the preliminary data generated from the Pilot Grant.

Drs. Buys, Hilton, Collingwood, and Gamble are just four of the countless researchers who have benefitted from the CCTS. The Nascent Project Panels, Panels Done Quickly, and Translational Investigator Exchange Service are making new connections daily and providing unprecedented feedback to UAB investigators looking to make their ideas realities. The research possibilities are endless, and the Center for Clinical and Translation Science is there to take your ideas and make them realities.

References

1. Buys, D. (2013, Oct. 1). Interview by Catherine Ritchey.

2. CCTS Logo. 2009. UAB Center for Clinical and Translational Science, Birmingham, AL. Eventbrite.com. Retrieved 10 Jan 2014.

3. Gamble, K. (2013, Oct. 4). Interview by Catherine Ritchey.

4. Hilton, D. (2013, Oct. 4). Interview by Catherine Ritchey.

5. Keyser, K. (2013, Sep. 24). Interview by Catherine Ritchey.
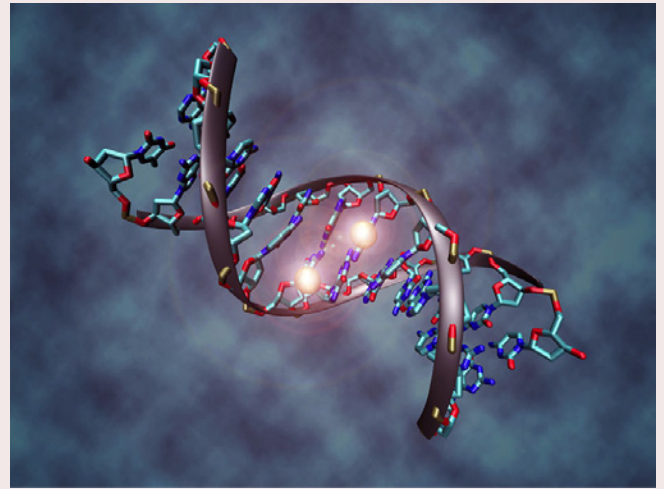
The pleasure of memory formation: DNA methylation regulates associative reward learning

Roxie Lockhart

The brain encourages certain behaviors which increase the chances of survival by connecting pleasure to these actions. Eating delicious foods, producing offspring, and other pleasurable activities have all increased the chances of humans' survival. Published recently in Nature Neuroscience, our very own UAB researchers have unlocked the mechanism for memory formation relating to pleasure.

"We believe reward memory may serve as a good model for understanding the molecular mechanisms behind many types of learning and memory," said David Sweatt, Ph.D., chair of the UAB Department of Neurobiology and director of the Evelyn F. McKnight Brain Institute at UAB. "Our results provide a leap in the field's understanding of reward-learning mechanisms and promise to guide future attempts to solve related problems such as addiction and criminal behavior."

Dr. Jeremy Day, a member of Dr. Sweatt's laboratory and author of this published research, was initially interested in understanding what brain changes occur when you make a memory about something considered pleasurable. Day and his research team began by observing dopamine neurons and found that during memory formation there is a specific change in gene expression that involves an epigenetic mechanism—an external event which affects how genes are expressed. For example, DNA methylation is the attachment of a methyl group to a DNA sequence at a certain area. Methylation has the ability to turn genes off or on depending on environment or behavioral factors. Therefore, this type of regulation affects gene expression without changing the inherited sequence itself. The brain's pleasure center is generally located in the ventral tegmental area (VTA). Memory formation proceeds through nerve cells that signal using the neurochemical dopamine. Past research has debated that dopamine-producing neurons in the VTA and those in the nucleus accumbens (NAC), downstream of the VTA, were both involved in natural reward- and drug-addiction-based memory formation. By using a mix of DNA methylation and demethylation, which blocked the important chemical changes in memory formation in the VTA, rats were prevented from forming new reward memories. This was the first demonstration that formed memories involve pleasurable events. This study was also the first to illustrate epigenetic changes that influence memory-related genes occur in the specifically the VTA. "We observed an important distinction, not in circuitry, but instead in the epigenetic regulation of that circuitry between natural reward responses and those that occur downstream with drugs of abuse or psychiatric illness," said Dr. Day.

Rendition of DNA methylation. Image retrieved from Wikipedia.org.

Using an animal model, rats were trained to associate a sound tone with the availability of sugar pellets in their feed ports. This same animal model has been used to study the function of dopamine neurons since the 1990s. To separate the effects of memory-related brain changes from those arising from the pleasure of the eating itself, the rats were separated into three groups. One group received sugar pellets each time they heard a sound cue. The second group heard the sound the same number of times and received as many sugar pellets but never simultaneously. A third group only received a tone and no sugar reward. Rats paired with sounds were significantly more likely to poke their noses into the feed ports than the control rats, signifying a successful pleasurable memory formation. The pleasurable memory rats also had significantly higher expression of the memory genes *Egr1* and *Fos* than the control rats. These two genes are known to regulate memory in other brain regions by coordinating the signaling capacity of the connections between neurons. In the next series of experiments, methylation and demethylation manipulations drove the changes in gene expression as memories formed. This study discovered that two sites upstream from the *Egr1* gene were demethylated during reward experience. Within both *Egr1* and *Fos* genes methylation occurred as reward memories were formed. This simple yet elegant experiment demonstrated that rats receiving a sugar pellet paired with sound were significantly better at forming memories. DNA methylation and demethylation patterns drove changes for gene expressions in memory formation. Therefore, a model of reward-related experiences caused both types of DNA methylation and epigenetic gene regulation to occur.

For his future studies, Dr. Day is interested in exploring more avenues to treating addiction as well as better understanding memory formation. "Dopamine neurons are remarkably dynamic. Changes in the neurons are important to formation of pleasure-related memories, but we don't know what maintains the memories over a long time. We can have memories that involve pleasure for months, days, or years even; but, we don't know what maintains that to the future. Another aspect is applying this concept to addiction. Memories related to drugs of abuse are powerful regulators of behavior. If a former addict sees some kind of cue that is associated with drugs it can be a trigger for drug relapse," stated Dr. Day when discussing the significance of this type of memory function as well as a future for therapeutic treatment.

"When designing therapeutic treatments for psychiatric illness, addictions, or memory disorders, you must profoundly understand the function of the biological systems you're working with. Our field has learned from experience that attempts to treat addiction with drugs that globally impair normal reward memories do not succeed. Our study suggests the possibility that future treatments could dial down drug addiction or mental illness without affecting normal rewards," added Dr. Day. This ground-breaking research provides a new light in better understanding how the brain adapts to addictions. It also opens new doors for more target-specific treatments. "Epigenetics is not a new field. It is a field that connects environmental factors and behavior, as well as provides hope for future care," said Dr. Lubin, a member of the Evelyn F. McKnight Brain Institute at UAB. By better understanding the mechanisms for which humans adapt to their surroundings at the molecular level, researchers are providing a new hope to those not only suffering from addiction but also those with other neurological disorders.

program spotlight

The Science and Technology Honors Program: Preparing undergraduates for research and science careers

Bliss Chang

Around the world, experts and non-experts alike are realizing the importance of fostering research among the younger generations to help keep pace with the rapid developments in sectors that affect the quality of living. As a biomedical research institution, the University of Alabama at Birmingham developed an initiative which encourages students to pursue research careers: the Science and Technology Honors Program.

The Science and Technology Program accepts 50 students annually and prepares them for research and other science-based careers through extensive specialized courses and mentoring. Similar to students pursuing a masters or doctoral degree, each student in the program develops a research proposal with the aid of his/her mentor, carries out experiments to validate or refute a hypothesis, and defends a thesis in front of a committee. Students also have the opportunity to take writing and public speaking classes geared toward scientific communication. These preparatory mechanisms allow students to find success in disseminating their work to local and national audiences through publications and conference presentations.

When asked about the importance of undergraduate research, program director Dr. Diane Tucker emphasizes, "When a student assumes ownership of an in-depth project, there is a level of intellectual curiosity and investigation beyond that which is encountered in most courses." Furthermore, Tucker

Diane Tucker, Director of the UAB Science and Technology Honors Program.

agrees that research provides a means for students to learn a topic of interest on a more advanced level than is available through most traditional classes. Most importantly, research requires students to reason through a challenging problem and synthesize new knowledge out of existing knowledge and new information. This ability to think critically and expand upon the knowledge base is the ultimate product of education.

As with any initiative, however, development of the research-focused program was not without its challenges. Although Tucker drew from her experiences as an undergraduate and emphasized curricula that reflect opportunities for

students to think critically and communicate about problems, sometimes commitment and performance problems arise as students become busy with their academic and social lives. Tucker explains that one of her biggest challenges has been acquiring and maintaining all the information about each student's involvement in their respective labs. This is necessary to maintain a good working relationship with the mentors who willingly offer their time and money to train undergraduates.

UAB's Science and Technology Honors Program is nurturing the scientific potential that lies dormant in many students who attend college. As a field that is not highly publicized, research has often been cast into the shadows by students focusing on the academics, arts, and sports. However, UAB is moving towards increased participation in undergraduate research: a course of action consistent with its identity as a biomedical research institution.

short report

White matter hyperintensity load in adults with chronic stroke is related to motor function but not response to CI therapy

Jarrod M. Hicks[1], Tyler Rickards[1], Victor W. Mark[2], Gitendra Uswatte[1,3], and Edward Taub[1]

[1] Department of Psychology, [2] Department of Physical Medicine and Rehabilation,
[3] Department of Physical Therapy
University of Alabama at Birmingham

Abstract

Objective: Determine the relationship between white matter hyperintensity (WMH) volume, motor function, and response to constraint-induced movement (CI) therapy, an efficacious rehabilitation method, in patients with chronic stroke with upper-extremity hemiparesis.

Participants and Methods: Participants (n=35) with chronic stroke (63.2 ± 10.3 years) and mild to moderate motor impairment of their more affected upper extremity were randomly assigned to receive CI therapy (n=24), a comparison therapy (n=6), or no therapy (n=5). Fluid attenuated inversion recovery (FLAIR) MRI sequences were obtained prior to therapy and WMHs were traced using a semi-automated procedure. Hyperintensity overlap with the corticospinal tract (CST) and centrum semiovale (CS) was calculated. Hemiparetic arm function was measured prior to and after therapy with the Motor Activity Log (MAL) and Wolf Motor Function Test (WMFT).

Results: Increased global hyperintensity volume and hyperintensity overlap with the CST and CS were related to poorer pretreatment motor function on the WMFT. Improvement in motor function following CI therapy did not relate to global hyperintensity volume or hyperintensity overlap with the CST or CS.

Conclusion: Despite the contribution of WMH load to pretreatment deficit in motor performance on the WMFT, WMH load does not prevent patients from benefitting from CI therapy. These findings are consistent with previous data from this laboratory (Gauthier et al., 2009), which show similar relationships between lesion volume and motor function in patients with chronic stroke. Together, these suggest WMH may be an important factor to consider in upper extremity motor impairment.

Keywords: *stroke, white matter hyperintensities, CI therapy, neuroimaging, motor deficits*

Introduction

White matter hyperintensities (WMHs) are brain abnormalities that appear as bright areas on proton-density (PD), T2-weighted, and fluid attenuated inversion recovery (FLAIR) MRI scans as shown in Figure 1.[1] WMHs are presumably associated with damage to cranial white matter due to vascular abnormalities such as small vessel disease.[2] It is thought that affected vessels contribute to white matter lesions through hypoperfusion, leading to chronic plasma leakage into the white matter.[2-4] Several studies have associated WMHs with cognitive decline and aging.[5-9] WMHs are also correlated with physical disabilities such as reduced gait speed, balance, and muscle strength.[10-12]
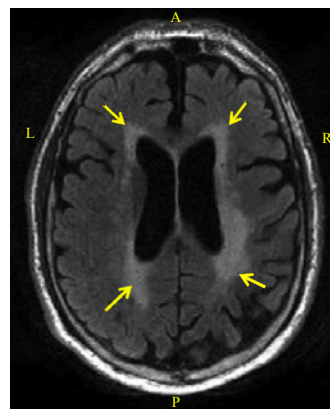

Figure 1. FLAIR MRI image showing white matter hyperintensities (WMHs), indicated by yellow arrows.

Table 1. Patient demographics (Mean ± SD)

Group	Age at entry	Years since stroke
CI therapy (n=24)	63.1±10.4	3.6±2.9
Comparison (n=6)	65.9±10.6	4.7±5.5
No therapy (n=5)	60.4±11.3	7.1±8.8
Total (n=35)	63.2±10.3	4.3±4.6

In patients with chronic stroke, i.e. stroke occurring more than 1 year post-injury, overall lesion volume is not related to motor function prior to therapy.[13-14] However, location specific lesion load, particularly in the corticospinal tract (CST), is associated with poorer motor ability following stroke.[15-20]

Constraint-induced movement (CI) therapy is a treatment shown to be efficacious in improving motor function following stroke.[21-22] While lesion load of the centrum semiovale (CS) region of the CST is correlated with reduced motor ability prior to treatment, such lesion load does not reduce the ability to improve motor function in response to CI therapy.[18]

This study examines the relationship between WMH load, motor function, and response to CI therapy in adults with upper-extremity hemiparesis following stroke.

Methods
Participants
Adult chronic stroke patients received either CI therapy (n=24) or a comparison therapy (n=6), and five patients received no therapy, as shown in Table 1.

Intervention
All therapy patients received in-laboratory impaired upper-extremity training for 3 hours each day for 10 consecutive weekdays. CI therapy components included: 1) massed practice training of impaired-arm movement; 2) training by the behavioral technique termed "shaping"; 3) restraint of the less-impaired arm with the use of a protective safety mitt for a target of 90% of waking hours; 4) a transfer package consisting of an additional 30 minutes of training daily involving monitoring of real-world use of the more-affected arm, home practice assignments, problem solving to overcome apparent barriers to arm use, and a behavioral contract. Mass practice training consisted of functionally based activities, such as writing or wrapping a present, performed continuously for a period of 15 to 20 minutes. Shaping tasks are characterized by reaching behavioral objectives in small, successive steps. An example of a shaping task is placing blocks onto a box. In this case, successive adjustments of difficulty could include increasing box distance from patient, increasing box height, or changing the block size. The comparison therapy involved the same in-laboratory treatment and target 90% waking-hours restraint; however, it did not include the transfer package.

Motor measures
Two measures were used to assess motor function in patients, both within one week prior to and within one week following therapy. The Motor Activity Log (MAL) is an established measure with strong clinimetric properties of the amount and quality of spontaneous use of the more-impaired upper extremity in 30 tasks of daily living activities in real-world situations.[21] The Wolf Motor Function Test (WMFT) is a validated laboratory measure of maximum motor ability made on request. The WMFT assessed the average maximal performance speed on 15 tasks.[23]

Imaging analysis
FLAIR MRI scans were obtained for all subjects within one week prior to receiving therapy; scans for subjects receiving no therapy were also obtained at this time. Subject scans were normalized to a FLAIR template in Montreal Neurological Institute (MNI) space prior to tracing. WMHs were traced by a trained experimenter under supervision of the project's neurologist (V. W. M.) using a semi-automated intensity thresholding method available through MRIcron software (http://www.mccauslandcenter.sc.edu/mricro/mricron/index.html). Contralesional and ipsilesional CST and CS regions of interest (ROIs) were created in MNI space using the "SPM Anatomical toolbox" in SPM 5 (The Wellcome Dept. of Imaging Neuroscience, London; www.fil.ion.ucl.ac.uk/spm).

WMH volume calculations included measurements of total WMH volume, periventricular WMH (PVWMH) volume, deep WMH (DMWH) volume, and total WMH percent overlap with the CST and CS ROIs. An example of WMH and CST ROI overlap is demonstrated in Figure 2.

Let PVWMH volume be defined as the portion of WMH volume lying within a 2 cm space surrounding the lateral ventricles. Also, let DWMH volume be defined as the total WMH volume minus the PVWMH volume. Overlap percentages are reported as WMH/ROI overlap volume divided by ROI volume multiplied by 100. Pearson correlations were used to examine the association between WMH characteristics and measures of motor function.

Results and Discussion
For all subjects prior to treatment, higher total WMH volume and PVWMH volume corresponded with poorer WMFT performance (both $p < 0.01$). Also, WMH overlap with the

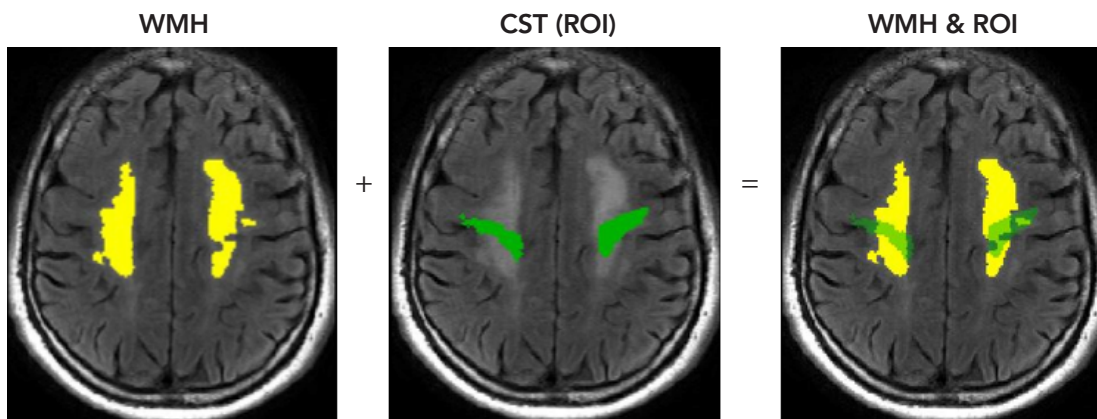| WMH	CST (ROI)	WMH & ROI

Figure 2. A traced WMH region (left; yellow), the CST ROI (center; green), and both superimposed on the same image (right), showing overlap between the two.

ipsilesional CST and ipsilesional CS related to decreased pre-treatment WMFT performance (all correlations $p < 0.01$). The relationship between DWMH volume and WMFT performance approached significance ($p = 0.059$). WMH overlap with the contralesional CST and contralesional CS was not significantly associated with reduced WMFT performance prior to therapy. These results are summarized in Table 2.

Additionally, no measures of WMH load were significantly associated with pretreatment MAL scores.

Improvement in maximal motor function following CI therapy, as measured by the in laboratory WMFT, did not relate to WMH volume or WMH overlap with the CST or CS. WMH volume and WMH overlap with ROIs also did not reduce amount of improvement in spontaneous use of the affected arm in the life situation, as measured by the MAL.

Conclusions
In patients with chronic stroke, increased global hyperintensity volume and hyperintensity overlap with the CST and CS were related to poorer pretreatment motor ability, as measured by the WMFT, but not to spontaneous use of the more-affected arm, as measured by the MAL. This suggests that spontaneous use of an arm affected by stroke in the life situation and maximal motor ability exhibited on request in the laboratory represent two different domains of movement that are not well correlated with one another after stroke.

Despite the contribution of WMH load to pretreatment deficit in motor performance on the WMFT, WMH load does not prevent patients from benefiting from CI therapy. These findings are consistent with previous data from this laboratory relating: total lesion load,[13,14,18] lesion overlap with the CST and CS,[18] and interruption and displacement of the CST.[20] Together, these suggest WMH may be an important factor in upper extremity motor impairment prior to the application of CI therapy. However, these defects in the central nervous system do not prevent a patient from obtaining maximal benefit from this treatment.

Table 2. Correlations between WMH load and maximum motor function prior to therapy. Significant results are presented in bold-face type.

Volume Measure	Pearson Correlation (r)	Significance (P)
Total WMH	**-0.461**	< 0.01
PVWMH	**-0.486**	< 0.01
DWMH	-0.327	0.059
Ipsilesional CST Overlap %	**-0.556**	< 0.01
Contralesional CST Overlap %	-0.303	0.082
Ipsilesional CS Overlap %	**-0.544**	< 0.01
Contralesional CS Overlap %	**-0.293**	0.092

References

1. Fazekas, F. *et al.* (1993). Pathologic correlates of incidental MRI white matter signal hyperintensities. *Neurology* 43, 1683-1689.

2. Debette, S., Markus, H. S. (2010). The clinical importance of white matter hyperintensities on brain magnetic resonance imaging: systematic review and meta-analysis. *BMJ* 341.

3. O'Sullivan, M. *et al.* (2002). Patterns of cerebral blood flow reduction in patients with ischemic leukoaraiosis. *Neurology* 59, 321-326.

4. Marstrand, J. R. *et al.* (2002). Cerebral perfusion and cerebrovascular reactivity are reduced in white matter hyperintensities. *Stroke* 33, 972-976.

5. Yoshita, M. *et al.* (2006). Extent and distribution of white matter hyperintensities in normal aging, MCI, and AD. *Neurology* 67, 2192-2198.

6. Young, V. G., Halliday, G. M., Kril, J. J. (2008). Neuropathologic correlates of white matter hyperintensities. *Neurology* 71, 804-811.

7. Silbert, L. C. *et al.* Trajectory of white matter hyperintensity burden preceding mild cognitive impairment. *Neurology* 79, 741-747.

8. Maillard, P. *et al.* (2012). Coevolution of white matter hyperintensities and cognition in the elderly. *Neurology* 79, 442-448.

9. van den Heuvel, D. M. *et al.* (2006). Increase in periventricular white matter hyperintensities parallels decline in mental processing speed in a non-demented elderly population. *J Neurol Neurosurg Psychiatry* 77, 149-153.

10. Silbert, L. C., Nelson, C., Howieson, D. B., Moore, M. M., Kaye, J. J. (2008). Impact of white matter hyperintensity volume progression on rate of cognitive and motor decline. *Neurology* 71, 108-113.

11. Starr, J. M. *et al.* (2003). Brain white matter lesions detected by magnetic resonance imaging are associated with balance and gait speed. *J Neurol Neurosurg Psychiatry* 74, 94-98.

12. Sachdev, P. S., Wen, W., Christensen, H., Jorm, A. F. (2005). White matter hyperintensities are related to physical disability and poor motor function. *J Neurol Neurosurg Psychiatry* 76, 362-367.

13. Mark, V. W., Taub, E., Perkins, C., Gauthier, L., Uswatte, G. (2008). MRI infarction load and CI therapy outcomes for chronic post-stroke hemiparesis. *Restor Neurol Neurosci* 26, 13-33.

14. Page, S. J., Gauthier, L. V., White, S. (2013). Size doesn't matter: cortical stroke lesion volume is not associated with upper extremity motor impairment and function in mild, chronic hemiparesis. *Arch Phys Med Rehabil* 94, 817-821.

15. Lindenberg, R. *et al.* (2010). Structural integrity of corticospinal motor fibers predicts motor impairment in chronic stroke. *Neurology* 74, 280-287.

16. Lo, R., Gitelman, D., Levy, R., Hulvershorn, J., Parrish, T. (2010). Identification of critical areas for motor function recovery in chronic stroke subjects using voxel-*based lesion symptom mapping*. *Neuroimage* 49, 9-18.

17. Zhu, L. L., Lindenberg, R., Alexander, M. P., Schlaug, G. (2010). Lesion load of the corticospinal tract predicts motor impairment in chronic stroke. *Stroke* 41, 910-915.

18. Gauthier, L. V., Taub, E., Mark, V. W., Perkins, C., Uswatte, G. (2009). Improvement after constraint-induced movement therapy is independent of infarct location in chronic stroke patients. *Stroke* 40, 2468-2472.

19. Shelton, F. N., Reding, M. J. (2001). Effect of lesion location on upper limb motor recovery after stroke. *Stroke* 32, 107-112.

20. Rickards, T. *et al.* (2013). Diffusion tensor imaging study of the response to constraint-induced movement therapy of children with hemiparetic cerebral palsy and adults with chronic stroke. *Arch Phys Med Rehabil*.

21. Taub, E. *et al.* (1993). Technique to improve chronic motor deficit after stroke. *Arch Phys Med Rehabil* 74, 347-354.

22. Taub, E. *et al.* (2006). A placebo-controlled trial of constraint-induced movement therapy for upper extremity after stroke. *Stroke* 37, 1045-1049.

23. Morris, D. M., Uswatte, G., Crago, J. E., Cook, E. W. 3rd, Taub, E. (2001). The reliability of the wolf motor function test for assessing upper extremity function after stroke. *Arch Phys Med Rehabil* 82, 750-755.

Tensor singular value decomposition with applications

Alexandra Fry and Carmeliza Navasca

Department of Mathematics, University of Alabama at Birmingham

Abstract

In this paper, tensor decomposition and its application to MRI data compression was introduced. The tensor singular value decomposition (SVD), which is the generalization of the matrix singular value decomposition, was specifically used. A truncated tensor SVD to approximate a low multilinear rank for tensor structured datasets (e.g. MRI data) was applied for tensor image compression. We implemented this method on a real-life MRI dataset of the brain with a small residual error.

Introduction

There are many applications for tensor decompositions, including identifying addresses on mail, reducing MRI scans for easy processing, compressing data like videos (Figure 1), extracting features like faces in face recognition software, and reducing noise for weather prediction.

Figure 1. A video or an image sequence represented as a third-order tensor of column x row x time, where time is the 3rd mode.

Recently, tensors have become popular in pattern recognition. Tensor SVD has been applied to face and handwriting recognition since the data often has a multidimensional structure. SVD is used to compute a small basis set that spans the main space of each digit. This set is then used to identify unknown digits. Since we can reduce the number of bases in each modal direction that provide salient information, SVD requires less memory and is more efficient without sacrificing accuracy. Essentially, an image or other data is compressed using truncated tensor SVD and is reconstructed from the individual parts. The algorithm gives an error of 5% when comparing the two sets of data, even after a substantial compression of the digits.[1]

Tensors are multi-dimensional arrays of numerical values. The order of a tensor is the number of dimensions or modes. An Nth order tensor can be defined as an element of the tensor product of N vector spaces.[2] Third-order tensors will be discussed, which are formally viewed as an element of products of vector spaces. A first-order tensor is a vector, a second-order tensor is a matrix, and tensors of order three or higher are called higher-order tensors, as shown in Figure 2.
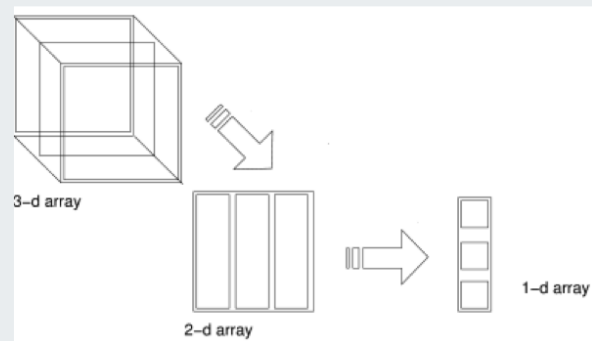

Figure 2. Representation of a tensor (3-d array), matrix (2-d array), and scalar (1-d array).

It can be convenient to rearrange the elements of a tensor so that they form a matrix. This unfolding or flattening is called *matricization*. For instance, a 2×3×4 tensor can be arranged as a 6×4 matrix or a 3×8 matrix. The matricizing of a tensor A is defined by specifying where an element in A is placed in the matrix. The computation of the SVD of a tensor can be done by separately computing the orthogonal matrices U_1, U_2, and U_3 of A.

The singular value decomposition (SVD) of an $m×n$ matrix A is a factorization shown in Equation 1:

$$A = USV^T \qquad (1)$$

U is an orthogonal $m×m$ matrix. S is the core, an $m×n$ rectangular diagonal matrix with positive real numbers (called singular values) on the diagonal. V^T (the conjugate transpose of V) is an orthogonal $n×n$ matrix. This is known as matrix SVD.[2]

Tensor SVD

Tensor SVD is more complex than matrix SVD because the core is usually not diagonal. There is only a sequence of better and better approximations that converge to infinitely

large matrices. Two types of tensor decompositions exist: CP and Tensor SVD. Tensor SVD decomposes an order-N tensor into a core tensor that has the same size as the original tensor together with N orthogonal side-matrices.[2]

The rank of a matrix is the number of linearly independent column vectors. The rank of a third-order tensor is based on the rank of each of the subspaces. Low-rank approximation is defined as finding the minimum number of linearly independent column vectors that approximate the linear subspace well. This truncated tensor SVD is calculated using Equation 2:

$$A = S \times_1 U_1 \times_2 U_2 \times_3 U_3 \qquad (2)$$

Finding a low rank reduced subspace of U_1, U_2, and U_3 leads to a truncated S, demonstrated in Figure 3.

Figure 3. Representation of the truncated tensor SVD. Tensor A is factorized into the core S and the subspaces U1, U2, and U3, shown in gray. These are reduced from the original versions that are outlined.

Materials and Methods

Consider a timed series of 22 images along the brain with a tumor for an MRI scan.[3] Each image is a two-dimensional data array, and, together with images at different parts of the brain, the data constitutes a third-order tensor. It is very beneficial to use the collected data without destroying its multidimensional structure. Tensors make it possible to capture what is sufficient to analyze the data and significantly reduce the size of the data to find tumors or other maladies more efficiently. To find the truncated tensor SVD, the core tensor must be calculated by first calculating the three SVDs for the set of images using the algorithm in Equations 3–6 and shown in Figure 5.

First, the three SVDs are computed:

$$A_{(1)} = U_1 S^{(1)} (V^{(1)})^T \qquad (3)$$

$$A_{(2)} = U_2 S^{(2)} (V^{(2)})^T \qquad (4)$$

$$A_{(3)} = U_3 S^{(3)} (V^{(3)})^T \qquad (5)$$

Followed by computation of the core tensor:
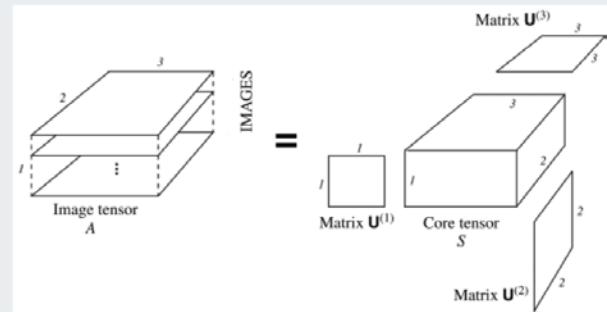
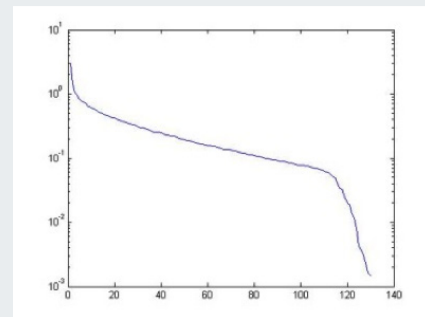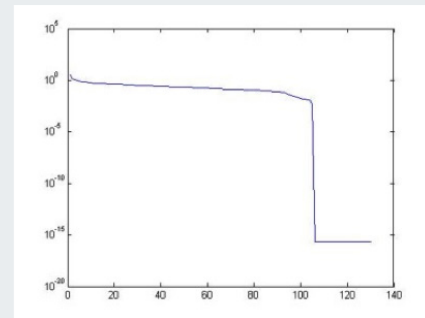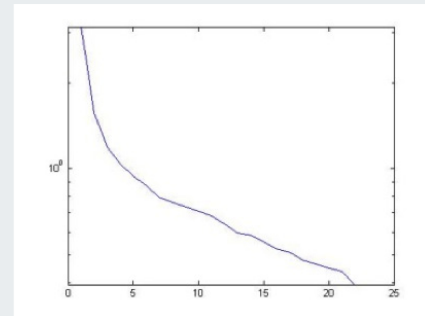$$S = A \times_1 U_1^T \times_2 U_2^T \times_3 U_3^T \qquad (6)$$

Figure 4. Computing the core tensor from the image tensor A.

Mode 1 singular values

Mode 2 singular values

Mode 3 singular values

Figure 5. The singular values for the three modes of the tensor.

The three modes of the tensor are calculated using an algorithm in MATLAB with the individual points in the graphs designated as singular values. The singular values eventually decay, and the set of non-important zeros is truncated. This is called a truncated tensor SVD through rank reduction. It is based on the drop-off point obvious in the graphs of modes 1 and 2 in Figure 5. The number of singular values that are kept determines the dimensions of each low-rank subspace. In Figure 5, the third mode is the set of 22 images, and therefore its singular values decay at 22. Unlike the first and second modes, its singular values were not truncated.

Results and Discussion

The sets of MRI scan images in Figure 6 are representative sets of 9 of the 22 total scans. The top set, which is the original set of images, is transformed using the truncated tensor SVD algorithm into the bottom two sets. In the bottom left set, the first two modes (R_1 and R_2) were prematurely truncated, so the MRI scans are blurry. The first two modes were appropriately truncated to create the bottom right set, so the rank is reduced at the approximate value of the first two graphs' decays in Figure 6. The singular values decay at approximately $R_1, R_2 = 110$ (Figure 5), so the rank was reduced at that particular value in the bottom right set of images in Figure 6. This set is a successful application of truncated tensor SVD, used properly with the correct rank reduction.
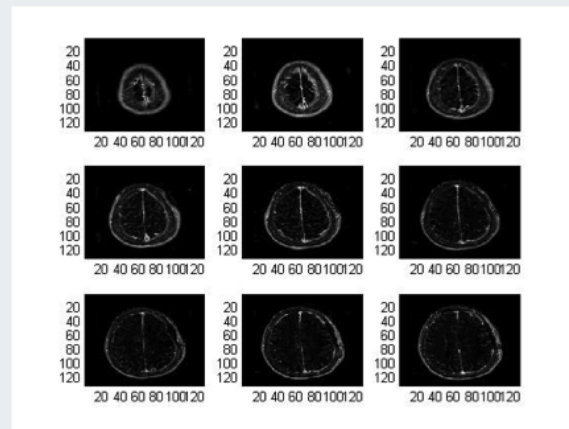
Conclusion

With advances in data acquisition and storage technology, massive multidimensional data sets are being generated with a wide range of emerging applications. Therefore, SVD is frequently employed to reduce the size of the data while keeping the important information. Future research should focus on more efficient methods for computing tensor decompositions and determining maximal tensor ranks. More applications, both inside and outside mathematics, will doubtlessly be found for tensor decompositions in the future.

Acknowledgements

References

1. Eldén, L. (2007). Matrix methods in data mining and pattern recognition, *SIAM*.

2. Kolda, T., Bader, B. W. (2009). Tensor decompositions and applications. *SIREV*, **51**(3), 455-500.
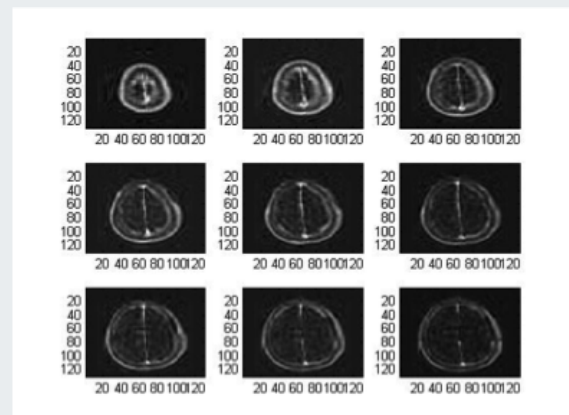
3. OsiriX. (2012). DICOM Viewer. http://www.osirix-viewer.com/

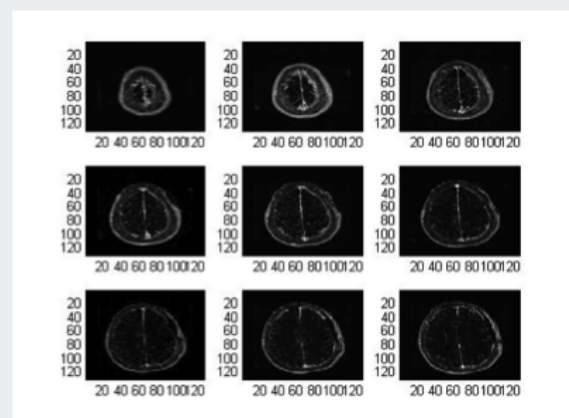

Tensor dimensions: 130 × 130 × 22

Original MRI of the brain with tumor

Truncated Tensor SVD

Rank reduction of: R_1=22, R_2=22, R_3=22

Rank reduction of: R_1=110, R_2=110, R_3=22

Reconstructed MRIs of the Brain with Tumor

short report

Metabotropic glutamate receptor 4 positive allosteric modulators attenuate LPS-induced inflammation in microglial cells

Ranjani Ponnazhagan, Ashley S. Harms, David G. Standaert

Department of Neurology, University of Alabama at Birmingham

Abstract

Metabotropic glutamate receptors (mGluRs) are G-protein coupled receptors that contain a binding site for glutamate. mGluR4 is localized to presynaptic terminals in the substantia nigra pars compacta (SNpc). Previous studies have shown that mGluR4 plays a functional neuroprotective role in neurodegenerative disorders such as Parkinson's Disease (PD), but the role of mGluR4 in inflammatory response is currently unknown. In this study, we examined whether treatment of microglial cells with the mGluR4 positive allosteric modulators (PAMs) ADX and VU813 afforded protection against lipopolysaccharide (LPS)-induced inflammatory response. We found that pre-treatment of microglial cells with 1 nM, 10 nM, and 100 nM ADX and 1 nM, 100 nM, and 1000 nM VU813 attenuated LPS-induced tumor necrosis factor (TNF) release, suggesting that administration of the PAMs attenuates the pro-inflammatory response. These findings indicate that mGluR4 PAMs are not only protective against motor dysfunction in PD, but also have anti-inflammatory properties, suggesting that they have potential as novel therapeutic agents for the treatment of PD.

Introduction

Parkinson's Disease (PD) is the second most common neurodegenerative movement disorder in the United States. The substantia nigra pars compacta (SNpc) and striatum are the brain areas most affected in PD,[1] and the areas in which dopaminergic neurons and axonal projections are highly concentrated. PD causes progressive loss of dopaminergic neurons, resulting in motor deficits, as well as an increased accumulation of aggregated forms of the protein α-synuclein (α-syn) in neurons in the SNpc and in other parts of the brain. Such accumulation leads to microglial activation, production of inflammatory cytokines and chemokines, T-cell infiltration, and neurodegeneration.[2]

Metabotropic glutamate receptors (mGluRs) are G-protein coupled receptors found on microglia that contain a binding site for glutamate. Upon the binding of glutamate to mGluRs, biochemical signaling cascades are activated that lead to changes in synaptic excitability and modulation of neuronal postsynaptic responses of neurons.[2]

mGluR4 has been found to be localized on presynaptic terminals in the SNpc[3] and has been shown to play a functional neuroprotective role in neurodegenerative disorders, but the exact relationship between mGluR4 localization and this role is unknown.[4] mGluR4 agonists, such as L-AP4, may therefore exert neuroprotective effects by increasing mGluR4 expression. Previously, selective activation of mGluR4 in rat models of PD was found to be functionally neuroprotective and also preserve motor function, suggesting that mGluR4 can be selectively targeted for PD therapies.[5, 6]

Inflammation in the brain is believed to play an important role in the neuronal cell death pathway in PD. Inflammation in the CNS is initiated by microglia, the resident immune cells of the central nervous system, which are responsible for responding to neuronal damage and removing damaged cells.[2] Inflammation and mGluR4 are both involved in PD progression, but the relationship between the two remains unknown. Although it has been shown that activation of mGluR4 is protective in PD,[4] possible anti-inflammatory properties have not yet been elucidated.

Allosteric binding sites, a target in drug therapies, are topographically different from endogenous binding sites, allowing for co-occupation of a single receptor by the ligand and an allosteric modulator. Positive allosteric modulators (PAMs) enhance the affinity of an agonist to bind to a binding site and have been shown to be protective in PD models.

Lipopolysaccharide (LPS) is a large molecule made up of a lipid and polysaccharide found in the outer membrane of Gram-negative, pathogenic bacteria. Upon binding to Toll-like receptor 4 (TLR4) expressed on immune cells such as microglia, LPS induces a strong pro-inflammatory cytokine response. Tumor necrosis factor (TNF, also referred to as TNFα) is a cytokine produced by LPS-activated immune cells and promotes an inflammatory response by activating surrounding cells (Figure 2).[7] In this study, we aimed to determine whether treatment of primary microglia cells with the synthetic mGluR4 PAMs ADX and VU813 attenuated lipopolysaccharide (LPS)-induced inflammation.

Materials and Methods

Microglia extraction

Primary microglia were isolated from wild type (WT) postnatal day 0 to 2 mouse pups as described by previously published protocols.[2] The brains were isolated, the meninges were removed, and the cells were allowed to dissociate. Mixed glial populations were plated and grown for 11 days or until they reached confluency. Upon confluency, microglia were isolated from the astrocyte bed by a mechanical shaking method previously described.[2] Prior to treatment, microglia were plated and allowed to adhere for 1 hour in serum-free and glutamate-free Sigma DMEM nutrient mixture.

Microglia treatment

After adhesion to the chamber slides, microglia were pre-treated with 1 nM, 10 nM, and 100 nM ADX and 1 nM, 100 nM, and 1000 nM VU813. As a positive control, microglial cells were also pre-treated with an mGluR4 agonist, L-AP4. Fifteen minutes after the addition of ADX, VU813, or L-AP4, 100 ng·mL^{-1} LPS was added to the cultures for 24 hours. At the end of the 24 hour treatment period, media was collected and analyzed by enzyme-linked immunosorbent assay (ELISA). The collected media was run according to the guidelines of the R&D Systems mouse TNF-a DuoSet ELISA assay.

Results

In this study, a TNF ELISA was used to measure the amount of LPS-induced TNF released by the microglia. We found that pre-treatment with ADX and VU813 attenuated the LPS-induced TNF release by microglial cells (Figure 1A, 1B), indicating that mGluR4 PAMs and the mGluR4 agonist L-AP4 have anti-inflammatory properties.

In order to ensure the anti-inflammatory effect of ADX and VU813 was mediated by the PAMs themselves and not the DMSO vehicle, we prepared primary microglial cells as explained above and treated with 0.1% DMSO for 15 minutes prior to stimulation with LPS for 24 hours. We found that the concentrations of TNF in the serum-free media and DMSO vehicle samples were relatively similar. This effect was also observed with LPS treatment (Figure 1c).
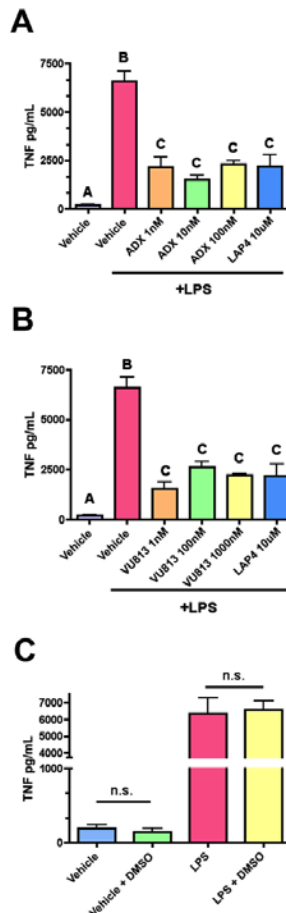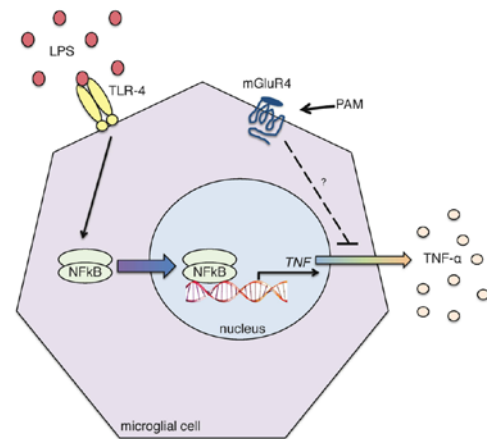

Figure 1. Administration of mGluR4 PAMs protects against LPS-induced TNF release from microglial cells. (A) Administration of ADX at the concentrations of 1 nM, 10 nM, and 100 nM 15 minutes prior to 100 ng·mL^{-1} LPS treatment attenuates TNF release as measured by ELISA. (B) Administration of VU813 at concentrations of 1 nM, 100 nM, and 1000 nM 15 minutes prior to 100 ng·mL^{-1} LPS stimulation attenuates TNF release as measured by ELISA. (C) Treatment of primary microglia with 0.1% DMSO did not induce significant TNF release over vehicle and LPS controls. Data was analyzed by one-way ANOVA with Tukey's multiple comparison post-hoc test. A-B p<0.001, B-C p<0.001, A-C p<0.05, n.s. not significant.

Figure 2. Schematic showing that LPS binds to TLR-4 on microglial cells, initiating a signaling cascade that results in TNF gene transcription and subsequent release from the cell. mGluR4 PAMs bind to mGluR4 receptors expressed on the surface of microglial cells, where downstream events result in the inhibition of TNF release from the cell.

Discussion

The decreased levels of TNF expression in the samples treated with ADX and VU813 support our initial hypothesis that ADX and VU813 attenuate LPS-induced inflammation in microglia.

As shown in Figure 1, the level of attenuation achieved by ADX at concentrations of 1 nM, 10 nM, and 100 nM and VU813 at concentrations of 1 nM, 100 nM, and 1000 nM were relatively similar, suggesting that the drug doses administered exceeded the dose response, but were still highly effective in blocking LPS-induced inflammation in microglial cells.

According to Figure 2, the PAMs used in this experiment bind to mGluR4 and block TNF release, which was initially activated by LPS. Although the pathway that blocks TNF release when

mGluR4 is activated remains unknown, future study of this pathway may reveal a role for PAMs in the modulation of PD symptoms beyond inflammation.

Lowering the administered concentrations of the PAMs could result in varied protectiveness against inflammation, including inflammation from stimuli other than LPS, such as α-syn. Further studies involving decreased PAM concentrations must be conducted to determine a dose response curve for PAM administration *in vitro*. To determine the viability of PAM administration as a treatment for PD, *in vivo* future studies will use neurotoxin and α-syn based animal models of PD. Studies using animal models will allow for the observation of the effect of PAMs on inflammatory responses *in vivo*, while also allowing for behavioral tests of motor function. Motor function loss is progressive in PD and may correlate with the level of inflammation found in PD brains. If a correlative relationship between inflammation and decreased motor function is found, the role of the PAMs may be extended to a possible treatment option for degenerative motor function in PD. Possible *in vivo* complications may include using higher than necessary concentrations of the PAMs in order to establish a drug dose response curve.

Conclusion

This study tested whether mGluR4 PAMs are protective against LPS-induced inflammation in microglia, which was quantitatively measured by TNF release. Compared to the LPS-induced TNF release in the positive control sample, the ADX and VU813 compounds showed a significant decrease in TNF expression, suggesting that administration of the PAMs attenuated LPS-induced inflammatory response. As mGluR4 activation has previously been shown to be protective in PD animal models through behavioral and motor tests,[6] future animal studies will show whether they can be targeted to protect against inflammation in PD. Various findings obtained by animal models of PD have suggested that neuroinflammation manifested by glial reactions is an important contributor to the pathogenesis of PD.[8] These results, coupled with future findings, will hopefully lead to the development of alternative therapeutic strategies for PD specifically targeting mGluR4.

References

1. Lang, A.E., Lozano, A.M. (1998). Parkinson's disease. Second of two parts. *The New England Journal of Medicine* **339**(16), 1130-1143.

2. Harms, A.S., Cao, S., Rowse, A.L., Thome, A.D., Li, X., Mangieri, L.R., *et al.* (2013). MHCII is required for alpha-synuclein-induced activation of microglia, CD4 T cell proliferation, and dopaminergic neurodegeneration. *The Journal of Neuroscience: The Official Journal of the Society for Neuroscience* **33**(23), 9592-9600.

3. Bradley, S.R., Standaert, D.G., Rhodes, K.J., Rees, H.D., Testa, C.M., Levey, A.I., *et al.* (1999). Immunohistochemical localization of subtype 4a metabotropic glutamate receptors in the rat and mouse basal ganglia. *The Journal of Comparative Neurology* **407**(1), 33-46.

4. Marino, M.J., Hess, J.F., Liverton, N. (2005). Targeting the metabotropic glutamate receptor mGluR4 for the treatment of diseases of the central nervous system. *Current Topics in Medicinal Chemistry* **5**(9), 885-895.

5. Zhou, F., Hongmin, B., Xiang, Z., Enyu, L. (2003). Changes of mGluR4 and the effects of its specific agonist L-AP4 in a rodent model of diffuse brain injury. *Journal of Clinical Neuroscience : Official Journal of the Neurosurgical Society of Australasia* **10**(6), 684-688.

6. Betts, M.J., O'Neill, M.J., Duty, S. (2012). Allosteric modulation of the group III mGlu(4) receptor provides functional neuroprotection in the 6-hydroxydopamine rat model of Parkinson's disease. *British journal of pharmacology* **166**(8), 2317-2330.

7. Raetz, C.R., Whitfield, C. (2002). Lipopolysaccharide endotoxins. *Annual Review of Biochemistry* **71**, 635-700.

8. Tufekci, K.U., Meuwissen, R., Genc, S., Genc, K. (2012). Inflammation in Parkinson's disease. *Advances in Protein Chemistry and Structural Biology* **88**, 69-132.

short report

Most prevalent drugs in death cases: a six-year study

Phillip Ritchey[1], Justin E. Sanders[2], Curt E. Harper[2]

[1] Department of Chemistry, University of Alabama at Birmingham
[2] Toxicology Discipline, Alabama Department of Forensic Sciences

Abstract

The purpose of this study was to determine the most prevalent drugs in postmortem cases encountered by the Alabama Department of Forensic Sciences Toxicology Section. These data span the years 2007 to 2012. Each year was separated into two categories: homicide and non-homicide postmortem cases. Homicide is defined as the killing of one person by another person. The total number of postmortem cases per category and the number of instances of each drug in each category were determined. These drugs included illicit drugs, drugs of abuse, prescription medication, over-the-counter medication, and alcohol. Metabolites, chemical compounds created in biological systems for the purpose of elimination, are commonly analyzed in forensic toxicology and were included in this study. A list of the most prevalent drugs per category per year was compiled and the percentage of each drug per category per year was calculated. Ethanol (drinking alcohol) was the most prevalent drug found in postmortem cases (28% of cases). Ethanol, cocaine, methamphetamine, marijuana, and hydrocodone were the five most prevalent drugs (excluding metabolites) over the entire span of this study. The analysis of these data can be utilized to educate the public on emerging trends of drug abuse.

Keywords: *toxicology, postmortem, ethanol, forensic science, homicide*

Introduction

Formed in 1935, the Alabama Department of Forensic Sciences, the nation's third oldest crime lab, analyzes thousands of cases per year.[1] The Toxicology Section specifically looks for the presence of drugs or alcohol in the body, testing biological specimens such as blood, urine, and vitreous fluid. These biological samples come from law enforcement personnel, coroners, and medical examiners and represent tissue from both living and deceased subjects.[2] Methods such as enzyme-linked immunosorbent assay (ELISA), gas chromatography/mass spectrometry (GC/MS), liquid chromatography-tandem mass spectrometry (LC/MS/MS), and headspace gas chromatography (HSGC) are used by the Toxicology Section in their analyses. These techniques help to determine which, if any, drugs are in the system at the time the biological sample was obtained and how much of each drug is present.

This study focused on postmortem cases analyzed by the Toxicology Section spanning the years 2007 – 2012. The purpose of this study was to determine which drugs were most prevalent in postmortem cases over this time span. It was not in the scope of this study to determine the lethality of the drugs, but simply their prevalence. The analysis of these data can be used to educate the public on emerging trends in drug abuse by revealing which drugs were most common in death cases in recent years.

Methods

Raw data from the postmortem cases of the Alabama Department of Forensic Sciences Toxicology Section was transferred from the Laboratory Information Management System (LIMS) to a Microsoft Excel spreadsheet. For each year, the data were separated into homicide and non-homicide postmortem cases. Each category was limited to blood analysis only. No evaluation was made of urine and tissue cases since they constitute a small percentage of the cases analyzed. The total number of cases per category per year was determined, and the total number of instances of each drug was determined for each category each year. Any drug with fewer than ten instances in its category was excluded. Once the number of instances of each drug was determined for a given category, the percentage of each drug relative to its category was calculated, and a list of the twenty-five most prevalent drugs was created. In the homicide category, fewer than twenty-five drugs met the ten-or-higher instance requirement in any year.
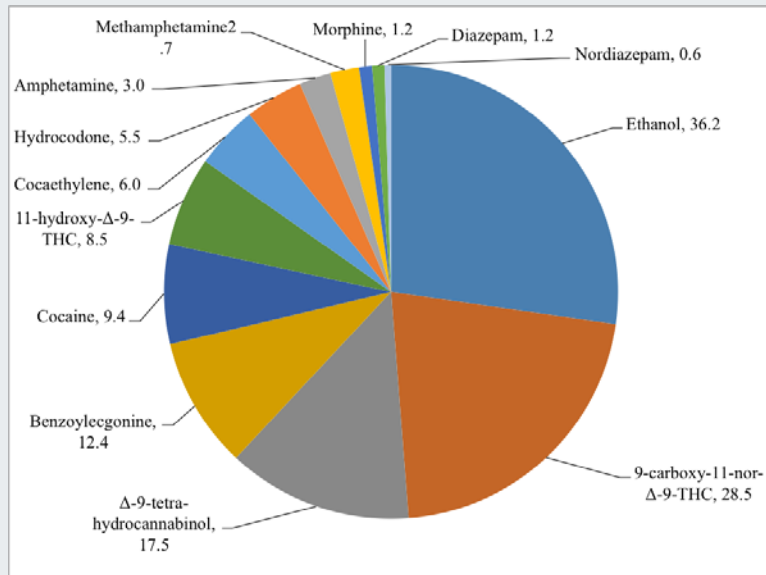
Figure 1. Most prevalent drugs in homicide cases, 2007 – 2012, n=1797 (reported in %).
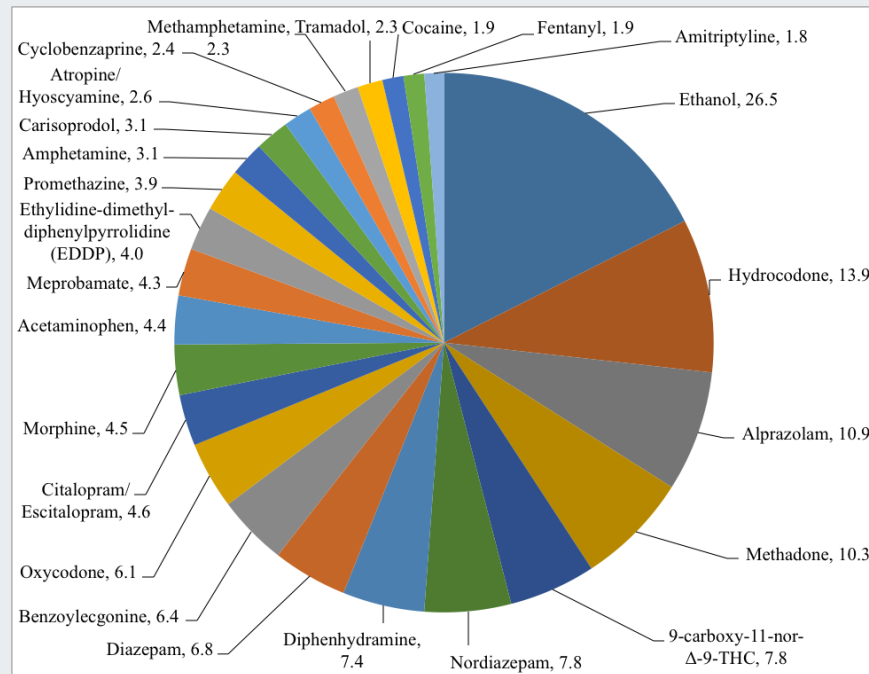

Figure 2. Most prevalent drugs in non-homicide cases, 2007 – 2012, n=11 487 (reported in %).

Results and Discussion

Figures 1 and 2 depict the top drugs in the homicide and non-homicide categories. Ethanol was the most prevalent drug found in homicide (36%) and non-homicide (26%) cases. It was present in 28% of all cases over this span (data not shown). Its prevalence in death cases is consistent with its acceptance and prevalence in society. Marijuana (THC and metabolites)

was the second most prevalent drug in homicide cases. Cocaine (and/or its metabolites) and methamphetamine were among the top five drugs in homicide cases. The percentage of cases which reported these drugs for each year can be seen in Table 1.

Table 1. Most prevalent drugs (%) in the homicide category each year.

	2007	2008	2009	2010	2011	2012
Ethanol	35.4	35.0	37.8	33.5	33.0	41.3
Marijuana	27.4	26.3	30.2	31.2	26.1	29.8
Cocaine	8.5	15.1	13.8	11.5	12.9	11.8
Methamphetamine	5.2	4.3	N/A*	4.1	N/A*	3.2

Methamphetamine did not meet the 10-case threshold in 2009 and 2011; therefore, the percentage was not calculated.

Table 2. Most prevalent drugs (%) in the non-homicide category each year.

	2007	2008	2009	2010	2011	2012
Ethanol	31.4	26.2	26.3	26.9	24.7	26.4
Hydrocodone	13.3	12.8	13.5	14.2	15.5	14.5
Methadone	12.3	11.2	10.5	9.1	9.0	10.2
Alprazolam	13.1	7.9	8.7	13.1	12.4	12.4

In the non-homicide category, hydrocodone (the prescription painkiller Lortab®) was the second most prevalent drug. Methadone (used for pain management, acute pain, and opioid addiction recovery) and alprazolam (the prescription anti-anxiety medication Xanax®) were in the top five drugs in non-homicide deaths overall. Table 2 provides the percentage of cases which reported these drugs for each year.

Marijuana use as indicated by the presence of 9-carboxy-11-nor-Δ9-THC was 114% more prevalent in homicide cases than in non-homicide cases. Marijuana is an illicit drug that carries heavy prison sentencing; therefore, individuals who use marijuana are more likely to be in high risk, volatile environments and are more prone to violent behavior, thus providing one possible explanation for the vast difference between the homicide and non-homicide categories.[3] Cocaine (and/or its metabolites) was 64% more prevalent in homicide cases than in non-homicide cases. Methamphetamine was 16% more prevalent in homicide cases. These drugs are also both illicit drugs, and individuals who use these drugs are more likely to be in situations similar to those involved in obtaining marijuana. Thus, the prevalence of cocaine and methamphetamine in the homicide category are consistent with the risks involved in obtaining the drugs.

Hydrocodone was 87% more prevalent in non-homicide cases. This prevalence is consistent with the fact that hydrocodone is the most prescribed medicine in the United States.[4] Methadone and alprazolam were only present in the non-homicide cases in this study. Alprazolam was among the 25 most-prescribed medications in the United States during this span, and its use increased by 56% from 2008 – 2012 in non-homicide death cases.[4]

Conclusion
Ethanol was the most prevalent drug overall in this study. Marijuana, cocaine, and methamphetamine were among the five most prevalent drugs in the homicide category. Hydrocodone, methadone, and alprazolam were among the five most prevalent drugs in the non-homicide category. The data collected in this study will help the public (citizens, law enforcement agencies, substance abuse specialists, physicians, and healthcare professionals) by providing additional data on drug abuse and drug prevalence.

References
1. Alabama Department of Forensic Sciences. History of the Alabama Department of Forensic Sciences. http://www.adfs.alabama.gov/About.aspx.

2. Alabama Department of Forensic Sciences. Forensic Toxicology. http://www.adfs.alabama.gov/Toxicology/ToxicologyMain.aspx.

3. Yacoubian, G. S. (2007). Assessing the relationship between marijuana availability and marijuana use: A legal and sociological comparison between the United States and the Netherlands. *Journal of Alcohol and Drug Education* **51**(4), 17-34.

4. Manchikanti, L., Helm II, S., Fellows, B., Janata, J. W., Pampati, V., Grider, J. S., Boswell, M. V. (2012). Opioid epidemic in the United States. *Pain Physician* **15**, ES9-ES38.

short report

A novel evaluation of daytime vigilance in patients with Parkinson's disease using a virtual reality street-crossing task

Kristin Ford[1], David C. Schwebel[2], Anna Johnston[2], Gary Cutter[3], David G. Standaert[1], and Amy Amara[1]

[1] Department of Neurology, [2] Department of Psychology, [3] Department of Biostatistics
University of Alabama at Birmingham

Abstract

Introduction: Patients with Parkinson's disease (PD) commonly experience sleep dysfunction, including daytime sleepiness. Excessive daytime sleepiness affects vigilance and attention, which can impact safety in tasks such as driving or crossing a street. No reliable measures of vigilance in this population currently exist. **Methods**: 25 subjects with Parkinson's disease completed subjective evaluation of daytime sleepiness (Epworth Sleepiness Scale) and a virtual reality street-crossing task. Subjects also completed the Useful Field of View (UFOV) test as a measure of visual processing. The primary vigilance outcome measure was the number of looks left and right per minute with higher values indicating better vigilance. We hypothesized a negative correlation between looks per minute (visual attention) and subjective sleepiness. **Results**: Preliminary analysis of this small sample shows a non-significant trend toward a negative correlation (r = −0.06) between visual attention and sleepiness. Adjusted for UFOV scores, subjective sleepiness still cannot predict visual attention. However, the Epworth is strongly positively correlated with near misses (r = 0.46, p = 0.02). Additionally, the UFOV is a strong predictor of visual attention and there is a significant negative correlation between visual attention and UFOV (r = −0.56, p = 0.005). **Conclusions**: Preliminary data indicate no significant correlation between subjective daytime sleepiness and vigilance. Interestingly, daytime sleepiness did correlate with close calls to pedestrian crashes, and visual processing (UFOV) negatively correlated with visual attention (looks/minute), indicating that subjects with PD may not correct for visual processing deficits. Failure to reject the null hypothesis may indicate that subjects with Parkinson's disease underestimate their daytime sleepiness.

Keywords: *Parkinson's disease, excessive daytime sleepiness, Useful Field of View, Virtual Reality street-crossing simulator, vigilance*

Introduction

Parkinson's disease (PD) is a progressive neurodegenerative disorder with motor symptoms including tremor, stiffness, slowness, and lack of balance as well as non-motor symptoms such as sleep dysfunction and excessive daytime sleepiness.[1-2] Though motor symptoms are disabling, non-motor symptoms also negatively affect quality of life in individuals with this disorder.[3-4] Fifty to seventy-five percent of all PD patients report excessive daytime sleepiness.[5] Daytime sleepiness affects alertness and attention, which can hinder the successful and safe completion of everyday tasks such as driving or crossing a street.[4] An objective measure of daytime vigilance is needed in order to better understand the extent to which daytime sleepiness affects attention and safety in real life situations.

Several methods can be used to evaluate daytime sleepiness and vigilance. Questionnaires (such as the Epworth Sleepiness Scale[6]) ask patients about their level of alertness over the past month. The psychomotor vigilance task[7] is used to measure the impact of sleep loss on vigilance. These methods are useful, but they do not evaluate how sleepiness and vigilance affect safety during daily activities.

This observational study will investigate the relationship between performance on a virtual reality (VR) street-crossing simulator[8-9] and validated measures of daytime sleepiness and vigilance in subjects with Parkinson's disease. Our hypothesis is that the virtual reality street-crossing simulator task will be feasible in this patient population and that performance on the task will correlate with validated measures of daytime sleepiness and vigilance.

This research is novel in that this virtual reality simulation has never been used with PD patients, although it has been validated in other populations.[8-9] If it is found that the VR simulation is indeed a feasible objective measure that can be used to evaluate vigilance and daytime sleepiness in realistic situations, it can potentially be used as an outcome measure in other studies that involve sleep or medications in PD.

Methods

For this pilot study, 25 patients with Parkinson's disease were recruited from the population of individuals followed in the Movement Disorders Clinics at the University of Alabama at Birmingham. Inclusion criteria for the study included clinical diagnosis of Parkinson's disease, asymmetric onset of PD, and the ability to walk without assistance. Exclusion criteria included atypical features indicative of a Parkinson's Plus

disorder, neuroleptic treatment, history of multiple strokes or head injuries, and blindness.

All VR studies were performed at 10 a.m. (±30 minutes) to control for variation in circadian factors during the day. Upon arrival to the Youth Safety Lab, each participant completed the Epworth Sleepiness Scale (ESS), a subjective questionnaire used to evaluate daytime sleepiness in different situations over the previous month.

Next, each patient participated in the virtual reality street-crossing task, a measure of vigilance and attention. The VR environment consists of an elevated platform that represents a street-side curb with three screens on which the subject views the virtual environment of a two-lane street with bidirectional traffic (Figure 1). The subject observes the traffic and, when he or she feels it is safe to cross the street, steps off the platform. This triggers a cartoon representation of the subject to cross the street. The average number of looks left and right per minute is monitored, as this denotes visual attention to traffic, with higher numbers of looks suggesting greater attention to traffic. An important secondary outcome is the number of times that the participant is "hit" or nearly hit ("close calls") by a car, as these are an important safety measure. Performance on the UFOV is included as a covariate.

Figure 1. Screenshot of the virtual reality street-crossing task.

Prior to starting the VR task, the walking speed of the participant is measured to calculate a pedspeed for the virtual reality task. The pedspeed determines the speed at which the cartoon representation of the participant crosses the virtual street. A member of the study team demonstrates both a safe crossing and an unsuccessful crossing ("hit") on the VR task prior to the subject's first orientation trial to eliminate curiosity. Before participating in orientation or data trials, the participant is fitted with a headband holding a head-tracking device to measure looks left and right. The participant then completes a total of twelve orientation trials, each consisting of one street crossing.

Between the orientation and data collection trials of the VR task, the Useful Field of View Test (UFOV) is administered. The UFOV is a measure of visual processing speed during which the participant identifies objects that are displayed in the central and peripheral visual field on a touch-screen computer. This test, which consists of three subtests of increasing difficulty, allows assessment of deficiencies in

visual processing speed that could influence performance on the virtual reality street-crossing task.

After the completion of the UFOV, the participant completes twelve data collection trials in the virtual reality environment. These trials are administered in the same manner as the twelve orientation trials. Both orientation and data collection trials are recorded via a video camera for hand-scoring as an additional measure of looks left and right.

Results

Based on this pilot study, individuals with Parkinson's disease were able to perform the virtual reality task in the virtual reality environment with minimal difficulty, showing that use of this task in the PD population is feasible. Table 1 gives the demographics of the first 25 PD participants. The summary statistics of outcome measures are featured in Table 2, and the distributions of outcome measures can be seen in Figure 2.

Table 1. Subject demographics

	Mean ± S.D.	Minimum	Maximum
Age (years)	64.4 ± 8.7	43	83
Gender (% male)	68	___	___
Duration of disease (years)	8.5 ± 5.5	1	20

Table 2. Summary statistics of outcome measures

	Mean	SD	95% CI
Looks·min^{-1}	33.07	11.38	28.38, 37.77
ESS	9.76	4.75	7.80, 11.72

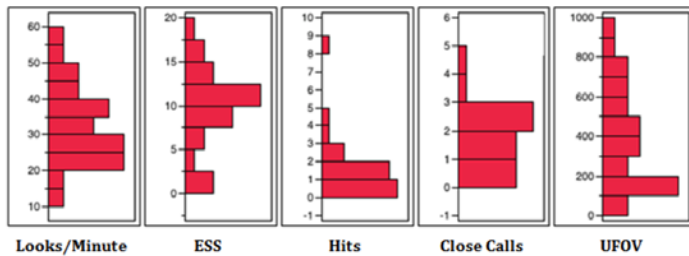|	Median	Minimum	Maximum
Hits	1	0	8
Close calls	1	0	4
UFOV	387	70	904

Figure 2. Distributions of outcome measures.

Correlations between outcome measures were calculated using Pearson Correlation coefficients (Table 3). Analysis of the primary outcome measure shows a non-significant trend toward a negative correlation between visual attention (looks left and right per minute) and subjective sleepiness, as measured by the Epworth Sleepiness Scale. Following adjustment for UFOV scores, it was found that subjective sleepiness still cannot predict visual attention to traffic.

Evaluation of secondary outcome measures (Table 3) shows that the Epworth Sleepiness Scale is strongly positively correlated with close calls to pedestrian crashes. Additionally, the Useful Field of View test is a strong predictor of both visual attention (looks per minute) and close calls.

Table 3. Pearson correlations for outcomes

	Epworth	Hits	Close calls	UFOV
Looks·minute^{-1}	-0.06	-0.392	-0.069	-0.557
	p = 0.78	*p = 0.53*	*p = 0.75*	***p = 0.005***
ESS		0.101	0.46	0.277
		p = 0.632	***p = 0.021***	*p = 0.190*
Hits			0.215	0.333
			p = 0.303	*p = 0.112*
Close calls				0.454
				p = 0.026

Discussion

This preliminary data indicates no significant correlation between subjective daytime sleepiness and vigilance, suggesting either that patients with PD may underestimate their degree of daytime sleepiness or that the VR task is unable to adequately measure visual attention in this population. However, daytime sleepiness, as measured by the Epworth Sleepiness Scale, is positively correlated with close calls to pedestrian crashes, indicating that excessive daytime sleepiness may be a cause for concern for this population in regard to safety. Visual processing (measured by the UFOV) is negatively correlated with visual attention (looks per minute) which suggests that subjects with PD may

not correct for visual processing deficits. This may also be a safety concern, as close calls are positively correlated with visual deficits. Continued study to evaluate a larger sample size is ongoing.

Acknowledgements

References

1. Lees, A. J., Blackburn, N. A., Campbell, V. L. (1988). The nighttime problems of Parkinson's disease. *Clin Neuropharmacol* **11**(6), 512-9.

2. Rye, D. B. *et al.* (2000). FAST TRACK: daytime sleepiness in Parkinson's disease. *J Sleep Res* **9**(1), 63-9.

3. Amara, A. W. *et al.* (2012). Unilateral subthalamic nucleus deep brain stimulation improves sleep quality in Parkinson's disease. *Parkinsonism & Related Disorders* **18**(1), 63-68.

4. Fabbrini, G. *et al.* (2003). Excessive daytime somnolence in Parkinson's disease. Follow-up after 1 year of treatment. *Neurological Sciences* **24**(3), 178-179.

5. Valko, P. O. *et al.* (2010). Fatigue and excessive daytime sleepiness in idiopathic Parkinson's disease differently correlate with motor symptoms, depression and dopaminergic treatment. *European Journal of Neurology* **17**(12), 1428-1436.

6. Johns, M. W. (1991). A new method for measuring daytime sleepiness: the Epworth sleepiness scale. *Sleep* **14**(6), 540-5.

7. Dinges, D. F. (1985). Microcomputer analysis of performance on a portable, simple visual RT task during sustained operations. *Behavioral Research Methods, Instruments, & Computers* **17**(6), 652-5.

8. Schwebel, D. C., Gaines, J., and Severson, J. (2008). Validation of virtual reality as a tool to understand and prevent child pedestrian injury. *Accident Analysis & Prevention* **40**(4), 1394-1400.

9. Schwebel, D. C., Stavrinos, D., and Kongable, E. M. (2009). Attentional control, high intensity pleasure, and risky pedestrian behavior in college students. *Accident Analysis & Prevention* **41**(3), 658-661.

A new perspective: Treating patients from the laboratory
Daniel Gilliam

I have always known that I wanted a career through which I would never cease to learn, and my fascination with the scientific enterprise has been fueled by this desire more than anything else. Learning is my favorite activity, but I am also intrigued by the possibility of generating new knowledge and actualizing this knowledge to impact the world in a meaningful way. My experiences in college have changed my vision of a future career from that of a practicing physician to that of a physician-scientist. In an effort to create synergy between my interests in research and in improving clinical outcomes for patients, I am planning to pursue a dual M.D./Ph.D. degree and a career in translational biomedical research.

As soon as I arrived at UAB, eager to begin finding opportunities to learn, I started looking into the work being done here in my chosen field of neuroscience. I read publications from different labs in which I was interested and began to form an appreciation for the sheer breadth of knowledge that I have yet to learn as well as the amount that remains unknown to anyone. One subject in particular—the epigenetic mechanisms underlying memory—stood out as particularly interesting. I identified the lab that appealed to me most and made contact with the principal investigator— Dr. David Sweatt in the Department of Neurobiology.

I started working in the lab, hoping to learn something new, but I was ultimately most concerned with filling another slot on my medical school applications. By learning in classes, engaging in research, and taking advantage of opportunities to experience what a potential career might entail, I gradually came to the realization that I could not picture having a career completely apart from research. In a research setting, where the entire goal is to challenge the boundaries of knowledge and understanding, I could never reach a point where I felt as though I had learned enough. The possibility that some facet of human knowledge could be revealed, at least in part, by my own investigation, is simply too enticing to refuse.

My scientific interests have always had a focal point in medicine, but I only recently discovered that my interest in medicine, while ultimately founded on an interest in helping patients, is largely academic. One of the more prominent experiences that led to this realization came while shadowing physicians. I often found myself considering the clinical presentation of certain conditions from the perspective of a researcher. For example, while observing the cogwheel rigidity and bradykinesia characteristic of Parkinson's disease, I began to speculate about the biochemistry and neuropathology underlying these symptoms. The questions I later posed to the physician explored these causal factors, and I pursued discussion related to the development of potential treatments and the voids that remain in our understanding. During such discussions, and as I later perused relevant scientific literature, I became increasingly aware that future treatments for patients will ultimately derive from work being done in laboratories at this moment, and that I could play a role in the development of these treatments.

My experience so far in Dr. Sweatt's laboratory has proved tremendously helpful in shaping my career aspirations. I am currently working on a project investigating the epigenetic aberrations, molecular perturbations, and cognitive deficits evoked in the brain by diet-induced obesity as well as potential methods to mitigate these defects in a mouse model. My work requires an average of fifteen hours per week in the lab, and although the time commitment required to receive the full benefit is substantial, this challenge has been immensely rewarding. This experience has introduced me to many of the key concepts and investigative techniques involved in biomedical research; just as importantly, my time in the laboratory has exposed me to what a future in research may entail. In a world where so many questions await answers and so many patients await new treatments, it is clear that we need physician-scientists. I intend to take advantage of the opportunity to work between these increasingly connected worlds of research and medicine.

"In a research setting, where the entire goal is to challenge the boundaries of knowledge and understanding, I could never reach a point where I felt as though I had learned enough."

short report

Intact brain volume is related to therapy responses in chronic stroke and real-world arm use in hemiparetic multiple sclerosis patients

Ameen Barghi[1], Victor W. Mark[2,3], Tyler Rickards[1], Chelsey Sterling[1], Michelle Haddad[1], Gitendra Uswatte[1,4], and Edward Taub[1]

[1] Department of Psychology, [2] Department of Physical Medicine and Rehabilitation, [3] Department of Neurology, [4] Department of Physical Therapy
University of Alabama at Birmingham

Introduction

The Brain Parenchymal Fraction (BPF) is a measure of structural brain tissue integrity from standard MRI. It is the total amount of white and grey matter divided by the total intracranial space.[1] Previous research from this laboratory has shown that stroke patients with greater BPF show greater improvement in maximal movement ability following constraint-induced movement therapy (CIMT).[2] Previous studies have also correlated BPF with various measures of physical disability in multiple sclerosis (MS), including overall disability (EDSS score) and a composite score comprised of upper and lower extremity movement ability and cognitive function, the Multiple Sclerosis Functional Composite (MSFC).[3-5]

The purpose of this study was to evaluate whether BPF is associated with spontaneous hemiparetic arm use in MS. Additionally, we analyzed how these correlations compare to the BPF values of people affected by stroke. Due to the small sample size, rehabilitation outcomes after CI therapy in relation to BPF were not analyzed in the MS cohort; the study is ongoing.

Methods

Subjects

This study was composed of eighteen adults with chronic hemiparetic MS (aged 49.9 ± 8.0 years) who were randomized to undergo either CI therapy or a holistic program of Complementary and Alternative Medicine. The patients randomly received either CIMT (n = 18) or a comparison therapy (n = 25). The comparison therapy group received all components of CIMT except for the transfer package (described below).

Stroke Intervention: Constraint-Induced Movement Therapy

CIMT consists of in-laboratory training of the impaired upper extremity for ten consecutive weekdays for three hours each day. Therapy components include massed practice and shaping of movement. Additionally, a transfer package was administered to the experimental group. The control group received the same therapy without the transfer package. The transfer package involves an additional 0.5 hours spent in the laboratory and includes: 1) daily monitoring of real-world use of the more affected arm, 2) problem-solving with a therapist to overcome perceived barriers to using the extremity in the real world, 3) home practice of motor task exercises and selected activities of daily living (ADLs; changed daily), 4) a behavioral contract between the therapist and participant (and separately with the caregiver) in which they agree that the participant will use or try to use the more affected arm as much as safely possible outside of the laboratory, and 5) a daily home diary in which the participants record how much they have used the more affected arm for the activities laid out by the behavioral contract. CIMT involves restraint of the less impaired arm for a target of 90% of waking hours in a padded mitt that prevents arm use.

Outcome Measures

The Motor Activity Log (MAL) is a reliable and valid structured interview of use of the more impaired arm in real-world situations.[6-7] The MAL consists of both the Quality of Movement scale (QOM) and the Amount of Use scale (AOU). We were specifically interested in the QOM scale. The Wolf Motor Function Test (WMFT) is a validated laboratory measure of motor ability in prompted movement.[8-9]
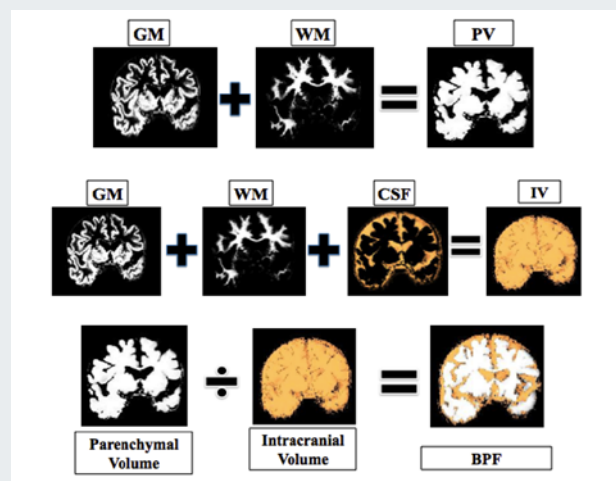

Figure 1. Structural depiction of the various components of the BPF calculation.

Imaging

T1 MRI scans were obtained from patients on a 3T Philips Intera MRI scanner immediately prior to treatment. Raw

T1 images were given a N3 inhomogeneity correction to improve differentiation/contrast between tissue and non-tissue.[10] Scans were segmented into grey matter (GM), white matter (WM), and cerebrospinal fluid (CSF) using SPM8, and viewed in FSL. Voxels in GM and WM segments (parenchymal volume, PV) divided by voxels in GM, WM, and CSF segments (intracranial volume, IV) is equal to Brain Parenchymal Fraction (BPF) (Figure 1).

Results

The CIMT and control therapy groups for stroke did not differ pre-treatment in their BPF values ($t(41)$ = 0.70, p = 0.41), with BPFs of 0.754 and 0.769, respectively. The mean BPF for MS was 0.74. MS patients with greater pre-treatment QOM showed less change on the MAL (Table 1). A similar correlation was seen in stroke patients (Figure 2).

Figure 2. Correlations were found between pre-treatment QOM and change QOM in patients who received CI movement therapy.

Table 1. Pearson Correlations of Brain Parenchymal Fraction with Pre-Treatment and Treatment Change Motor Scores

	Motor Activity Log–Quality of Movement		Wolf Motor Function Test	
	Pre	Change	Pre	Change
CIMT Stroke	0.06	0.49*	0.022	-0.45+
Control	-0.13	-0.21	0.259	0.17
MS	0.21	-0.52	0.042	-0.081

*+ approaching significance (.1 > p > .05), * significant (p < .05); Significance tests were two-tailed.*
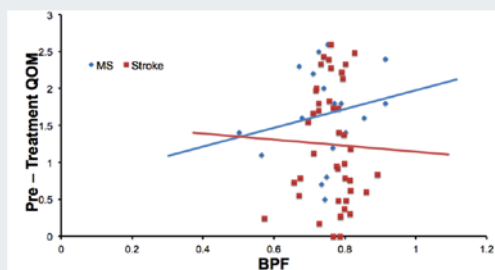

Figure 3. Pre-treatment QOM relationship with BPF.

Discussion

In this small sample study, MAL scores were not significantly correlated with BPF in persons with chronic MS. However, the results suggest that a larger volume of intact brain tissue in the chronic stroke phase (i.e. greater BPF value) predicts better quality of movement in the more-impaired arm during activities of daily living (Table 1). Additionally, it was found that patients in the chronic stroke phase with a larger volume of intact brain tissue have greater gains in maximum motor

ability after CIMT, as revealed by the WMFT. There was no difference between groups in BPF values, and BPF itself did not change as a result of CIMT.

BPF may be considered a surrogate marker for overall CNS atrophy. It appears that the characteristics of non-infarcted tissues are important predictive factors for the potential of a patient to recover motor function following rehabilitation. It should be emphasized that previous studies on the relationship between BPF and functional status showed stronger correlations, but from much larger patient samples.

References

1. Rudick, R. A., Fisher, E., Lee, J. C., Simon, J., Jacobs, L. (1999). Use of the brain parenchymal fraction to measure whole brain atrophy in relapsing-remitting MS. *Neurology* **53** 1698- 1704.

2. Rickards, T., Taub, E., Sterling, C., Graham, M. J., Barghi, A., Uswatte, G., Mark, V. W. (2012). Brain parenchymal fraction predicts motor improvement following intensive task-oriented motor rehabilitation for chronic stroke. *Restorative Neurology and Neuroscience* **30**, 355–361.

3. Bakshi, R. *et al.* (2008). Predicting clinical progression in multiple sclerosis with the magnetic resonance disease severity scale. *Archives of Neurology* **65**, 1449-53.

4. Sanfilipo, M., Benedict, R. H., Sharma, J., Guttman, B., Bakshi, R. (2005) The relationship between whole brain volume and disability in multiple sclerosis: a comparison of normalized gray vs. white matter with misclassification correction. *Neuroimage* **26**, 1068-77.

5. Kalkers, N. F. *et al.* (2001). Optimizing the association between disability and biological markers in MS. *Neurology* **57**, 1253-8.

6. Taub, E., Miller, N. E., Novack, T. A., Cook III, E. W., Fleming, W. C., Nepomuceno, C. S., *et al.* (1993). Technique to improve chronic motor deficit after stroke. *Archive Physical Medicine and Rehabilitation* **74**, 347-354.

7. Uswatte, G., Taub, E., Morris, D., Vignolo, M., McCulloch, K. (2005). Reliability and validity of the upper-extremity Motor Activity Log-14 for measuring real-world arm use. *Stroke* **26**, 2493-6.

8. Taub, E., Uswatte, G., Mark, V. W., Morris, W. M. (2006). The learned nonuse phenomenon: Implications for rehabilitation. *Europa Medicophysica* **42**, 241-255.

9. Wolf, S. L. *et al.* (2001). Assessing Wolf motor function test as outcome measure for research in patients after stroke. *Stroke* **32**, 1635-9.

10. Keihaninejad, S., Heckermann, R. A., Fagiolo, G., Symms, M. R., Hajnal, J. V., Hammers, A. (2010). A robust method to esti- mate the intracranial volume across MRI field strengths (1.5 T and 3 T). *Neuroimage* **50**, 1427-1437.

short report

Testing of United States currency for cocaine and methamphetamine

Jessi Mann[1] and Elizabeth Gardner[2]

[1] Department of Chemistry, [2] Department of Justice Sciences
University of Alabama at Birmingham

Abstract

A recent experiment at UAB showed an unusually high percentage of methamphetamine contamination on bills obtained from a home improvement store near Birmingham, Alabama. Cocaine contamination of bank notes is well documented worldwide; however, detecting other drugs of abuse is far less common. Even when found, other drugs tend to be present at much lower concentrations than cocaine. According to the National Substance Abuse Index (NSAI), methamphetamine abuse is a greater problem than cocaine abuse in Alabama,[1] and the Drug Enforcement Administration (DEA) reports that the number of clandestine methamphetamine labs and dump sites varies greatly from state to state.[2] This has raised questions about methamphetamine contamination of currency in other states. The objective of this project was to test for the presence of methamphetamine on currency in order to determine the percentage of $1 bills that test positive for cocaine and methamphetamine in different states.

Keywords: *controlled substances, acid-base extraction, gas chromatography-mass spectrometry, cocaine, methamphetamine*

Introduction

Many studies have focused on detecting trace amounts of illicit drugs on bank notes, including a variety of bills of different denominations and countries of origin. Many theories exist to explain the mechanism of drug contamination of bank notes. Carter's theory states that, over time, usage creates cavities in the linen-cotton fibers in US bills. These cavities provide a site where drugs like cocaine and methamphetamine can collect.[3] Sleeman suggests that oils from human hands can trap the compounds on the surfaces of the bills. He also proposes that drugs bind to fibers that make up the bills.[4]

The World Drug Report states that there were 6.2 million cocaine users in America in 2008. They also report that North America is among the most prominent regions in the manufacture of amphetamines. In 2008 alone, the number of clandestine laboratories rose by twenty percent.[5] The DEA reports that the Southeast had the highest number of confiscated labs in 2011.[2] The NSAI even goes as far as to say that methamphetamine abuse is surpassing that of cocaine in the state of Alabama.[1]

Previous experiments testing for controlled substances generally tested a small number of bills and found only cocaine. In 1998, Negrusz found that 3 out of 4 $1 bills were contaminated with cocaine.[6] Jenkins found 92% cocaine contamination on sets of ten bills from five cities across the country. Three of the bank notes, 6%, were also positive for methamphetamine.[7] Prior to Jenkins's study, methamphetamine was not detected or tested for on currency.

In the spring of 2012, methamphetamine was detected on $1 bills for the first time in four years of analyzing paper money for drugs of abuse at UAB. The objective of this study was to extend the testing to a larger geographic area in order to confirm that the methamphetamine contamination was not an anomaly. In all, bills from 14 different states were analyzed for cocaine and methamphetamine.

Materials and Methods

An acid-base method was used to extract any basic drugs from the currency. The bills were crumpled and placed into 20-mL vials; 10 mL of 0.1 M HCl was added to each. The vials were shaken for a minimum of 30 minutes on an orbital platform shaker set at 150 cycles minute^{-1}. The solution was transferred to a second 20-mL vial and 2 M NaOH was added dropwise until the pH reached 12. One mL of chloroform ($CHCl_3$) was added to each vial. The organic layer was extracted via glass pipette. The sample was then placed into a gas chromatography-mass spectrometry (GC-MS) vial to be analyzed by an Agilent 6890 gas chromatograph equipped with a DB-5 MS column interfaced with an Agilent 5973 MSD.

Chloroform was run as a blank between each sample as the negative control. The bills were compared to cocaine and methamphetamine controls purchased from Sigma Aldrich. The retention time (rt) for the cocaine standard was 11.214 ± 0.050 min. The fragment ions needed for confirmation of cocaine were *m/z* 82, 182, and 303. The retention time for the methamphetamine standard was 4.676 ± 0.060 min with the fragment ions *m/z* 58, 91, and 134 for confirmation. Example chromatograms and spectra of cocaine and methamphetamine confirming the presence of the drugs are provided in Figures 1–3.
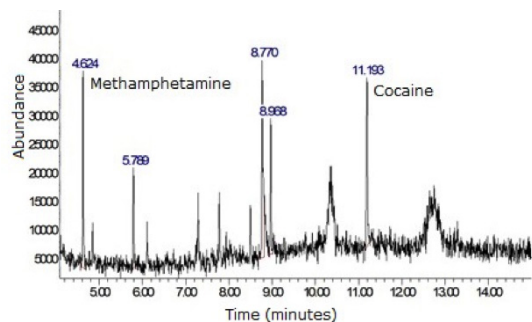
Figure 1. GC Chromatogram of an extraction from a bill. This sample was positive for both methamphetamine (rt 4.624 min) and cocaine (rt 11.193 min).
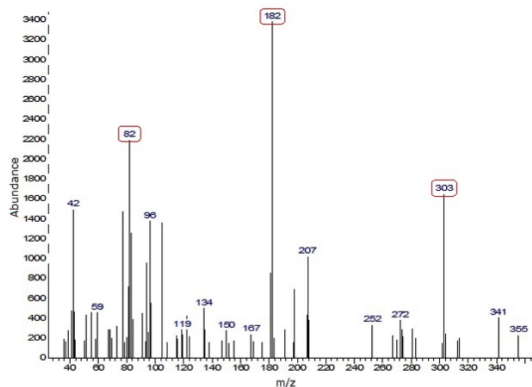

Figure 2. MS spectrum of cocaine. The fragments at m/z 82, 182, and 303 present at retention time 11.193 min confirm that this sample contains cocaine.
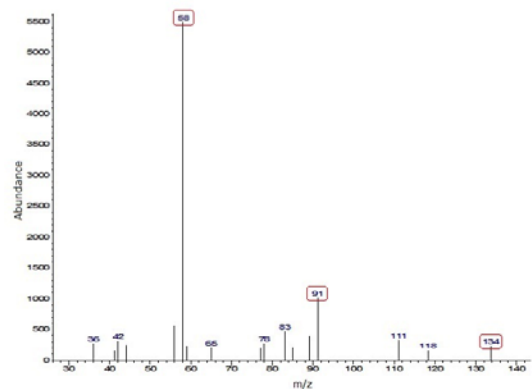

Figure 3. MS spectrum of methamphetamine. The fragments m/z 58, 91, and 134 present at retention time 4.624 min confirm that the sample is positive for methamphetamine.

Results and Discussion

In this study, 190 $1 bills from 14 states were tested for cocaine and methamphetamine. The bills were tested in sets of ten from each state except for Alabama (40 bills) and Georgia (30 bills). The sets of bills were collected from local stores, placed into a plastic bag inside an envelope, and mailed to the laboratory. Previous research has shown that uncirculated bills are not contaminated by drugs of abuse.[8] Overall, 67.9% of the bills were positive for either cocaine or methamphetamine. Traces of cocaine were found on 62.6% of the bills, while methamphetamine traces were found on

28.9% of all bills; 23.7% were positive for both substances. The results for each state are shown in Figure 4.
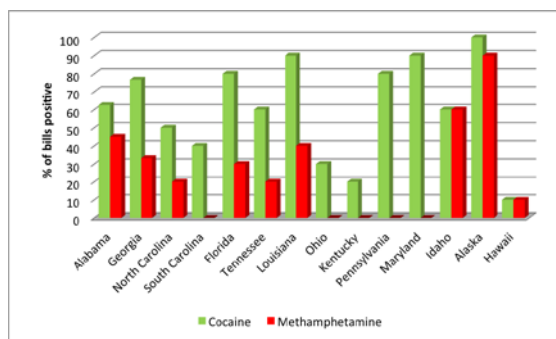

Figure 4. Percentages of contaminated bills per state. This data represents the 190 samples from the 14 states included in the study. Six of the seven southeastern states were positive for methamphetamine. Bills from all 14 states tested positive for cocaine.

All of the states represented had bills that tested positive for cocaine, ranging from 10% to 100% of the sample. However, no bills tested positive for methamphetamine in South Carolina or any of the states further north: Maryland, Pennsylvania, Ohio, and Kentucky. The following controlled substances were also found: oxycodone (1 bill, Georgia), methadone (2 bills, Ohio), heroin (1 bill, Maryland), hydrocodone (1 bill, Tennessee) and ketamine (1 bill, Alaska), which were confirmed via comparison to known standards from Sigma Aldrich.

Conclusions

In this study, 62.6% of the bank notes tested were contaminated with cocaine, 28.9% for methamphetamine, and 23.7% were contaminated with both. Methamphetamine was detected on bills from nine of the fourteen states. This presence of methamphetamine on bills collected throughout the larger geographical area confirmed that the findings from the previous experiment were not anomalous.

Multiple explanations have arisen as to the current contamination of bills with methamphetamine. Methamphetamine abuse could be increasing according to the NSAI.[1] Further research is being conducted in order to elucidate trends in the prevalence of bills contaminated with controlled substances both on a state by state basis and according to the age of the bills.

Acknowledgements

References

1. Alabama drug climate. (2013). Retrieved October 2013 from www.nationalsubstanceabuseindex.org/alabama

2. Methamphetamine lab incidents, 2011. (2013). Retrieved October 2013 from www.justice.gov/dea/resource-center/meth-lab-maps.shtml

3. Carter, J. F., Sleeman, R., Perry, J. (2003). The distribution of controlled drugs on bank notes via counting machines. *Forensic Science International* **132**, 106-112.

4. Sleeman, R., Burton, F., Carter, J., Roberts, D., Hulmston, P. (2000). Drugs on money. *Analytical Chemistry* **72.11**, 397-403.

5. United Nations (2010). *World Drug Report 2010*. New York.

6. Negrusz, A., Perry, J., Moore, C. (1998). Detection of cocaine on various denominations of United States currency. *Journal of Forensic Sciences* **43**, 626-629.

7. Jenkins, A. (2001). Drug contamination of US paper currency. *Forensic Science International* **121**, 189-193.

8. Fultz, B., and Gardner, E. A. Methamphetamine contaminated currency. Presentation at the Alabama State Academy of Forensic Sciences Annual Meeting, Gulf Shores, AL, Aug 7-10, 2012.

faculty spotlight

An interview with Dr. John Waterbor
Naveed Farrukh

He thought he would only spend two or three years down in the South, but it has been nearly three decades since John Waterbor said goodbye to Philadelphia, his beloved Phillies baseball team, and the University of Pennsylvania Medical School. Dr. Waterbor has taken an incredibly free spirited approach to becoming a public health researcher. His journey has been anything but a well-worn path and should demonstrate to undergraduates aspiring toward careers in research that there exists a dimension wherein creativity marries work. Dr. John W. Waterbor's current positions and research are born from a desire to chase his passions and intuition.

Dr. Waterbor's roots can be traced back to his father, a math teacher who instilled in him an aptitude for working with numbers. As Waterbor pored over anatomy, pathology, and pharmacology in pursuit of his medical degree, there was little time left for mathematics, calculations, and numerical trends. That was, until he sat down on a Tuesday afternoon for a short combined course in Epidemiology and Biostatistics. Most students paid it no heed, reading newspapers in the back of the classroom or outright skipping class, while Dr. Waterbor looked around astonished at the apathy. In just four afternoons, he fell in love with the subjects and knew that medical school was not the most conducive outlet for his passions. However, with the help of his friends and an impressive show of commitment, Dr. Waterbor stayed onboard and completed his medical degree from the University of Pennsylvania, though he never obtained a license to practice because his heart was set on another course.

He next sought a doctoral program and was given the opportunity to work with Dr. Cole, at the time the chair of Epidemiology at Harvard. Dr. Cole was transferring to the University of Alabama at Birmingham, and importantly, had funds to support doctoral students. Dr. Waterbor was also accepted to Johns Hopkins and Pittsburgh but was informed that funding from those schools would be limited. Despite his initial hesitation about moving to the South, he decided that the opportunity to work for Dr. Cole with money available was too fortuitous to pass up. The two clicked immediately, thus beginning Dr. Waterbor's career in cancer epidemiology, and he has attributed the spark of his interest to Dr. Cole's enthusiastic teaching.

Under Dr. Cole's guidance, Dr. Waterbor conducted an Occupational Mortality Study that formed the basis of his dissertation. Everyone dies due to some cause, and Occupational Mortality Studies quantify and characterize these causes in a given population. In this format, most researchers study deaths resulting from dangerous occupations; but Dr. Waterbor took a novel approach and decided to study positive exposure. He selected a cohort of baseball players: well-paid individuals living comfortable lifestyles with increased physical activity. He wondered whether the physical benefits of their lifestyles in their twenties and thirties would extend their lives. With his characteristic creative insight, Dr. Waterbor found a way to channel his love for baseball into a dissertation that was actually enjoyable to write. He gathered the death certificates of various players from their respective health departments as a primary means of data collection. The results, somewhat surprisingly, showed that strenuous physical activity and a comfortable lifestyle in early adult years did not affect the longevity of life. Baseball players had, on average, similar lifespans to those of the general population. His interpretation of the results centered on the tendency for these players to slide back into unhealthy habits, thus negating any benefits gained in their early adult years as athletes. He describes the aftermath of his dissertation as his "15 minutes of fame," during which he was flooded with inquiries from news stations about his study on baseball players, and the intriguing result that being fit for just one section of your life did not necessarily give you free reign for the rest of your life. While Dr. Waterbor appreciated the attention, he certainly

placed greater emphasis on being able to bring together his interests of epidemiology and baseball.

With his own educational story in mind, Dr. Waterbor has some simple but powerful advice for undergraduates. First, he suggests that students seek a similar relationship with a professor or researcher that he shared with Dr. Cole: one based on mutual respect, and one in which the student can see the mentor as a role model. Interested students can pursue research opportunities by approaching professors teaching classes that interest them. Even if the professor cannot facilitate a research project, they will probably have the knowledge and connections to point students in the right direction. Other times a subject can become interesting through the people with whom you work. Dr. Waterbor is Director of the CaRES (Cancer Research Experiences for Students) program, so he regularly sees graduate and medical students paired with mentors who have proposed projects for an 8-12 week summer program. Research can best be achieved when two goals are met: feasibility and personal interest. Also, while there are many interesting projects out there, students should take into account how long and arduous an undertaking they might have on their hands. How willing and patient are they prepared to be to see a project to completion?

Dr. Waterbor's personal research interests reveal a man adept at wearing many hats, one with a keen eye for seeking out interdisciplinary opportunities. While cancer epidemiology remains his main research, he has made great strides in the field of injury epidemiology as well. He has previously co-taught EPI 603: Injury Epidemiology (available to undergraduates) with Dr. Russ Fine and has gained appointment to the Injury Control Research Center. His most recent project involved studying head injuries caused by tornadoes, specifically the deadly 2011 Alabama tornadoes. Data gathered by Dr. Robert Brissie, a Jefferson county medical examiner, showed that nearly 50% of all fatalities due to these tornadoes resulted from head injuries. At the time, the CDC's only guidelines for protection included covering your head with your hands to protect against flying debris. Dr. Waterbor and his team proposed spreading messages about the utilization of bike or football helmets for protection. However, despite the down-to-earth, common sense nature of the approach, the CDC was reluctant to back it, citing the lack of sufficient studies. Their stance prompted Dr. Waterbor to address an epistemological question regarding the nature of research: where is the line between waiting for more research and implementing a very straightforward solution? Nevertheless, he and his colleagues hope to continue gathering data to make a case for simple and improved head protection guidelines.

In continuing to explore new opportunities, Dr. Waterbor has also immersed himself in providing healthcare to rural counties in Wilcox, AL. He and his team discovered a dearth of physicians and many basic preventive services in that area.

John Waterbor, M.S., M.D., Ph.D.

With a slice of luck, he remembered attending a few meetings with Dr. Conan Davis (outreach coordinator for the School of Dentistry) and Mrs. Mary Jean Sanspree (outreach coordinator for the School of Optometry), each of whom applied for funding from his or her respective school to provide a One-Stop healthcare shop in an abandoned high school in Wilcox. As a team, they provide cancer screenings, diet and exercise advice, basic dental services, and eye exams to the rural population. While they only have grant funding right now, they hope to eventually develop a sustainable model. The power of granting access to hundreds through this One-Stop healthcare shop developed from chance, enthusiasm, and execution. Dr. Waterbor saw an opportunity to work with leaders in other disciplines after learning of a problem and, most importantly, took the steps to ensure action.

Having lived in Birmingham for nearly 30 years, Dr. Waterbor has participated in the UAB community as a student and a professor. His experiences have helped him realize that UAB is constantly growing, and he has offered his own insights into some of the changes we should embrace. According to him, more infrastructure for meeting spaces and greater communication cross-campus should be high priorities. One fun way to accomplish this goal might be a central faculty dining facility where professors from entirely different schools can come to share their work and even make connections that may develop into partnerships. Dr. Waterbor points out that a large university, especially one growing as quickly as UAB, runs the risk of the right hand not knowing what the left is doing. He believes there needs to be a far more extensive and queryable database of researchers that anyone on campus can use to find scientists in different departments based on tags such as "rural health" and "community research."

Dr. Waterbor ascribes to the motto that you don't deserve to play until you've put in hard work. Even then, he admits with a wry smile that he is just one of those people who is more comfortable in a state of work. Most of his time outside his multiple ongoing projects is spent with his wife, stepdaughter, and tennis racket. As a UAB alumnus, he also enjoys attending many sporting events, including football and basketball games. Despite the years, time, and effort that he has poured into UAB and the community at large, he has yet to kick an old habit – checking Phillies.com to keep updated on how his baseball team is doing.

Small peptides as treatments for Alzheimer's disease

Alana Brock[1], Valentine Nwachukwu[2], Inga Kadish[1], Thomas Van Groen[1]

[1] Department of Cell, Integrative, and Developmental Biology
[2] Department of Biomedical Engineering
University of Alabama at Birmingham

Abstract

Alzheimer's disease (AD) pathology is characterized by the deposition of a protein called amyloid β (Aβ) in plaques and blood vessel walls. It is thought that AD is not caused by Aβ deposits, but instead by the oligomeric form of Aβ. This study aimed to investigate the efficacy of two peptides, D3 and D3D3, in reducing these oligomers and the pathology they cause and in improving cognition. The D3 peptide is a D-enantiomer obtained from a mirror image phage display selection against small oligomeric forms of $Aβ_{42}$. D3D3 is a dimer of D3 connected by a peptide bond. D3 had previously been shown to reduce oligomers and improve pathology and cognition in AD transgenic (APP/PS1) mice. We hypothesized that the D3D3 peptide would bind more strongly than D3 to Aβ oligomers and therefore be more effective as a treatment. Because Aβ oligomers have been shown to start causing damage to the brain years prior to the onset of symptoms, we chose to test the peptides in young mice (4-6 months). Behavioral and cognitive analysis included Morris water maze, open field, and zero maze. Histological analysis involved staining for Aβ and measuring levels of Aβ in the dentate gyrus and CA1 region of the hippocampus. Significant reduction in plaque accumulation was observed in the dentate gyrus and CA1 region with both peptides, but D3D3 was not superior to D3. Similarly, both experimental groups displayed significant improvement in cognitive functioning, but with no differences between D3D3 and D3.

Keywords: Alzheimer's disease, amyloid, limbic system, mouse, plaques, treatment

Introduction

Alzheimer's disease (AD) is a progressive neurodegenerative disease that affects millions of people worldwide. There are currently no curative treatments for this disease, and thus developing novel treatments is imperative. One of the key features of the disease is the accumulation of amyloid β (Aβ), a proteolytic fragment of amyloid precursor protein (APP), in plaques. These amyloid β deposits begin accumulating many years before the onset of cognitive symptoms. It was originally thought that Aβ plaques were the cause of the dementia; however, recent findings suggest that Aβ

oligomers are the real cause of the synaptic damage that leads to disconnections within the brain.

Aβ monomers are released from the cell membrane and bind to each other, leading to the formation of Aβ fibrils that are deposited in plaques. Smaller forms of these aggregates, referred to as oligomers, also form. Evidence suggests that these Aβ oligomers are implicated in the degeneration of neural connections, i.e. synapses, leading to cognitive deficits. Thus, these Aβ oligomers were the target of this study. We hypothesized that long-term treatment with small peptides that bind to $Aβ_{42}$ (the most toxic form of Aβ) would result in changes in amyloid deposition in our transgenic (Tg) AD model mice. Our lab has previously tested a small D-enantiomeric peptide (D3) that was shown to reduce the accumulation of Aβ oligomers and improve cognition in AD transgenic (APP/PS1) mice.[1] This D3 peptide targets Aβ oligomers and was obtained from a mirror image phage display selection against small oligomeric forms of Aβ42.[2] Following this study, a second D-enantiomeric peptide (D3D3) was created with the intention of improving the effects of the first. A comparison of the two peptides was designed in order to test the efficacy of the new D3D3 peptide.
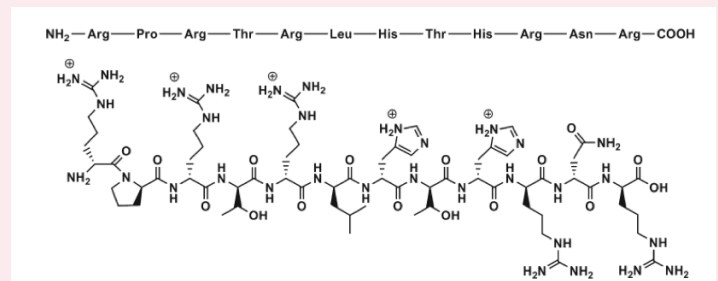

Figure 1. Amino acid sequence and chemical structure of the D3 peptide. D3D3 is a dimer of this peptide connected by a peptide bond between the N and C termini.

Methods

Animals
Our study used female, AD Tg mice (APPSweDI) divided into three groups: D3, D3D3, and control (saline). Female mice were chosen in order to maintain consistency with a previous

peptide study. The animals received 1 mg per month of D3 peptide, D3D3 peptide, or saline intraperitoneally over the course of one month (4.5-5.5 months of age) via an Alzet minipump (model 1004). The experiments were conducted in accordance with the local Institutional Animal Care and Use Committee (IACUC) guidelines.

Behavioral and cognitive analysis
The mice were analyzed in a battery of behavioral tests. To rule out differences in anxiety or stress levels, the open field and zero maze tests were applied. For the analysis of cognitive deficits, the mice underwent the Morris water maze test. During days 1 through 5 of the water maze testing period, the mice were trained to find a hidden platform that was kept in a constant position. Four trials per day were run so that all starting positions were used equally in a random order. The mice were given 60 s to find the platform and 10 s to stay on the platform. The inter-trial interval was approximately 2 min. Learning of the task was evaluated by recording the swimming speed, latency to find the platform, path length, and percentage of trials each animal found the platform. After the end of the four trials on day 5 of the testing period, the mice were tested in a 60 s probe trial (trial 21), with no escape platform present.

Mice that learned the platform position will predominantly search in the correct quadrant of the pool in the probe trial. All behavioral testing and statistical analysis of the behavioral data were performed in the UAB Behavioral Assessment Core.

Immunohistochemical and biochemical analysis
Following behavioral and cognitive analysis, the animals were anesthetized and perfused transcardially with a cold saline solution. The brain was dissected and the left hemisphere was frozen at −80 °C, then used for ELISA measurements of Abeta levels. The right hemisphere was fixed in 4% paraformaldehyde solution.

Histology
Brains were cut into 6 series of 30-mm sections (coronal plane). Sections were stained with amyloid β (WO2-antibody), glial fibrillary acidic protein (GFAP; astrocytes), and ionized calcium binding adaptor molecule 1 (Iba-1; microglia). Series 4 – 6 were stored for later analysis. Following incubation in the primary antibody for 18 h, the sections were rinsed in Tris-Buffered Saline with Tween and incubated with the appropriate biotinylated secondary antibody for 2 h. Following rinsing, the sections were put in a solution containing Extra-Avidin for 2 h, then rinsed and stained for approximately 3 min with Ni-enhanced diaminobenzidine. Stained sections were mounted on slides and coverslipped. Some sections of these series were counterstained with Congo red (Aβ plaques), mounted, and coverslipped.
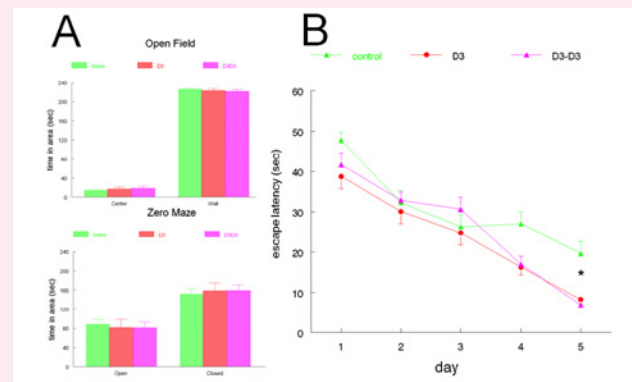
Results

Figure 2. (A) Time spent in the different areas of the open field and elevated plus mazes. Animals did not show significant differences in anxiety or activity. (B) Learning curves of the mice in the water maze. D3 and D3D3 treated mice showed significant improvement compared with control.
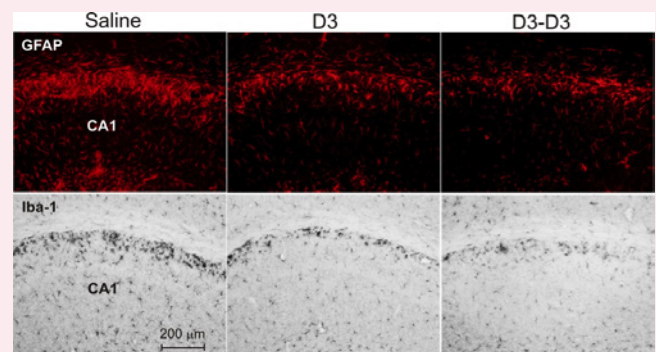

Figure 3. Photomicrographs of the dorsal hippocampus, stratum oriens. Upper panel: GFAP (astrocytes) stained sections; lower panel: Iba-1 (microglia) stained sections. Sections from peptide treated animals displayed decreased staining density.
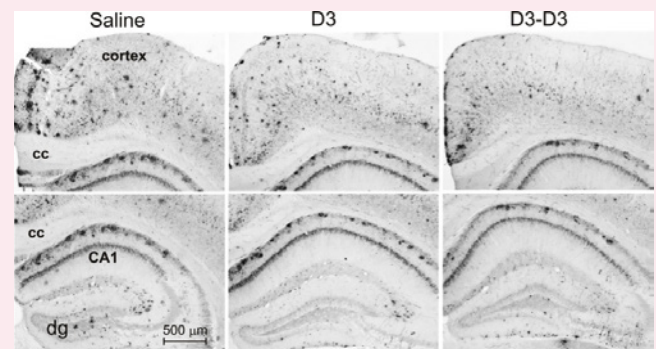

Figure 4. Photomicrographs of sections stained for human Aβ showing the dorsal, midline cortex and hippocampus. Sections from peptide treated animals displayed decreased staining density. Corpus callosum (cc) and dentate gyrus (dg) are shown.
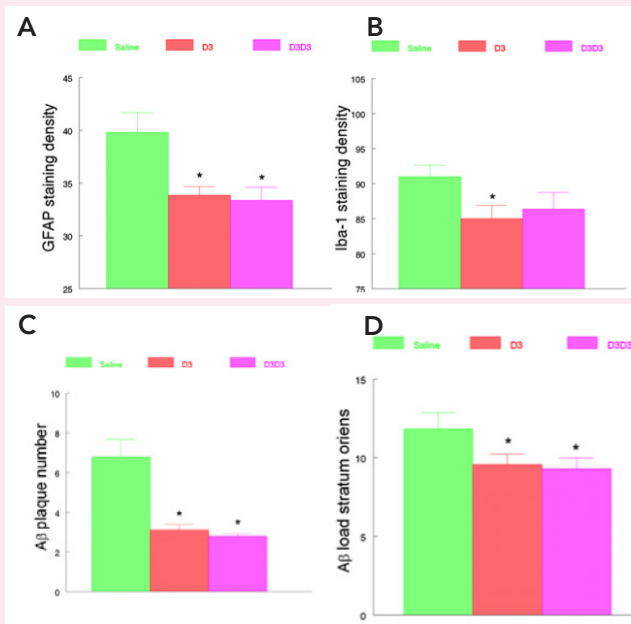
Figure 5. Quantification of the staining density of (A) GFAP, (B) Iba-1, (C) Aβ, and (D) Congo red. Staining density was significantly reduced in peptide-treated mice.

Tests for anxiety resulted in no difference between the control group and the two experimental groups (Figure 2A). Spatial learning and memory functioning was assessed by measuring escape latency in the water maze task. Animals in the D3 and D3D3 groups displayed significantly faster escape times by day five than those in the control group, indicating an improvement in cognitive functioning (Figure 2B). While a significant difference was seen in the learning curve, no significant difference was seen between groups in the probe trial (not shown graphically).

Figure 3 shows GFAP and Iba-1 staining of the dorsal hippocampus, specifically the CA1 region. The top section was stained with GFAP to detect astrocytes, which cluster around Aβ plaques. Significant reduction in astrocyte clusters can be seen in the D3 and D3D3 stains compared with the control region. The bottom panel was stained with Iba-1 to detect the presence of microglia, the immune cells of the nervous system. A significant reduction in microglia accumulation was seen in the D3 group but not in the D3D3 group compared with the control group. Figure 4 shows sections of the hippocampus stained for the presence of human Aβ. A significant reduction in plaque density can be seen in the D3 and D3D3 groups compared with the control group.

Figure 5 depicts graphical representations of the data presented in Figures 3 and 4 as well as results for Congo red staining (not pictorially represented). A significant reduction in the number of Aβ plaques observed was noted in the D3 and D3D3 groups compared with the control group. There was no significant difference in number of plaques between experimental groups.

Discussion

In this study, we intraperitoneally infused Tg AD model mice with one of two small D-amino acid peptides (D3 or D3D3) that have a high affinity for $Aβ_{42}$,[2-3] examined cognitive performance after 3 weeks, and measured the Aβ deposits in the hippocampus and cortex 4 weeks later. No difference in cognitive deficits was observed between D3- and D3D3-treated mice, but saline-treated mice were significantly impaired compared to the other two groups. The data demonstrate that short-term infusion with the D3 or D3D3 peptides leads to a reduction in the density of amyloid β deposits in the hippocampus and cortex, whereas infusion with the vehicle solution does not change amyloid β deposition patterns. Furthermore, analysis of glial stainings (GFAP and Iba1) shows significant reduction in both activated astrocytes and microglial cells surrounding Aβ plaques in both the D3 and D3D3 infused mice compared to the control mice.

One of the two pathological hallmarks of human AD is the presence of neuritic plaques.[4] Neuritic plaques have a dense core of aggregated Aβ peptides.[5] However, diffuse amyloid deposits have also been shown to be present in AD brains[4,6] and in the brains of AD model mice.[7] The data from our experiments show that both the D3- and D3D3-infused mice have a lower Aβ load, demonstrating that binding of the peptide to $Aβ_{42}$ reduces Aβ deposition in the hippocampus and neocortex. This is most likely due to changes in the aggregation properties of the $Aβ_{42}$-D peptide complex, lessening the propensity of $Aβ_{42}$ to aggregate.[8-9] This would lead to a decrease in the Aβ deposition rate by reducing either the number of plaques, the size of plaques, or both.[3] Conversely, it is possible that the clearance of the $D3-Aβ_{42}$ complex has improved compared to the clearance of $Aβ_{42}$.[10-12] Several mechanisms have been proposed for the clearance of Aβ, including receptor-mediated Aβ transport across the blood-brain barrier and enzyme-mediated degradation of the peptide.[10,12] It is more likely that Aβ transport out of the brain is improved than that Aβ degradation has increased, since the properties of the $D3-Aβ_{42}$ complex are not likely to improve enzymatic degradation.[13]

All plaques in our AD-model mice are accompanied by activated glial cells, both astrocytes and microglia.[14-15] The role of the activated glial cells is unclear; they could protect the brain by removing Aβ, or they could secrete inflammatory cytokines and generate NO, thus damaging and killing bystander neurons.[16] In our mouse model, no dead or dying neurons are present, even near plaques.[12] In the D3 and D3D3 infused mice, dense amyloid β deposits are associated with much lower numbers of activated microglia or activated astrocytes. This suggests that the binding of the D-peptides to deposited $Aβ_{42}$ changes the structure of $Aβ_{42}$, evoking fewer inflammatory responses.[9,13] Furthermore, the size of the Aβ deposits is smaller in both D-peptide-treated mice,

suggesting that the Aβ in the plaques, through binding with the D-peptide, exhibits lower aggregation kinetics. Finally, it should be noted that the number of deposits that stain for Congo red has also been significantly reduced. Either fewer new deposits were formed during the four weeks of treatment, or deposits were removed by microglia.

The data demonstrate that short-term infusion with the D3 and D3D3 peptides leads to a reduction in the density of amyloid β deposits in the hippocampus and cortex, whereas infusion with the vehicle solution does not. Cognitive deficits are not significantly different between control and D3-infused mice. Furthermore, the D3- and D3D3-infused mice demonstrate a significant reduction in both activated astrocytes and microglial cells surrounding Aβ plaques compared to the control mice. Together, this demonstrates that, while neither peptide is superior over the other, D3 and D3D3 have great potential as future treatments in Alzheimer's disease.

Conclusion

Treatment with both D-peptides improved cognitive functioning and significantly reduced Aβ load and inflammation in AD transgenic (APP/PS1) mice; however, D3D3 was not superior to D3. New peptides are currently being developed based on D3. We hope these new peptides will be more efficacious than D3 and/or D3D3.

A key demonstration of this study is that oral treatment with D3 and D3D3 peptides is able to improve cognitive deficits, decrease amyloid β pathology, and decrease inflammation. These findings suggest possible future use of these peptides toward treatment of Alzheimer's disease in humans.

References

1. van Groen, T., Wiesehan, K., Funke, S. A., Kadish, I., Nagel-Steger, L., Willbold, D. (2008). Reduction of Alzheimer's disease amyloid plaque load in transgenic mice by D3, a D-enantiomeric peptide identified by mirror image phage display. *ChemMedChem* **3**, 1848–1852. 33.

2. Wiesehan, K., Buder, K., Linke, R.P., Patt, S., Stoldt, M., Unger, E., Schmitt, B., Bucci, E., Willbold, D. (2003). Selection of D-amino-acid peptides that bind to Alzheimer's disease amyloid peptide Aβ1–42 by mirror image phage display. *ChemBioChem* **4**, 748-753.

3. Wiesehan, K., Stöhr, J., Nagel-Steger, L., van Groen, T., Riesner, D., and Willbold, D. (2008). Inhibition of cytotoxicity and amyloid fibril formation by a D-amino acid peptide that specifically binds to Alzheimer's disease amyloid peptide. *Protein Engineering, Design and Selection* **21**, 241-246.

4. Braak H, Braak E (1991) Neuropathological stageing of Alzheimer-related changes. *Acta Neuropathol* **82**, 239-259.

5. Selkoe, D. J. (2001). Alzheimer's disease: Genes, proteins, and therapy. *Physical Rev* **81**, 741-766.

6. Dickson, T.C., Vickers, J.C. (2001). The morphological phenotype of beta-amyloid plaque and associated neuritic changes in Alzheimer's disease. *Neuroscience* **105**, 99-107.

7. van Groen, T., Kiliaan, A. J., Kadish, I. (2006). Deposition of mouse amyloid beta in human APP/PSI double and single AD model transgenic mice. *Neurobiol Dis* **23**, 653-662.

8. Bartolini, M., Bertucci, C., Bolognesi, M.L., Cavalli, A., Melchiorre, C., Andrisano, V. (2007). Insight into the kinetic of amyloid beta (1-42) peptide self-aggregation: Euclidation of inhibitors' mechanism of action. *ChemBioChem* **8**, 2152-2162.

9. Iijima, K., Liu, H. P., Chiang, A. S., Hearn, S. A., Konsolaki, M., Zhong, Y. (2004). Dissecting the pathological effects of human Abeta40 and Abeta42 in Drosophila: A potential model for Alzheimer's disease. Proc Natl Acad Sci U S A 101, 6623-6628.

10. Ji, Y., Permanne, B., Sigurdsson, E. M., Holtzman, D. M., Wisniewski, T. (2001). Amyloid beta40/42 clearance across the blood-brain barrier following intra-ventricular injections in wild-type, apoE knock-out and human apoE3 or E4 expressing transgenic mice. *J Alzheimers Dis* **3**, 23-30.

11. Tanzi, R. E., Moir, R. D., Wagner, S. L. (2004) .Clearance of Alzheimer's Abeta peptide: The many roads to perdition. *Neuron* **43**, 605-608.

12. Wang, Y. J., Zhou, H. D., Zhou, X. F. (2006). Clearance of amyloid-beta in Alzheimer's disease: Progress, problems and perspectives. *Drug Discov Today* **11**, 931-938.

13. Yoshiike, Y., Chui, D.H., Akagi, T., Tanaka, N., Takashima, A. (2003). Specific compositions of amyloid-beta peptides as the determinant of toxic beta-aggregation. *J Biol Chem* **278**, 23648-23655.

14. Bondolfi, L., Calhoun, M., Ermini, F., Kuhn, H. G., Wiederhold, K. H., Walker, L., Staufenbiel, M., Jucker, M. (2002). Amyloid associated neuron loss and gliogenesis in the neocortex of amyloid precursor protein transgenic mice. *J Neurosci* **22**, 515-522.

15. van Groen, T., Kadish, I. (2005). Transgenic AD model mice, effects of potential anti-AD treatments on inflammation and pathology. *Brain Res Brain Res Rev* **48**, 370-378.

16. Akiyama, H., Barger, S., Barnum, S., Bradt, B., Bauer, J., Cole, G. M., Cooper, N. R., Eikelenboom, P., Emmerling, M., Fiebich, B. L., Finch, C. E., Frautschy, S., Griffin, W. S., Hampel, H., Hull, M., Landreth, G., Lue, L., Mrak, R., Mackenzie, I. R., McGeer, P. L., O'Banion, M. K., Pachter, J., Pasinetti, G., Plata-Salaman, C., Rogers, J., Rydel, R., Shen, Y., Streit, W., Strohmeyer, R., Tooyoma, I., Van Muiswinkel, F. L., Veerhuis, R., Walker, D., Webster, S., Wegrzyniak, B., Wenk, G., Wyss-Coray, T. (2000). Inflammation and Alzheimer's disease. *Neurobiol Aging* **21**, 383-421.

Optimization of piezoelectric PVDF films for electroactive strain measurements

Matthew Bailey[1], Derrick R. Dean[2], and Carrie Schindler[2]

[1] Department of Physics, University of Maryland Baltimore County
[2] Department of Materials Science and Engineering, University of Alabama at Birmingham

Abstract

Of the five crystalline phases that exist in poly(vinylidene fluoride), the β phase is responsible for piezoelectric properties in the material. These properties are desirable for actuating devices in applications such as aerospace, robotics, and medical technology. Five types of poly(vinylidene fluoride) were studied to determine a processing method that created films with a maximal amount of β crystalline phase while maintaining mechanical integrity. The films were prepared using two methods: melt pressing and solution casting. Differential scanning calorimetry showed that the poly(vinylidene fluoride) copolymers exhibited the lowest total crystallinity; however, FTIR spectroscopy and x-ray diffraction showed the highest β phase crystallinity. The optimized films were prepared by heat pressing the copolymers and cooling before stretching to a draw ratio of 2.1 at ambient conditions. A novel approach—use of a modified thermomechanical analyzer to measure the dimensional change—was adapted to characterize the piezoelectric responses of the films.

Introduction

Piezoelectric materials are defined by their ability to convert between mechanical and electrical energy; physical deformations induce a voltage difference and vice versa.[1] Because of this property, such materials can compete with mechanical actuators and sensors by replacing a mechanical device with the piezoelectric property. Electroactive polymers (EAPs) are a class of polymers that utilize a polarized crystal structure to induce deformation by applying a voltage.[2] These polymers show promise for a multitude of applications including biomimetic artificial muscles[3] and fabric woven into clothing to create electrical power from movement.[4-5] Furthermore, these materials are attractive as actuators and sensors due to the versatility of the polymeric nature.

Poly(vinylidene fluoride) (PVDF) is an EAP that offers excellent flexibility and chemical resistance while simultaneously being the most responsive piezoelectric polymer presently known.[6] However, not all forms of PVDF are piezoelectric; the piezoresponse of PVDF only occurs when the β crystalline phase is predominantly present.[7] The associated monomer of PVDF is $-CH_2-CF_2-$, which typically creates a head-to-tail chain. When not in an amorphous configuration, PVDF can exhibit five primary crystalline phases described by the trans (T) configurations, which create planar chains, and gauche (G[+] or G[-]) configurations, which skew the structure ±60° for helical chains. The α and δ crystalline phases have a trans-gauche (TG[+]TG[-]) molecular configuration, the β phase has all trans (TTT) in a planar zigzag formation, and the γ and ε phases have $T_3G^+T_3G^-$.[8]

Typically, the α and β phases are predominant and very little of the other phases are present in PVDF. The α phase is most energetically favorable due to the electroneutrality formed by the adjacent placement of fluorine atoms in the backbone of the polymer chain.[8] In contrast, the β phase requires more energy to form a polarized crystal structure in which the fluorine atoms align on the same side of the polymer chain. Previous methods of forcing the formation of the β phase include creating copolymers of PVDF,[9] orienting films by uniaxial strains,[7] and adding carbon nanotubes (CNTs).[10] Adding CNTs has also been explored to modify EAPs for higher sensitivity, energy efficiency, and conductivity. These properties, in addition to the ability to nucleate β phase in PVDF, make CNTs a valuable asset in creating piezoelectric films.

Several factors hinder the expansion of EAPs into more applications. The difficulty of consistently characterizing EAPs presents a roadblock for the creation of a reliable database of electro-mechanical properties.[2] In addition, the limited availability of inherent EAPs creates a lack of supply for mass-produced products. The development of electro-mechanically enhanced nanocomposites provides an alternative to inherent EAPs but requires characterization techniques to compare the performance of inherent EAPs to composite EAPs. Little research has been done to measure dimensional change resulting from applying voltage to piezoelectric polymers.

For these reasons, it is imperative that novel characterization techniques are thoroughly explored for the advancement of EAPs in diverse applications. The focus of this work is a comparison of the β phase content of various PVDF films and composite PVDF/CNT films in order to select the appropriate processing conditions to achieve the highest β content. The varying degrees of β crystallinity were tested for corresponding piezoelectric properties by direct strain measurements using a thermomechanical analyzer.

Materials and Methods

Materials

A PVDF homopolymer for general use with extrusion or injection molding, a high molecular weight PVDF homopolymer, a copolymer with hexafluoropropylene (HFP), and a copolymer with chlorotrifluoroethylene (CTFE) were provided in pellet form by 3M. A PVDF composite with carbon fibers was provided by SABIC Innovative Plastics. Multi-walled carbon nanotubes (MWCNTs) were purchased from Materials and Electrochemical Research (MER) Corporation and modified with fluorine (CNT-F) following the procedure of Abdalla et al.[11] N,N-Dimethylformamide (99%) (DMF) was purchased from Sigma-Aldrich for use as the solvent in solution cast films.

Fabrication and processing

Heat pressing

Films with an approximate thickness of 30 μm were prepared by melting each type of PVDF in a Carver press. Melting temperatures were determined by differential scanning calorimetry (DSC). Homopolymers and the composite showed a melting temperature of 170 °C, so the press was heated to 180 °C before inserting those materials; copolymers exhibited a melting temperature of approximately 160 °C, so the press was set to 170 °C for the copolymers. The PVDF/CTFE copolymer was first rinsed with acetone to remove impurities and then placed in a vacuum chamber to dry overnight before pressing at 170 °C. This method was chosen to avoid the formation of volatiles during melt pressing. The PVDF was inserted between aluminum plates and allowed 5 minutes to melt before a pressure of 5.0 – 5.5 tons was applied for another 5 minutes. Two sets of films were then created: one by removing the aluminum plates with the material inside to cool in the air over a period of 30 minutes (air-cooled) and another by leaving the plates in the press to cool over a period of 4 hours (slow-cooled).

Solution casting

PVDF solutions in DMF at a concentration of 20% (w/v) were stirred until dissolution on a hot plate at 55 °C for 2 hours. Solutions were then poured into aluminum dishes and heated in an oven at 60 °C for 30 minutes and left in the oven for 48 hours to dry. The resulting films were approximately 70 μm thick.

A second set of films was created using PVDF/CTFE with CNT-F, where the CNT-F concentrations were 0.25, 0.5, and 1.0% (w/v) of the PVDF/CTFE. Processing and DMF concentrations were the same as those for the previous set. Each of these three solutions was poured at three separate volumes to investigate the effect of solvent evaporation on CNT-F dispersion and β phase formation.

Orienting films

Drawing PVDF films to different strain ratios is a known method to convert α phase to β crystallinity.[12] To prepare films for stretching, samples were cut from each heat-pressed film with an ASTM standard dogbone-MET cutter 68 mm in length. Using a Satec mechanical testing instrument (Apex T5000 model), the samples were stretched at rates of 1 and 5 mm·min^{-1} to draw ratios of 1.7, 2.1, and 2.5 at room temperature. While higher draw ratios (e.g., between 3.0 and 6.5) have been shown to convert almost all α phase to β, these samples were more likely to break at ratios above 2.5 due to imperfections.

Structure evaluation methods

Differential scanning calorimetry

Differential scanning calorimetry (DSC; Q100 model from TA Instruments in New Castle, DE) was performed on each type of PVDF as it was received as well as on heat-pressed air-cooled and slow-cooled films. Plots of heat flow versus temperature were used to determine the melting temperature (T_m) and enthalpy of fusion (ΔH) for each sample. The T_m was primarily used in preparing the heat-pressed films, whereas the ΔH was used to determine the percent crystallinity (X_c) for the samples according to Equation 1, where ΔH_{crys} is the enthalpy of heat for 100% crystalline PVDF.[13]

$$X_c = 100 \; \frac{\Delta H}{\Delta H_{crys}} \qquad (1)$$

The value of ΔH_{crys} has been found to be a constant 104.7 J·g^{-1}. These measurements were also taken to determine a correlation between the amounts of α or β phases PVDF present in the samples.

Fourier transform infrared spectroscopy

Infrared spectra of the samples were collected using Fourier transform infrared (FTIR) spectroscopy (Nicolet 4700 model from Thermo Fisher Scientific Inc. in Waltham, MA), employing 64 scans per sample. The range in attenuated total reflection (ATR) was 4000 cm^{-1} to 400 cm^{-1}. These scans were analyzed to evaluate the fractions of α and β phase crystalline structures in the PVDF samples. The fraction of β phase, (β), was found by applying the Beer-Lambert law (Equation 2), using the 763 cm^{-1} and 839 cm^{-1} bands bands for characteristic α and β absorption bands A_α and A_β.[7-8,13]

$$F(\beta) = \frac{A_\beta}{(1.26 \, A_\alpha + A_\beta)} \qquad (2)$$

Wide-angle X-ray diffraction

Wide-angle x-ray diffraction (XRD) experiments were carried out using an x-ray generator (Kristalloflex 710 model from Siemens) on heat-pressed slow-cooled films and select other samples that showed a high $F(\beta)$ as measured by FTIR spectroscopy. Samples were scanned with a 2θ range of 10° to 30° at a rate of 0.05° s^{-1} with 0.05° intervals.

Scanning electron microscopy

A field emission scanning electron microscope (SEM; Quanta FEG 650 model from FEI in Hillsboro, OR) was used to observe the dispersion of carbon fibers in the associated heat-pressed slow-cooled film and the solution cast films with CNT-F. To prepare the films with carbon fibers or CNT-F, each was freeze fractured with liquid nitrogen as the cooling agent. The SEM was further used to compare the morphology in terms of spherulite size.

Strain measurements

Thermomechanical analyzer

Piezoelectric response testing was conducted with a thermochemical analyzer (TMA; Q400 model from TA Instruments in New Castle, DE) setup modified with a function generator (Figure 1). Conductive aluminum tape was placed on top of the TMA stage and served as the negative electrode with the associated wire connected between the tape and function generator. The wire leading to the positive electrode was taped to the side of the stage and bent such that the exposed wire lay at a distance equivalent to the thickness of the samples above the stage, parallel to the stage. Samples were inserted between electrodes, and the probe was lowered to provide a constant force of 0.1 N, ensuring contact between each component. Dimensional changes were then recorded by TMA at 35 °C as voltage and frequency were varied from the function generator. The ranges tested included ramps from 0 to 10 V and 10 mHz to 1 MHz as well as various constant values in the same ranges for both alternating and direct currents.

Figure 1. Modified TMA setup, with electrodes connected to a function generator. The TMA is programmed to measure dimensional change as a function of voltage or frequency.

Results and Discussion

Structure evaluation

Differential scanning calorimetry

Figure 2 shows the thermograms for the as-received PVDF and PVDF copolymers. The PVDF copolymers exhibited the lowest melting temperatures as well as the lowest crystallinities, which was consistent with the defects added into the polymer chain by the copolymer. The homopolymers exhibited the highest crystallinities and melting temperatures. This trend was consistent for each processing method. Although the types of crystalline phases were unidentifiable with DSC, the CTFE copolymer and carbon fiber composite exhibited multiple crystal systems. The multiple crystalline phases were identified by the multiple peaks in the DSC curve during melting. The highest total crystallinity achieved was 71.6% by the slow-cooled general-use homopolymer film.
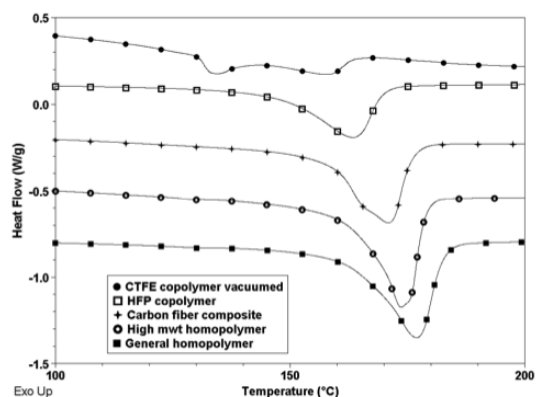

Figure 2. DSC thermograms for each grade of as-received PVDF indicating the different melting profiles for each sample.

Figure 3 (top) demonstrates the typical result of pressing films with different cooling profiles. The slow-cool processing allowed the polymer chains more time to pack into ordered crystallites in comparison to air-cool processing. This is supported by the broadening of the melting peak, which contributes to a higher enthalpy of fusion (total area of the peak). An exception occurred with the carbon fiber composite, shown in Figure 3 (bottom), for which the enthalpy of fusion was lower with slower cooling. This may be attributed to the interaction of two separate crystalline phases, evidenced by the presence of two distinct peaks. The formation of multiple crystalline systems may indicate the growth of β phase. A similar phenomenon was observed in the CTFE copolymer, with the exception that the area of the peak with the lower melting temperature, visible in Figure 2, was reduced by processing.
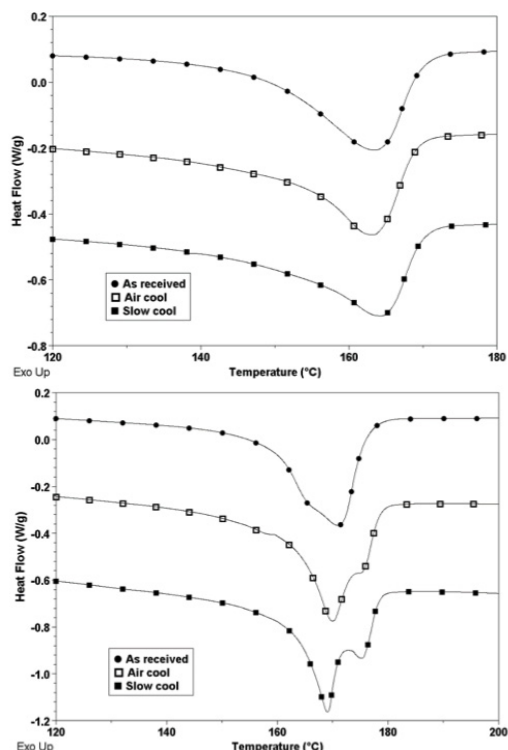
Figure 3. DSC thermograms including various processing methods for the HFP copolymer (top) and the carbon fiber composite (bottom). The grade with carbon fibers shows the formation of two crystalline phases with slower cooling.

Fourier transform infrared spectroscopy

FTIR spectra for the CTFE copolymer can be seen in Figure 4. The other grades of PVDF had comparable results with the same absorption pattern. Bands at 970 cm⁻¹, 870 cm⁻¹, 854 cm⁻¹, 796 cm⁻¹, 763 cm⁻¹, 612 cm⁻¹, and 532 cm⁻¹ have been associated with α phase PVDF, whereas the 839 cm⁻¹ and 510 cm⁻¹ bands correspond to β phase. Other bands at 882 cm⁻¹ and 812 cm⁻¹ can be used to identify γ phase crystallinity, though γ and δ phases appear much less than α and β phases with the processing techniques used. Table 1 summarizes the intensity values of the α and β absorption bands with the resulting fraction of β phase $F(\beta)$. While each processing method greatly increased $F(\beta)$ in the as-received samples, the largest $F(\beta)$ values resulted from the solution cast films, followed by stretching the heat pressed copolymers to a draw ratio of 2.1. Literature has shown that higher draw ratios contribute to higher β phase, whereas our results showed a decrease at the ratio 2.5, which was the highest draw ratio used. One possible explanation is that recoil effects while releasing the sample may have converted β crystals to α; a holding period in future studies may eliminate these effects.

Prior to stretching, slow-cooled films exhibited higher $F(\beta)$ values than air-cooled films; after stretching, the values were much closer. The solution cast films demonstrated the highest values for $F(\beta)$ and the lowest absorbance for characteristic α bands, which indicated that the nanotubes assist in nucleating β phase in PVDF as anticipated.
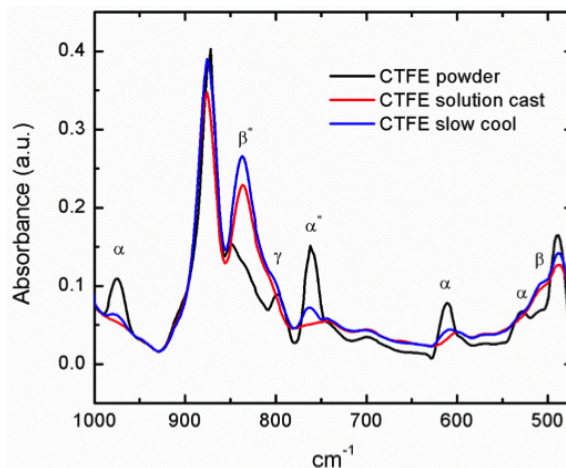

Figure 4. FTIR scans for PVDF/CTFE films with α, β, and γ labeled at wavenumbers characteristically absorbed by the crystalline structures. An asterisk (*) indicates a peak used for calculations in Table 1. Other PVDF grades had the same relative differences, but the copolymers excelled. The draw ratio 2.1 consistently gave higher β peaks than the ratios 1.7 and 2.5.

Table 1. FTIR-ATR spectroscopy data for the copolymers comparing the area of the characteristic bands for α and β phases.

Sample	A_α (612 cm⁻¹)	A_β (839 cm⁻¹)	$F(\beta)$*
HFP as received	1.935	6.767	0.735
HFP slow cool, draw 2.1	0.639	8.852	0.917
HFP solution cast	0.269	7.118	0.955
CTFE as received	2.089	4.46	0.629
CTFE slow cool, draw 2.1	0.532	7.499	0.912
CTFE solution cast	0.238	6.263	0.954
CTFE solution cast, 0.5% CNT-F high volume	0.151	6.701	0.972

*Weighted ratio of A_β with the sum of A_α and A_β as given by Eq. 2.

X-ray diffraction

Characteristic α peaks for XRD occurred with 2θ values of 17.7°, 18.4°, and 19.9° with diffraction in the (100), (020), and (201) planes, respectively, while the characteristic β peak appeared at a 2θ value of 20.4° due to diffraction in both the (110) and (200) planes.[7] XRD plots shown in Figure 5 are consistent with the corresponding FTIR plots in terms of relative effects of processing on α and β peak heights. Some samples even indicated that the α phase was almost entirely removed in processing.

Considering one grade of PVDF and multiple processing methods, raising percent crystallinity measured by DSC typically correlated with an increasing $F(\beta)$ measured by FTIR along with lower α and higher β intensity peaks in XRD. Some DSC scans of such sets are depicted in Figure 3, which also shows that the melting point T_m of a PVDF sample was mostly

unchanged with any processing that was performed. However, across all five types of PVDF for one processing method, lower T_m and X_c measured by DSC correlate with higher $F(\beta)$ measured by FTIR and observed with XRD; the difference between grades of PVDF overrides the generalization that higher crystallinity indicates greater prevalence of β phase. Furthermore, all processing effects increased only β phase; increasing other phases would also raise the total crystallinity, which would make it more difficult to correlate DSC data with the amount of β phase present.

Scanning electron microscopy

SEM images for PVDF/CTFE solution cast films with various concentrations of CNT-F are depicted in Figure 6. The spherical objects in all images represents the crystalline spherulites of the polymer films. The size and shape of the spherulites were analyzed to describe the interconnectivity of the samples: larger and less defined spherulites indicated a more integrated network of crystalline domains. The piezoelectric properties of the films are linked to the connectivity of the crystalline domains: interconnected domains cooperatively move to cause higher deformation or better piezoelectric properties. Higher CNT-F concentrations visibly increased the interconnectivity of the material, which is presumed to assist with conductivity. The films with CNT-F showed generally good dispersion, though there were some clusters of CNT-F. Carbon fibers were very well dispersed in films of the carbon fiber resin. Solution cast PVDF films have been documented to show spherulites about 5 μm in diameter with

SEM imaging, and heat-pressed films were expected to have a more compressed form based on the high pressure during crystallization and lower resulting thickness. The PVDF/CTFE in solution cast samples appeared clustered into spherulites, which could be reduced to a smooth top by heat pressing the films. At magnifications around 10 000x, large domains were observed to rotate or oscillate. A possible explanation for this phenomenon was that the motion indicated a piezoresponse from the electric field present in the microscope.[14]

Thermochemical analyzer

No film tested produced a piezoresponse to the function generator measured by TMA. Because piezoelectric motions were observed in SEM, this result was likely due to a flawed procedure rather than the properties of the samples. The lack of response may have been caused by the large area of the electrodes, which greatly reduced the current density. Furthermore, the top electrode in the setup used may have been too stiff, preventing the samples from deforming beneath the probe. This could be avoided if the probe itself were used as the electrode, which can be accomplished either by attaching a very light wire to it or by using a conductive probe. Further study of the piezoelectric properties of PVDFs may involve conductive atomic force microscopy (AFM). The advantage of this method is that it uses a very small conductive probe as one of the electrodes to create a high current density so that a voltage difference in the same range as that used with TMA will have an amplified effect.
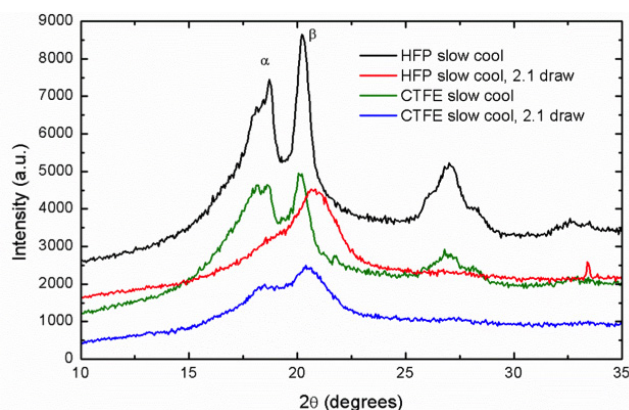

Figure 5. Wide-angle XRD scans for copolymer films with α and β labeled at angles characteristically reflective for the crystalline structures. Both heat-pressed films showed a dramatic decrease in α phase after being drawn, agreeing with FTIR data.
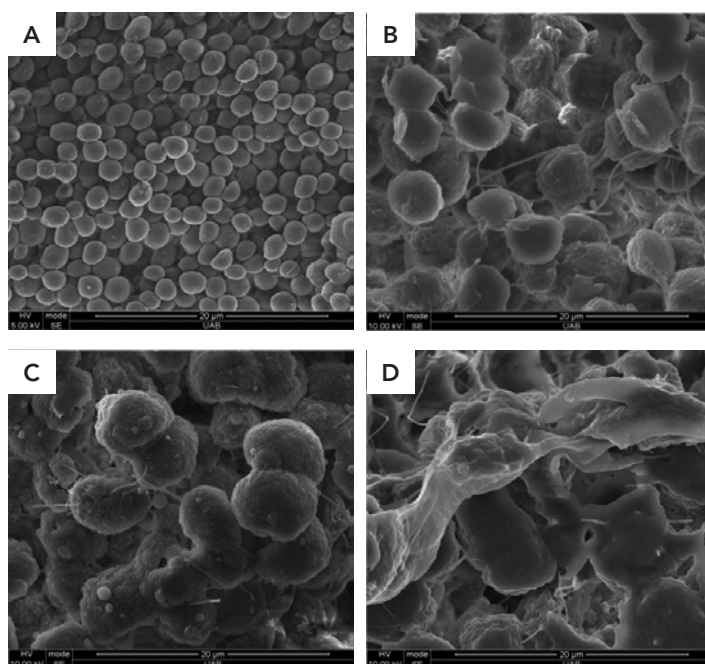

Figure 6. Field emission SEM images of solution cast PVDF/CTFE films at 10 000x with (A) 0%, (B) 0.25%, (C) 0.5%, and (D) 1.0% (w/v) CNT-F. Larger amounts of CNT-F induce a more interconnected structure and nucleate β.

The conductive probe also eliminates the electrode weight problem experienced in the TMA experiments. In addition, images can be obtained to depict the deformation caused by actuating the polymer films with different driving voltages.

Conclusion

Solution cast films with CNT-F gave the highest β phase content with improved mechanical integrity after heat pressing. However, the heat pressed copolymers stretched to a draw ratio of 2.1 had superior strength and flexibility while maintaining comparable $F(\beta)$ values. Solution cast films exhibited higher amounts of β phase than the stretched films but lacked mechanical strength. The addition of nanotubes improved both characteristics.

Piezoelectric response results were inconclusive, possibly due to the weight or large size of the electrode used in the modified TMA experiment. Some piezoelectric response was observed while taking SEM images, suggesting that the unsuccessful TMA experiment was due to the procedure. Suggestions have been made to improve the procedure for future studies, and an alternative experiment has been proposed that would cross-check electroactive strain measurements using conductive atomic force microscopy.

Acknowledgements

References

1. Ikeda, Y. (1990). Fundamentals of piezoelectricity.

2. Yoseph, B. C., Kwang, J. K., Hyouk Ryeol, C. John, D. W. M. (2007). Electroactive polymer materials. *Smart Materials and Structures* **16**.

3. Bar-Cohen, Y. (2006). SAMPE '06: Creating New Opportunities For The World Economy, April 30, 2006 – May 4, 2006. Soc. for the Advancement of Material and Process Engineering, Long Beach, CA, United States, **51**.

4. Jean-Mistral, C., Basrour, S., Chaillout, J. J. (2008). Dielectric polymer: scavenging energy from human motion. 692716-692716

5. Pelrine, R., Kornbluh, R. D., Eckerle, J., Jeuck, P., Oh, S., Pei, Q., Stanford, S. (2001). Dielectric elastomers: generator mode fundamentals and applications. 148-156.

6. Rao, S. S., Sunar, M. (1994). Piezoelectricity and its use in disturbance sensing and control of flexible structures: a survey. *Applied Mechanics Reviews* **47**, 113-123.

7. Gregorio, Jr., R., Ueno, E. M. (1999). Effect of crystalline phase, orientation and temperature on the dielectric properties of poly (vinylidene fluoride) (PVDF). *Journal of Materials Science* **34**, 4489-4500.

8. Salimi, A., Yousefi, A. A. (2004). Conformational changes and phase transformation mechanisms in PVDF solution-cast films. *Journal of Polymer Science Part B: Polymer Physics* **42**, 3487-3495.

9. Cho, J. W., Tasaka, S., Miyata, S. (1993). Cocrystallization and miscibility in blends of vinylidene fluoride-tetrafluoroethylene and vinylidene fluoride-hexafluoroacetone copolymers. *Polym J* **25**, 1267-1274.

10. Nasser, S., Sherif, A., Qingshi, M., Hung-Yao, H., Cheng, Y., Sara, A., Sang-Heon, L., Yanan, X., Jun, M., Sirong, Y. (2014). Superior piezoelectric composite films: taking advantage of carbon nanomaterials. *Nanotechnology* **25**, 045501.

11. Abdalla, M., Dean, D., Adibempe, D., Nyairo, E., Robinson, P., Thompson, G. (2007). The effect of interfacial chemistry on molecular mobility and morphology of multiwalled carbon nanotubes epoxy nanocomposite. *Polymer* **48**, 5662-5670.

12. Mohammadi, B., Yousefi, A. A., Bellah, S. M. (2007). Effect of tensile strain rate and elongation on crystalline structure and piezoelectric properties of PVDF thin films. *Polymer Testing* **26**, 42-50.

13. Sperling, L. H. (2006). *Introduction to Physical Polymer Science*. John Wiley and Sons Inc., 4th ed.

14. Esterly, D. M. (2002). Master's Thesis.

Method for the determination of trajectory angles of directional secretory vesicles in cultured astrocytes

Chapin E. Cavender[1], Manoj K. Gottipati[1], Erik B. Malarkey[1,2], and Vladimir Parpura[1,3]

[1] Department of Neurobiology, University of Alabama at Birmingham, [2] Department of Cell, Developmental, and Integrative Biology, University of Alabama at Birmingham
[3] Department of Biotechnology, University of Rijeka, Rijeka, Croatia.

Abstract

Astrocytes provide a principal pathway for glutamate uptake in the mammalian brain, a task accomplished by the powerful action of excitatory amino acid transporters (EAAT) 1 and 2. These transporters are synthesized within the endoplasmic reticulum and are then trafficked to the plasma membrane. The characteristics of their intracellular traffic within astrocytes have not been investigated. We monitored the trafficking of secretory vesicles laden with the recombinant fluorescent protein chimera of EAAT2 in cultured astrocytes. Such vesicles appeared as fluorescent puncta, and their trafficking parameters were obtained using original algorithms, which we describe here in detail. We determined the maximal displacement, average instantaneous speed, and trajectory angle of individual puncta/vesicles, with angles near 0° indicating radial movement directly away from or toward the nucleus and angles near 90° indicating tangential movement. Analysis of these trafficking parameters demonstrated that trafficking of EAAT2-laden vesicles has typical characteristics expected of the trafficking of secretory vesicles in cultured astrocytes. The distribution of trajectory angles for directional vesicles, i.e. those with a maximal displacement greater than 1 μm within the 40-s time-lapse imaging, was found to be unimodal, with angles near 0° being the most prominent (mode 7°). These measurements are in good agreement with previous measurements of trajectory angles of similar trafficking vesicles carrying cannabinoid receptor 1, evidencing the validity and robustness of our analytical approach and algorithms.

Introduction

Research in the past two decades has shown that astrocytes, a type of glial cell and the most numerous cell in the mammalian brain, have central roles in the structural and functional development and homeostasis of the nervous system.[1-2] One of these roles is to remove excess neurotransmitter molecules from the extracellular space, particularly in the vicinity of synaptic sites. While neurotransmitters mediate typical signaling between neural cells, excessive buildup of these molecules outside of the cells can have deleterious consequences. For example, the major excitatory amino acid neurotransmitter glutamate can cause neuronal death when present in high concentrations in the extracellular space. This condition is known as excitotoxicity and has been implicated in the progression of neurodegenerative diseases such as Alzheimer's disease.[3]

Astrocytes provide a principal pathway for the uptake of glutamate. About 80% of all glutamate released during synaptic transmission is taken up by astroglial cells, while most of the remaining 20% is taken up by post-synaptic neurons.[4-5] This uptake of glutamate by mature astrocytes is accomplished by the plasma membrane sodium-dependent excitatory amino acid transporter 2 (EAAT2). This membrane protein is trafficked by secretory vesicles from the endoplasmic reticulum to the plasma membrane along tracts in the cytoskeleton. In addition to ubiquitous actin- and microtubule-based mechanisms for vesicle trafficking, astrocytes exhibit trafficking mechanisms dependent on the intermediate filament proteins glial fibrillary acidic protein and vimentin.[6-7]

Previous analysis has yielded two categories of trafficking vesicles in astrocytes. These are distinguished by the magnitude of the vesicles' maximal displacement, the greatest distance between any two points on the vesicle's trajectory, within a specified time interval.[7-9] For the lengths of those experiments (15 s or 40 s), non-directional vesicles have a maximal displacement less than 1 μm, and their motion is governed by simple diffusion; directional vesicles have a maximal displacement greater than 1 μm, and their motion is more complex.

One parameter associated with vesicle trafficking that has not been studied extensively is the trajectory angle, defined as the angle between the trajectory of a vesicle and a vector in the radial direction away from the nucleus of the cell (see materials and methods and Figure 1).[9] This parameter is useful for defining a preferred direction of motion for the directional vesicles. Indeed, it has been instrumental in discovering a preference for radial trafficking (motion directly toward or away from the nucleus) of vesicles carrying fluorescently tagged cannabinoid receptor 1 (CB1R) in rat astrocytes,[9] as evident from detecting a mode near 0° for a unimodal distribution of angles. Consequently, the goal of this article

is to describe a method for determining the trajectory angles of directional vesicles. This method utilizes a custom-written Visual Basic routine for Microsoft® Excel, referred to in the present study as a custom script.

Trafficking of fluorescently tagged EAAT2 vesicles in cultured mouse cortical astrocytes was studied, and the results were compared to those of previous trafficking studies. Overall, the EAAT2-laden vesicles display preferential radial trajectories.
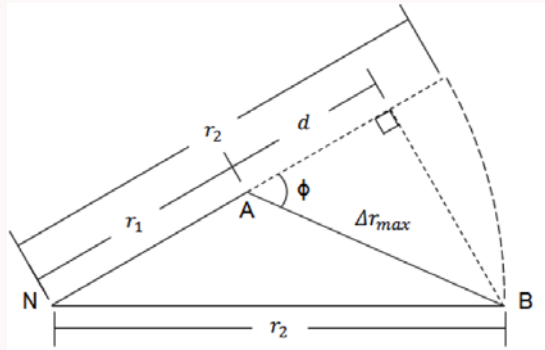

Figure 1. Geometry of vesicular trafficking. The centroid of the nucleus is located at vertex N. The vector representing maximal displacement of a vesicle/punctum is defined by the endpoints A and B. r_1 represents the distance between the centroid of the nucleus and the earlier endpoint (point A) of the maximal displacement vector, and r_2 represents the distance between the centroid of the nucleus and the later endpoint (point B) of the maximal displacement vector. The dashed curve represents the rotation of the vector **NB** around an axis through N perpendicular to the page to assist in the visualization of the distances r_2 and r_1. The angle marked φ is the angle between the radial vector **NA** and the maximal displacement vector **Δr_{max}**.

Materials and methods

Purified astrocytic cell culture
Purified astrocytic cultures were made as described elsewhere.[10-11] Visual cortices from 0- to 2- day-old C57BL/6 mice pups were isolated and treated with papain (20 I.U./mL; Sigma-Aldrich, Sr. Louis, MO) in the presence of L-cysteine (0.2 mg/mL) for 1 hour at 37 °C. Cortices were treated with trypsin inhibitor (type II-O, 10 mg/mL; Sigma-Aldrich) for 5 minutes at room temperature to neutralize the enzymatic activity of papain and then triturated in cell culture media using a glass serological pipette until no visible clumps appeared. The resulting cell suspension was plated into 25 cm² tissue culture flasks and left for 1 hour at 37 °C in a 95% air / 5% CO₂ incubator to allow for cell attachment, after which the flasks were washed with Hank's balanced salt solution (HBSS). The HBSS was replaced with cell culture media containing α-minimum essential medium (without phenol red; Invitrogen™, Life technologies Corp., Grand Island, NY) supplemented with fetal bovine serum (10% v/v,

HyClone™, Thermo Fisher Scientific Inc., Waltham, MA), sodium bicarbonate (14 mM), sodium pyruvate (1 mM), D-glucose (20 mM), L-glutamine (2 mM), penicillin (100 I.U./mL), and streptomycin (100 µg/mL) (pH 7.35). The flasks were returned to the incubator and the cells were allowed to grow and proliferate for 10 to 14 days to reach approximately 60% confluency, after which the flasks were purified for astrocytes using a previously described procedure.[12] The flasks were washed with ice cold culture media to kill the neurons and side-tapped to detach the microglia, dead neurons, and debris. The flasks were then shaken twice on a horizontal orbital shaker at 37 °C and 260 rpm, first for 1.5 hours followed by two exchanges with ice cold cell culture media and again for 18 hours. At this juncture, purified astrocytes attached to the flask were detached using trypsin (10 000 N$_\alpha$-benzoyl-L-arginine ethyl ester hydrochloride units/mL; Invitrogen™) diluted in HBSS for 2 to 3 minutes and pelleted by centrifugation for 10 minutes at 100 x *g*. The pellet was resuspended in cell culture media, plated onto round glass coverslips (12 mm in diameter) coated with polyethyleneimine (PEI, 1 mg/mL),[13] inlayed in plastic tissue culture dishes (round, 35 mm in diameter) containing 4 segments—each segment receiving one coverslip—and returned to the incubator for 1 hour, after which the cell suspension was replaced with cell culture media.

Transfection
The cells were transfected one day after plating with an EAAT2-EGFP plasmid (kindly provided by Dr. Jeffrey D. Rothstein, The Johns Hopkins University, Baltimore, MD) encoding EAAT2 tagged at its C-terminus with the enhanced green fluorescent protein (EGFP). Each dish received 1 µg of the plasmid and 2 µL of TransIT-293 (Mirus Bio, LLC, Madison, WI), premixed as per manufacturer's instructions. Four hours after transfection, the dishes were washed with HBSS, which was replaced with fresh culture media, and the dishes were returned to the incubator for 3 days until used in experiments.

Image acquisition
Coverslips (thickness #1, 0.13-0.16 mm, refractive index 1.5255 at λ = 564 nm and 20 °C; D-263 borosilicate glass, Erie Scientific Company; purchased via Fisher Scientific, cat. no. 12-545-82-12CIR-1D) containing cultured astrocytes were mounted onto an imaging chamber filled with an aqueous external solution (pH 7.4) consisting of sodium chloride (140 mM), potassium chloride (5 mM), calcium chloride (2 mM), magnesium chloride (2mM), D-glucose (5 mM), and HEPES (10 mM) at 20 °C - 24 °C and standard atmospheric pressure. An inverted microscope equipped with differential interference contrast (DIC; halogen lamp, 100 W) and wide-field epifluorescence illumination (xenon arc lamp, 100 W) was used with a standard fluorescein isothiocyanate (FITC) filter set (excitation 480/30x nm, dichroic 505DCXR and emission 535/40 nm), a 60x Plan Apochromatic objective lens (numerical aperture, 1.4), and Nikon Type A immersion

oil (refractive index 1.515 at 23 °C) to visualize the cells expressing EAAT2-EGFP. DIC imaging was used to visualize the cell nuclei. The Rayleigh transverse and axial resolutions of the objective were calculated to be 233 nm and 833 nm, respectively, at the 535-nm emission wavelength. Still images and time-lapse images were acquired using a CoolSNAP®-HQ cooled charge coupled device camera (Photometrics, Tucson, AZ) with an exposure time of 500 ms and MetaMorph® 6.1 software (Molecular Devices, Chicago, IL). One pixel corresponds to a square with 104.7-nm sides.

Vesicle trafficking
Trafficking of intracellular vesicles (appearing as intracellular fluorescent puncta) was performed using MetaMorph® imaging software. Time-lapse images of individual cells taken at 1.2 frames s^{-1} for 40 s were filtered using a smoothing kernel—referred to as background flattening in MetaMorph®—to accentuate the edges, resulting in false shading images. Subsequently, an intensity threshold was applied to these images. At this juncture, puncta, whose edge intensities exceeded the set threshold value and whose area was between 4 and 70 pixels, were selected for analysis, and the coordinates of their centroids were obtained in each frame. Of note, an apparent fluorescent punctum size exceeds that of the physical object studied, i.e. a trafficking vesicle, which in astrocytes is reported to be approximately 300 nm in diameter in live astrocytes.[14] For brevity, we shall refer to the coordinates of the centroid of a punctum as the position of the punctum. Puncta located fewer than 10 pixels (approximately 1 μm) from the lateral plasma membrane, puncta that could not be tracked in every frame, and puncta whose paths intersected those of other puncta were excluded from the analysis. Trafficking data for each punctum was analyzed using a custom Visual Basic script in Microsoft® Excel. The script calculated the maximal displacement, average instantaneous speed (the average of the speeds of the punctum for each time step), and trajectory angle for each punctum and plotted the trajectory of the punctum with respect to the centroid of the nucleus. To obtain the centroid of the nucleus, we first hand-traced the outline of the nuclear region based on the DIC image of the cell, which was further used to obtain the centroid using ImageJ software 1.47 (NIH, Washington, DC).

Determination of trajectory angles
Let N be the point representing the coordinates of the centroid of the nucleus, and let A and B be the endpoints of the vector representing the maximal displacement of a directional punctum (Figure 1). Also, let r_1 represent the distance between points N and A, and let r_2 represent the distance between points N and B. Then, the angle φ between the radial vector **NA** and the maximal displacement vector **Δr$_{max}$** is given by

$$\phi = \arccos\left(\frac{d}{\Delta r_{max}}\right) \qquad (1)$$

If the distance between the punctum and the nucleus centroid is much greater than the maximal displacement, i.e. $r_1 \gg r_2$, then $d \approx r_2 - r_1$. In such a case, the expression for φ can be written as

$$\phi = \arccos\left(\frac{r_2 - r_1}{\Delta r_{max}}\right) \qquad (2)$$

Since the trajectory angle must fall between +90° and −90°, we define the trajectory angle using the following expression:

$$\theta = \arccos\left(\left|\frac{r_2 - r_1}{\Delta r_{max}}\right|\right) \qquad (3)$$

We assign positive angles to the vesicles moving away from the nucleus and negative angles to the vesicles moving toward the nucleus. Thus, vesicles which move directly away from or toward the centroid of the nucleus have trajectory angles of ±0°, respectively, and vesicles which move in a tangential direction with respect to the centroid of the nucleus have trajectory angles of ±90°. The sign of the trajectory angle was determined by comparing the coordinates of the endpoints of the maximal displacement and the frames in which the punctum was positioned at those endpoints. If the x-coordinate of one endpoint was exactly equal to that of the other endpoint, the custom script threw an error and the punctum (1 of 1111 studied) was excluded from angle analysis.

Results
Astrocytes expressing EAAT2-EGFP displayed bright fluorescent puncta throughout the cell, with an apparent greater density of puncta in peripheral areas (Figure 2A), which are thinner than 1 μm and are well suited for vesicular tracking.[8-9,15] Once an astrocyte of interest was located based on its fluorescence, we acquired a corresponding DIC image of the cell. This image was used to obtain the coordinates of the centroid of the nucleus (Figure 2B). Trafficking of intracellular vesicles/puncta was performed on time-lapse images, lasting 40 s, of individual astrocytes. Each image frame was kernel-smoothened to obtain the corresponding false shading images (Figure 2C), to which we applied an operative threshold value to define putative puncta (Figure 2D, orange). The trajectories of the puncta whose edge intensities exceeded the threshold value and whose areas were between 4 and 70 pixels were determined (Figure 2D); for additional exclusion criteria, consult materials and methods.

Mobility was characterized by calculating the maximal displacement, average instantaneous speed, and trajectory angle for each punctum. Puncta whose maximal displacement
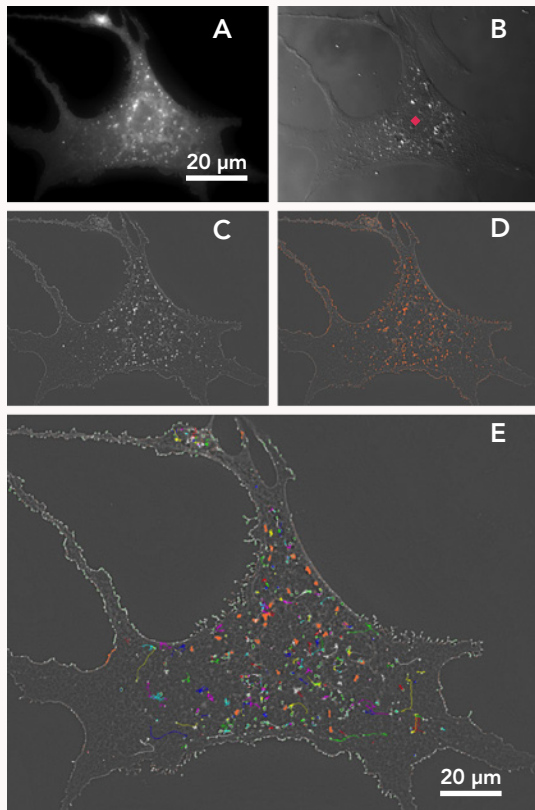
Figure 2. Visualization of EAAT2-EGFP vesicles in cultured astrocytes. (A) A typical astrocyte imaged using a FITC filter set to visualize the fluorescent puncta. (B) The cell shown in A imaged under DIC to disclose the nucleus. The red rhombus is positioned at the centroid of the nucleus. (C) Fluorescence image shown in A kernel-smoothened to obtain a false shading image. (D) An operative intensity threshold applied to the image shown in C. Puncta whose edge fluorescence intensities exceeded the threshold were identified (orange). (E) Composite motility of puncta from the 40-s time-lapse acquisition. Colored curves (other than orange) are overlaid on the false shading image to show the trajectories of the puncta within the astrocyte.

was less than 1 µm were classified as non-directional, and puncta whose maximal displacement exceeded 1 µm were classified as directional, as this distance is larger than the greatest distance which can be traveled by an average-sized secretory vesicle in 40 s under the influence of simple diffusion.[8-9] Examples of typical trajectories for non-directional and directional puncta are shown in Figure 3A. The majority of vesicles analyzed (57%; 1482 of 2593 tracked puncta from 15 astrocytes) were classified as non-directional based on their maximal displacement (Figure 3B). The distributions of average instantaneous speeds for non-directional and directional puncta were non-normal (D'Agostino test, D' = 15066.7 and 9839.2, respectively; both $p < 0.01$). The distributions were analyzed using non-parametric statistics, and, as expected, the average instantaneous speed of

directional puncta was significantly greater than that of non-directional puncta (median values of 0.142 µm/s and 0.052 µm/s, respectively; Figure 3C; Mann-Whitney U-test, $p < 0.0001$). Trajectory angles were determined for directional puncta using the method described above (Figure 3D). One punctum out of 1111 was excluded from angle analysis (see materials and methods). The distribution of trajectory angles of EAAT2-EGFP puncta was non-normal (D'Agostino test, D' = 10675.3, $p < 0.01$). However, the distribution of angles was found to be unimodal (Hartigan's dip test, $D(F_{1110}) = 0.0071$, $p > 0.05$) with angles near 0° being the most prominent (mode 7°).

Discussion

The trafficking parameters analyzed here for EAAT2-EGFP puncta compare favorably to the measurements obtained for astrocytic vesicles in similar studies. The greater proportion of non-directional vesicles (whose movement is due to diffusion) over directional vesicles (whose movement is due to active transport mechanisms) is consistent with the results from studies of trafficking of atrial natriuretic peptide vesicles[6,8] and of CB1R vesicle;[9] the directional vesicles are known to interact with actin filaments, microtubule filaments, and intermediate filaments.[6,8] Furthermore, the greater instantaneous speed of directional vesicles over non-directional vesicles is consistent with the results from the study of trafficking of CB1R vesicles.[9] Thus, movement of EAAT2 vesicles is characterized as typical of vesicular trafficking in cultured astrocytes.

The unimodality of the distribution of trajectory angles for directional puncta and the prominence of angles near 0° corroborates with the previous analysis of trajectory angles in CB1R vesicles.[9] From the consistency of these results with the previous analyses, we conclude that the method described above for determining the trajectory angles of directional vesicles is valid under the restriction that the maximal displacement of vesicles analyzed must not be on the same order of magnitude as the distance of the vesicle from the centroid of the nucleus, which is unlikely due to the size of the nucleus. Further analysis is needed to determine how large the maximal displacement needs to be with respect to the distance from the centroid of the nucleus in order to introduce noticeable error into the approximation. Although some error may be introduced by the analysis in two dimensions of vesicles that move in three dimensions, the thin areas (approximately 1 µm) of cultured astrocytes used for analysis greatly limit the motion of vesicles in the direction perpendicular to the imaging plane. Thus, this motion is unlikely to significantly affect the measurement of punctum mobility.[8] Future research concerning vesicular trafficking will utilize the method described here to characterize the trajectories of secretory vesicles in cultured astrocytes. Possible applications include methods for increasing the trafficking of EAAT2 vesicles in astrocytes, i.e. delivery of these transporters to the plasma membrane, as a means to increase the uptake of glutamate and reduce excitotoxicity.

Figure 3. Trafficking parameters for EAAT2-EGFP vesicles in cultured astrocytes. (A) Examples of typical trajectories of non-directional (lower cluster, maximal displacement 0.609 μm) and directional (upper cluster, maximal displacement 2.699 μm) puncta. Trajectories are color-coded by time (color-coding shown in the inset). The position of the centroid of the nucleus is represented by the large open circle (top right corner, not to scale). (B) Frequency of maximal displacements of puncta as a percentage of all puncta (n = 2593) from 15 astrocytes. Non-directional puncta (maximal displacement less than 1 μm) and directional puncta (maximal displacement greater than 1 μm) are marked. (C) Comparison of instantaneous speeds of directional puncta (n = 1111) to those of significantly slower non-directional puncta (n = 1482) (Mann-Whitney U-test, p < 0.0001). Boxes represent median values ± interquartile range. (D) Frequency of trajectory angles of directional puncta as a percentage of all directional puncta for which trajectory angles could be calculated (n = 1110; see materials and methods) from 15 cells. The distribution was determined to be unimodal (Hartigan's dip test, p > 0.05) with angles near 0° being the most prominent. The black arrowhead indicates the mode for the distribution (7°).

References

1. Nedergaard, M., Ransom, B., Goldman, S.A. (2003). New roles for astrocytes: redefining the functional architecture of the brain. *Trends in neurosciences* **26**, 523-530.

2. Parpura, V., Verkhratsky, A. (2012). Homeostatic function of astrocytes: Ca(2+) and Na(+) signalling. *Translational neuroscience* **3**, 334-344.

3. Hynd, M. R., Scott, H. L., Dodd P. R. (2004). Glutamate-mediated excitotoxicity and neurodegeneration in Alzheimer's disease. *Neurochemistry international* **45**, 583-595.

4. Danbolt, N. C. (2001). Glutamate uptake. *Progress in neurobiology* **65**, 1-105.

5. Hertz, L., Dringen, R., Schousboe, A., Robinson, S. R. (1999). Astrocytes: glutamate producers for neurons. *Journal of neuroscience research* **57**, 417-428.

6. Potokar, M., Kreft, M., Li, L., Daniel Andersson, J., Pangrsic, T., Chowdhury, H. H., Pekny, M., Zorec R. (2007). Cytoskeleton and vesicle mobility in astrocytes. *Traffic* **8**, 12-20.

7. Kreft, M., Potokar, M., Stenovec, M., Pangrsic, T., Zorec, R. (2009). Regulated exocytosis and vesicle trafficking in astrocytes. *Annals of the New York Academy of Sciences* **1152**, 30-42.

8. Potokar, M., Kreft, M., Pangrsic, T., Zorec, R. (2005). Vesicle mobility studied in cultured astrocytes. *Biochemical and biophysical research communications* **329**, 678-683.

9. Osborne, K. D., Lee, W., Malarkey, E. B., Irving, A. J., Parpura, V. (2009). Dynamic imaging of cannabinoid receptor 1 vesicular trafficking in cultured astrocytes. *ASN neuro* **1**, 283-296.

10. Reyes, R. C., Perry, G., Lesort, M., Parpura, V. (2011). Immunophilin deficiency augments Ca2+-dependent glutamate release from mouse cortical astrocytes. *Cell Calcium* **49**, 23-34.

11. Gottipati, M. K., Kalinina, I., Bekyarova, E., Haddon, R. C., Parpura, V. (2012). Chemically functionalized water-soluble single-walled carbon nanotubes modulate morpho-functional characteristics of astrocytes. *Nano letters* **12**, 4742-4747.

12. McCarthy, K. D., de Vellis, J. (1980). Preparation of separate astroglial and oligodendroglial cell cultures from rat cerebral tissue. *The Journal of cell biology* **85**, 890-902.

13. Lee, W., Parpura, V. (2012). Dissociated cell culture for testing effects of carbon nanotubes on neuronal growth. *Methods Mol Biol* **846**, 261-276.

14. Malarkey, E. B., Parpura, V. (2011). Temporal characteristics of vesicular fusion in astrocytes: examination of synaptobrevin 2-laden vesicles at single vesicle resolution. *The Journal of physiology* **589**, 4271-4300.

15. Haydon, P. G., Lartius, R., Parpura, V., Marchese-Ragona, S. P. (1996). Membrane deformation of living glial cells using atomic force microscopy. *Journal of microscopy* **182**, 114-120.

Dark matter and the mystery of orbital velocities

Joshua Plottel[1], Joseph Harrison[2]

[1]Department of Physics, Rensselaer Polytechnic Institute, Troy, New York
[2]Department of Physics, University of Alabama at Birmingham, Birmingham, Alabama

Abstract

Beginning with the seminal work of Fritz Zwicky, the existence of dark matter has been one accepted explanation for why orbiting objects in galaxy clusters do not obey the expected Newtonian fall-off with distance. The composition of dark matter has been hypothetically described in several ways, including "Massive Astrophysical Compact Halo Objects" and "Weakly Interacting Massive Particles." This paper explores the possibility that dark matter is actually the relativistic mass associated with the gravitational potential energy (U) of these systems, i.e., U/c^2. Data were acquired on the orbital velocities and radii of several galaxies, and analysis revealed that U could be directly related to an integral that could be evaluated solely from that data. The inertial masses for those systems were also extracted from the same data. The calculated inertial masses were in reasonable agreement with published values. However, relativistic masses were found to be five to seven orders of magnitude smaller than inertial masses. Further work is required before a definitive conclusion may be reached, and suggestions for such work are discussed.

Introduction

The orbital velocities of galaxies do not fall off in the expected Newtonian fashion (as $1/\sqrt{r}$), but rather they approach a constant with increasing radius (Figure 1). Without redefining fundamental laws of nature, this implies that galaxies must contain more mass than we have previously accounted for.[1] There are several possible explanations for this discrepancy. Perhaps the most intriguing involve dark matter (first proposed to exist by Fritz Zwicky in 1933, to explain his own observations of the Coma Cluster[2]), as hypothetically described in terms of Massive Astrophysical Compact Halo Objects (MACHOs)[3-4] and/or Weakly Interacting Massive Particles (WIMPs).[4] Other proposed explanations, including MOND (Modified Newtonian Dynamics)[5], have involved fundamental modifications of basic equations such as Newton's Law of Gravitation; however, these are outside the scope of this paper.
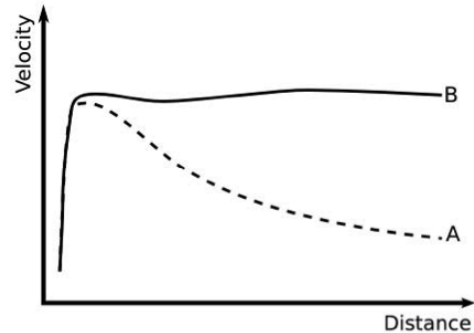

Figure 1. An illustration of the rotation curve of a typical spiral galaxy, where curve A represents the Newtonian prediction and curve B shows the actual observation.

Theory

In the traditional Newtonian formulation of the orbiting mass in a gravitational field, the centripetal force relation is

$$m\frac{v^2}{r} = G\frac{Mm}{r^2} \qquad (1)$$

where m is the mass of the orbiting object, r is the distance from the center of orbit, v is the centripetal velocity, and G is the universal gravitational constant (approximately $6.67 \cdot 10^{-11}$ N·m²·kg⁻²). Equation 1 simplifies to

$$\frac{v^2}{r} = \frac{GM}{r^2} \quad \rightarrow \quad v^2 = \frac{GM}{r} \qquad (2)$$

which leads to the following relationship of the orbital speed v to the radius r:

$$v = \sqrt{\frac{GM}{r}} \qquad (3)$$

One may also arrive at this relationship using a more general approach based on the Virial Theorem.[6] However, these calculations contradict observations, and this discrepancy led Zwicky to predict the existence of previously unobserved "dark" matter. We approach the problem of calculating the mass of this dark matter in two different ways.

The first method utilizes the following relationship between the centripetal force and the gravitational field:

$$\frac{v^2}{r} = |\vec{g}| = |-\vec{\nabla}\Phi|$$

(4)

where the gravitation potential (Φ) associated with the mass density (ρ) is given by

$$\Phi = -G \iiint \frac{\rho(\vec{r}')}{|\vec{r} - \vec{r}'|} d^3r'$$

(5)

Equation 5 leads to

$$\Phi = -G \iiint \rho(r') Y_{00}(\theta', \phi') \sum_{l=0}^{\infty} \frac{4\pi}{2l+1} \frac{r_<^l}{r_>^{l+1}} \sum_{m=-l}^{l} Y_{lm}^*(\theta', \phi') Y_{lm}(\theta, \phi) \, d\Omega' r'^2 \, dr'$$

(6)

Because r has a spherical form, the orthonormality of the spherical harmonics reduces the series in l, m to only the term for l = 0, m = 0. Thus, Equation 6 becomes

$$\Phi(\vec{r}) = -4\pi G \int_0^{\infty} \rho(r') r'^2 \frac{1}{r_>} \, dr' = -\frac{4\pi}{r} \int_0^r \rho(r') r'^2 \, dr' - 4\pi \int_r^{\infty} \rho(r') r' \, dr'$$

(7)

By choosing a spherically symmetric form for the dark matter density (ρ), such as

$$\rho(r) = \sum_{n=-1}^{2} a_n r^n e^{-\alpha_n r}$$

(8)

one can indirectly fit the density of matter in the following way. Inserting Equation 8 into Equation 7 results in a closed form for $\Phi(r)$. Taking the gradient of this expression and using it in Equation 4 to obtain the specific form that was utilized for this method yields

$$v^2 = 4\pi G \cdot \sum_{n=-1}^{2} \left(a_n \cdot \left(\frac{-e^{-\alpha_n r}}{r} \cdot \left(\sum_{b=0}^{(n+2)} (-1)^b \cdot \frac{(n+2)! \cdot r^{((n+2)-b)}}{((n+2)-b)! \cdot (-\alpha_n)^{(b+1)}} \right) - \left(\frac{(-1)^{(n+2)}}{r} \cdot \frac{(n+2)!}{(-\alpha_n)^{(n+3)}} \right) \right) \right)$$

(9)

Thus, using Equation 9 to fit data for the orbital speeds at different radial distances provides the parameters a_n and α_n, which give a fit of the density (Equation 8).

The second method of accounting for the dark matter density is based on the assumption that the dark matter itself is merely the relativistic mass given by the gravitational potential energy (U) divided by the square of the speed of light.[7] The gravitational potential energy of the system is given by

$$U = -\frac{G}{2} \cdot \iint \frac{\rho(\vec{r}')\rho(\vec{r})}{|\vec{r} - \vec{r}'|} d^3r' \, d^3r = -\frac{G}{2} \cdot \int \left(\vec{\nabla} \bullet \left[(\vec{\nabla}\Phi(\vec{r}))\Phi(\vec{r}) \right] - (\vec{\nabla}\Phi(\vec{r}))^2 \right) dr$$

(10)

Using the Poisson equation:

$$\nabla^2 \Phi = 4\pi G \rho(\vec{r})$$

(11)

Equation 10 can be rewritten as

$$U = -\frac{1}{8\pi G} \iiint \left(\left[\vec{\nabla} \bullet (\Phi(\vec{r})\vec{\nabla}\Phi(\vec{r})) \right] - |\vec{g}|^2 \right) d^3r$$

(12)

Using the Divergence Theorem $\iiint_V \vec{\nabla} \bullet \vec{A} \, d^3r = \oiint \vec{A} \bullet \hat{n} \, dS$, the first term in Equation 12 turns into a surface integral: $\oiint (\Phi(\vec{r})\vec{\nabla}\Phi) \bullet \hat{r} \, dA$, where dA is the surface area differential. It is expected that $(\Phi(\vec{r})\vec{\nabla}\Phi)$ will drop off as $1/r^3$ while the surface area will grow as r^2. Thus, for large surface area, this term will go to zero. Under these conditions, the first term of Equation 12 can be neglected. Additionally, by making use of Equation 4, the second term of Equation 12 can be rewritten as

$$U = \frac{1}{8\pi G} \cdot \int_0^\infty 4\pi v^4 dr \qquad (13)$$

Yielding the following expression for the mass:

$$\frac{U}{c^2} = mass = \frac{1}{2Gc^2} \cdot \int_0^\infty v^4 dr \qquad (14)$$

Then, by using a smooth spline of the data for v, Equation 14 can be used to obtain values for the inertial mass.
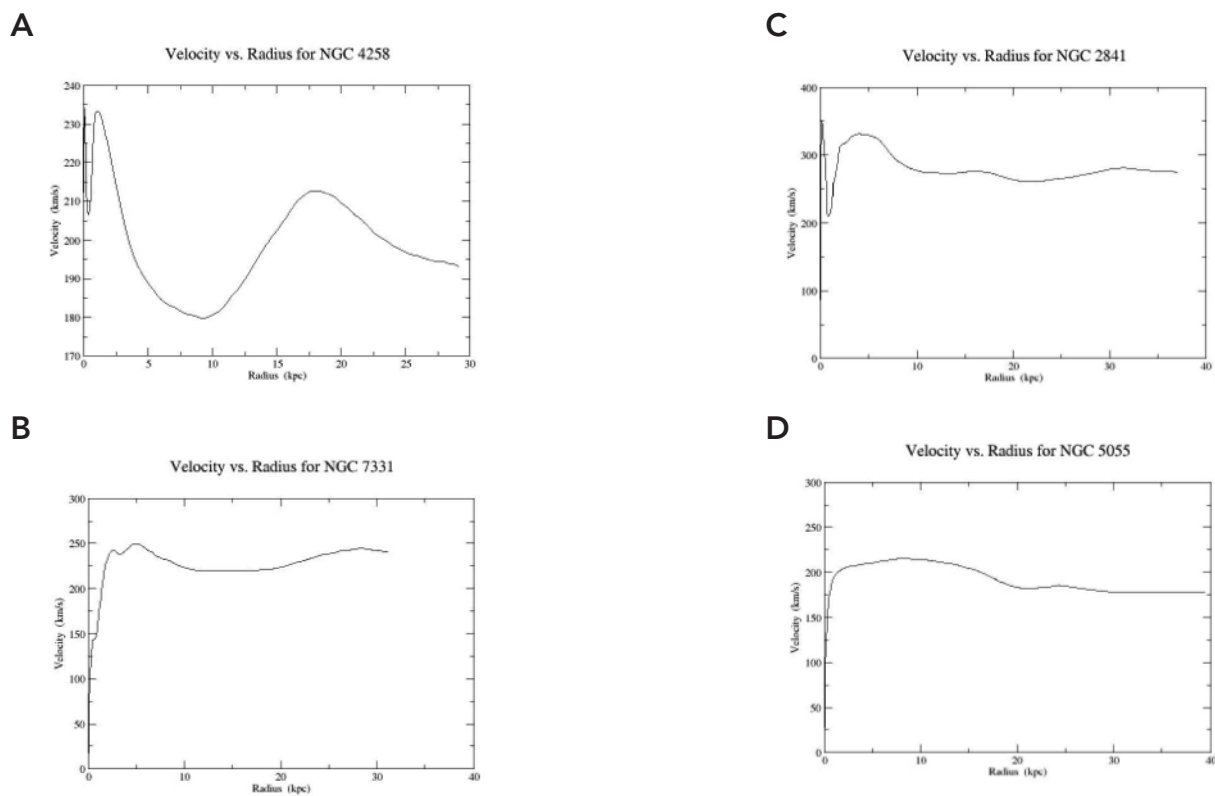
A

C

B

D

Figure 2. Orbital velocity vs. radius data for four galaxies. These data were manipulated using the fit formulas above. (A) NGC 4258; (B) NGC 7331; (C) NGC 2841; (D) NGC 5055.

Methods

In order to test the formulas derived herein, we utilized previously collected data relating orbital velocity to radius for several different galaxies (Figure 2).[8]

Non-linear regression analysis techniques were implemented to analyze and acquire fits to the data. First, the orbital velocity vs. radius data were read-in and plotted. A cubic spline was performed on the resulting curve to yield more data points. Then, the orbital velocity data points were squared and plotted against radius. Next, the fit formula (Equation 9) was applied to the data curve using the non-linear curve fitting command. This process was repeated using different weight factors to achieve better fits. Integrating these fits led to a numerical expression for the mass. The effects of choosing different weighting schemes were analyzed. The number of terms and the weighting factors were both chosen in order to acquire an adequate fit within a reasonable amount of time.

Results

Figure 3 shows an example of the change in the fit curves when a special weight factor is considered. Table 1

demonstrates how the fit coefficients change when a weight factor is considered. Notice that the fit coefficients change dramatically with different weight factors. Table 2 shows that the effect of the weighting factors on the computed values of the inertial masses is nearly negligible. It is reassuring that the calculated values in Table 2 do not dramatically change with the application of different weight factors. However, there were some unusually small exponential fit coeffcients that, when integrated, resulted in an abnormally large masses, thereby indicating an unacceptable fit.
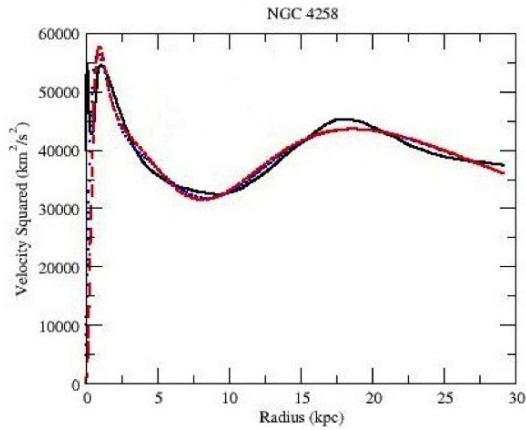

Figure 3. Change in fit curves with application of a weighting factor. The black solid curve is the original data; the blue dotted curve is a fit curve with a weight factor of $1/y^2$ applied; and the red dashed curve is a fit curve with a weight factor of x applied.

Table 1. Fit coefficients for NGC 4258 with three different weight factors applied.

Fit Coefficients	Weightings		
	none	$1/y^2$	x
a_0	415946	7.53622	16553.5
α_0	1.84251	0.000168461	0.254778
a_1	5.54981×10^{08}	12155.1	9.84164×10^{06}
α_1	3.19916×10^{06}	0.374986	5.53256
a_2	115.6	-4575.73	-2901.03
α_2	0.310573	0.52443	0.586648
a_3	3.11283×10^{06}	406326	7968.32
α_3	16.2339	2.18831	0.53555

Table 2. Effect of weighting factors on the computed values of the inertial masses. The weight factor applied is listed in parentheses. Units are in 10^{11} Solar Masses (M_{Sun}).

Galaxy Name	Inertial Mass (none)	Inertial Mass (x)	Inertial Mass (x^2)	Inertial Mass (1/y)	Inertial Mass $(1/y^2)$
NGC 4258	2.568487	2.53515	2.54748	2.47193	7328308.0*
NGC 7331	90.89388	784450800.0*	3453.271*	27.61070	8.59987
NGC 2841	24.74469	13.07116	12.27777	9.62400	80.72964
NGC 5055	64.67777	80.60132	42172660.0*	452144.7*	3.67188

*Anomalous results discussed in text.

The relativistic mass plots in Figure 4 have no obvious plateaus. This is indicative of the lack of orbital velocity data beyond that of the luminous matter. Because these plots do not flatten out by 40 kiloparsecs (kpc), we cannot predict what happens to the orbital velocity beyond that radius.

As can be seen in Figure 5, the inertial masses do eventually become relatively constant at a radial distance between approximately 30 and 80 kpc.

It is clear from Figure 6A that between 25 kpc and 30 kpc, there is a crossover of the monotonic increase of the relativistic mass where the inertial mass plateaus. Table 3 gives a side-by-side comparison of the calculated values for both the relativistic mass and the inertial mass of each galaxy.

Table 3. Comparison of relativistic and inertial masses (calculated with no weight factor considered).

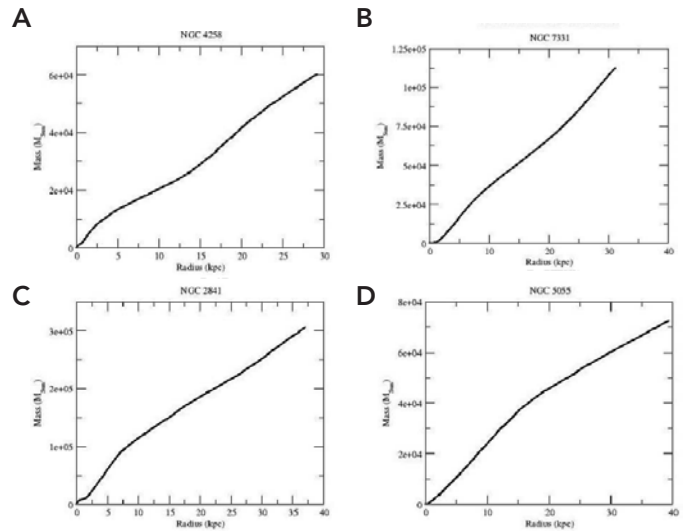| Galaxy	Relativistic Mass (10^4 Solar Masses)	Inertial Mass (10^{11} Solar Masses)
NGC 4258	6.00774	2.56847
NGC 7331	11.24428	90.89388
NGC 2841	30.53165	24.74469
NGC 5055	7.24629	64.67777

Figure 4. Distribution of the relativistic mass as a function of radius for four galaxies: (A) NGC 4258; (B) NGC 7331; (C) NGC 2841; (D) NGC 5055.
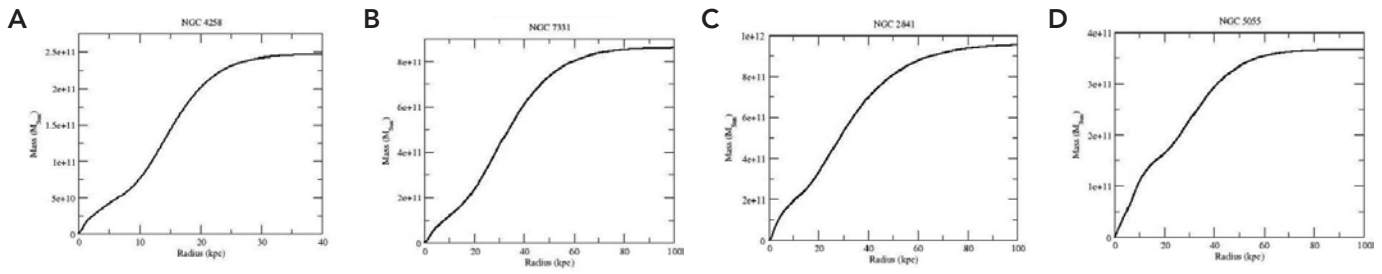
Figure 5. The distribution of the inertial mass as a function of radius for four galaxies: (a) NGC 4258; (b) NGC 7331; (c) NGC 2841; (d) NGC 5055.
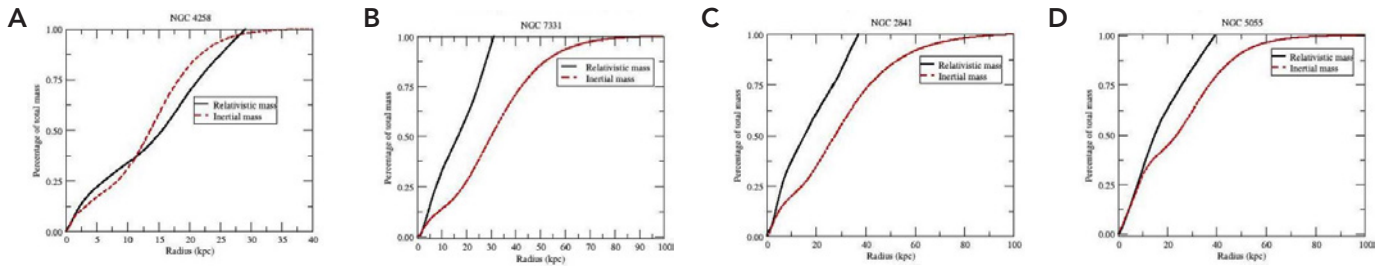

Figure 6. The distribution of the overall mass as a function of radius for four galaxies: (A) NGC 4258; (B) NGC 7331; (C) NGC 2841; (D) NGC 5055.

Discussion

Einstein's famous mass-energy relation, $E = mc^2$, is not simply a relationship between an intrinsic energy and an object's rest mass; that is just a special case of the more general statement. Ascribing inertial properties to an object based on its energy content was an unexpected outcome of Einstein's work with special relativity. It was so groundbreaking and surprising that it prompted Einstein to publish a short comment after his first paper on special relativity.[7] One salient quote from that paper embodies our point: "If a body gives off the energy L in the form of radiation, its mass diminishes by L/c^2. The fact that the energy withdrawn from the body becomes energy of radiation evidently makes no difference, so that we are led to the more general conclusion that the mass of a body is a measure of its energy content."

In this study, the energy content of the gravitational field was assessed for its inertial content by integrating the energy density $\frac{1}{8\pi}|\vec{g}|^2$. The field strength $|\vec{g}|$ was inferred from the velocity data for the various galaxies (Equation 4). The shortfall, discussed below, is that velocity data were only available out to a certain radius, and so a proper treatment of the field strength beyond that point could not be obtained.

The fit formula (Equation 9) was first computed for n = 0 through n = 2. Then, an n = −1 term was added to that interval. Including the n = −1 term allowed the formula to better account for the more rapid change of the density with radius in this region. In the future, addition of an n = 3

term may further improve the fit. The calculations described are limited by the radius of the available data; i.e., we can only compute the mass of the dark matter that is contained within the observed luminous matter halo. Thus if there is a dark matter halo that extends farther from the center of the galaxy than the measured luminous matter halo, then limiting the radius of the data impacts the results. Essentially, the measurement is restricted by the boundary of the luminous matter (Figure 7).
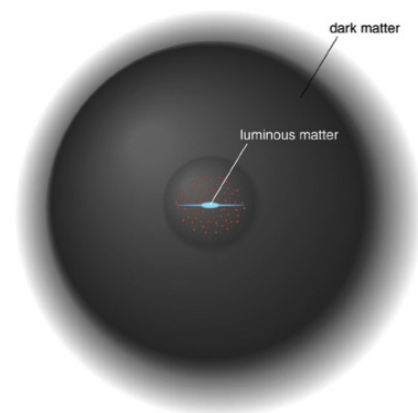

Figure 7. An artist's rendering of a dark matter halo surrounding the luminous matter of a galaxy.[9]

Calculated inertial masses were in agreement with published literature values. Relativistic masses, however, were found to be approximately 5 to 7 orders of magnitude smaller than

inertial masses. Relativistic masses, unlike inertial masses, did not approach asymptotic values. Reaching an asymptotic value implies that the mass density beyond a certain radius is negligible, so that integration beyond that point does not change the value of the total mass. The lack of an asymptotic value for the relativistic masses indicates that our data do not encompass such a radial value. Unfortunately, it is unclear how to evaluate the gravitational potential energy beyond where orbital velocity data are available, unless further assumptions are made. The reason for this is that calculations in this paper were based on orbital velocity data, of which there are no measurements beyond a certain radial extent. It may be possible to solve this issue by fitting the relativistic mass density with a functional form (Equation 14) similar to that of Equation 8, and then integrating the expression to yield relativistic mass.

$$relativistic\ mass = \int_0^\infty \frac{v^4}{2Gc^2r^2}dr \quad (15)$$

One area of future work will be to apply this analysis to larger systems, such as galaxy clusters.

Acknowledgments

This manuscript was prepared with the AAS LATEX macros v5.2.

References

1. Hibbs, P. (2005). GalacticRotation2.png. Image. Retrieved 15 July 2013 from *www.commons.wikimedia.org/wiki/File:GalacticRotation2.png*.

2. Zwicky, F. (1933). *Helv. Phys. Acta* **6**, 110127. Swiss Physical Society. Translated in Gen Relativ Gravit (2009). **41**, 207-224.

3. Griest, K. (1990). *Astrophys. J.* **366**, 412-421.

4. Griest, K. (1993). *Annals of the New York Academy of Sciences* **688**, 390-407.

5. Kroupa, P. *et al.* (2012). *Int. J. Mod. Phys. D* **21**, 1230003.

6. Taylor, J. (2005). *Classical Mechanics*. University Science Books: Sausalito, CA.

7. Einstein, A. (1905). Ist die Trägheit eines Körpers von seinem Energiegehalt abhängig? *Annalen der Physik* **18**, 639. Translated in Perrett, W., Jeffrey, G. B. Does the Inertia of a Body Depend on its Energy-Content? Retrieved from www.fourmilab.ch.

8. Sofue, Y. *et al.* (1999). *Astrophys. J.* **523**, 136-146.

9. Luminous Matter: Diagram. 22-01.jpg. Image. Retrieved 24 July 2013 from www.physast.uga.edu/~rls/astro1020/ch22/ovhd.html. Image available directly at www.physast.uga.edu/~rls/1020/ch22/22-01.jpg.

research paper

Comparison of the X-ray Crystal Structures of Two Mo(CO)5(Ph2PXR) (R = Pri; X = O; R = C6H4-4-Me) Complexes

Shakyra Tyus and Gary M. Gray

Department of Chemistry, University of Alabama at Birmingham

Abstract
Transition metal complexes of the type $Mo(CO)_5(PPh_2(XR))$ (X = O, R = (CH_3) (**1**); X = NH, R = C_6H_4-*p*-CH_3 (**2**)), where PPh_2 = diphenylphosphine, were synthesized in a previous study, and **2** has been recrystallized and characterized by small molecule X-ray crystallography. In this study the recrystallization of **1**, along with an analysis of the X-ray crystallographic data obtained, is presented. Complex **1** crystallizes in a *P*-1 space group and is arranged in a primitive triclinic Bravais lattice with cell dimensions $\underline{a}$ = 12.0804(5) Å, $\underline{b}$ = 13.4548(5) Å, $\underline{c}$ = 13.5947(6) Å, α = 92.405(2) °, β = 99.725(3) °, γ = 106.263(2) °, Z=2. Various bond lengths, bond angles, and torsion angles from **1** are compared to those of **2** in order to deduce steric and electronic properties of the molecules.

Keywords: *molybdenum, X-ray crystallography, phosphorus-donor ligands*

Introduction

Over the past 60 years, researchers have been interested in transition metal complex chemistry. This interest is sparked by the fact that a wide range of organic reactions can be catalyzed by transition metal complexes.[1] Phosphorus-donor ligands have been found to be important for use in transition metal catalysts[2] because these ligands affect both the activities and the selectivities of the catalysts through bonding interactions of substrates with transition metal centers. Both electronic (Lewis donor ability and hard-soft nature) and steric properties contribute to the ligand effects. The hard-soft nature of the ligand is imperative because metals that are hard acids tend to bond strongly with second row bases, while metals that are soft acids prefer third, fourth and fifth row bases.[3] Overall, hard acids would prefer to bond with hard bases and soft acids to soft bases.
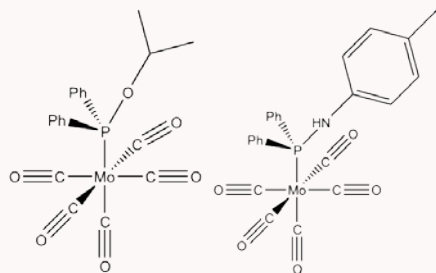

Figure 1. Mo(CO₅)(phosphorus-donor ligand) complexes 1 (left) and 2 (right).[2]

One of the best tools for characterizing the steric and electronic effects of ligands in transition metal complexes is X-ray crystallography. In this paper, we report the X-ray crystal structure of $Mo(CO)_5(PPh_2(OCH_3))$ (**1**, Figure 1 left) and compare the results to those previously obtained for $Mo(CO)_5(PPh_2(NHC_6H_4$-*p*-$CH_3))$ (**2**, Figure 1 right). The effects of the unique substituent on the phosphorus donor ligand's electronic properties are also described.

Materials and Methods

Synthesis and characterization of the complexes
Both complexes were previously prepared and the procedures for their syntheses are found in the chemical literature.[4] Complex **1** was purified by flash chromatography through silica gel with a 1:1 dichloromethane/hexanes eluent mixture. The resultant solution was thermally recrystallized, yielding X-ray quality crystals. The crystal structure of **2** has been previously reported.[2]

X-Ray data collection and solution
A suitable single crystal of **1** was mounted on a MiTeGen loop in immersion oil and aligned upon a Bruker SMART APEX CCD area-detector using Cu Kα radiation (λ = 1.54178 Å) and equipped with an Oxford Cryosystems low-temperature device. The frames were integrated with the Bruker SAINT software package using a narrow-frame algorithm. The integration of the data yielded reflections to a maximum θ angle of 66.90° (0.84 Å resolution). All of the reported angles were greater than $2\sigma(F^2)$. The final cell constants are based upon the refinement of the XYZ-centroids of 50 reflections above 20 σ(I) with 9.079° < 2θ < 59.92°. Data were corrected for absorption effects using the numerical method (SADABS). The space groups of the crystals were assigned on the basis of systematic absences and intensity statistics. Analytical scattering factors of each compound were corrected for both *Δf'* and *iΔf''* components of anomalous dispersion.[5]

The structure was solved and refined using the Bruker SHELXTL Software Package. Full-matrix refinements of the positional and anisotropic thermal parameters for all non-hydrogen atoms versus F^2 were carried out. All hydrogen atoms were placed in calculated positions with the appropriate molecular geometry and δ (C-H) = 0.96 Å. The isotropic thermal parameter of each hydrogen atom was fixed equal to 1.2 times the U_{eq} value of the atom to which it was bound.

Crystallographic data has been deposited in the Cambridge Crystallographic Database.[5]

Results

The crystal structure of **1** (Figure 2) has two molecules in the asymmetric unit, which will hereafter be referred to as molecule 1 and molecule 2. Important bond lengths for both molecules are given in Table 1, important bond angles are given in Table 2, and important torsion angles are given in Table 3. The number in parentheses to the right of the bond lengths, bond angles and torsion angles are the estimated standard deviations in the last significant digit of each number. For example, the C18-Mo1-P1-Cl2 torsion angle is listed as -111.65(15)°, meaning that the measured angle was found to be -111.65°, and has an estimated standard deviation of 0.15°. Significances in the difference between two measurements were computed using Eq. 1.[6]

$$q = \frac{(x_1 - x_2)}{\sigma_1^2 + \sigma_2^2} \qquad (1)$$

In the equation above, x corresponds to the respective measurements and σ is the respective standard deviations. A difference is significant with 99% certainty when $q > 2.58$.

The bond lengths in Table 1 are used to compare the bonds between the molybdenum and the ligands of the two molecules within the unit cell. The bond angles in Table 2 and the torsion angles in Table 3 are used to compare the conformations of the two molecules in the asymmetric unit.
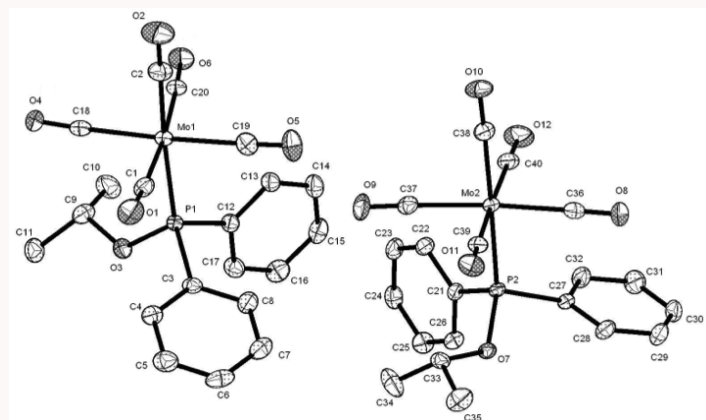

Figure 2. ORTEP drawing of 1, showing two molecules in the asymmetric unit. Thermal ellipsoids are drawn at 30% and hydrogen atoms are omitted for clarity.

*Table 1. Bond lengths (Å) of **1**.*

Atom 1	Atom 2	Bond length (esd) (Å)
Mo1	C2[a]	2.011(4)
Mo1	C1[b]	2.060(4)
Mo1	C18[b]	2.050(4)
Mo1	C19[b]	2.064(4)
Mo1	C20[b]	2.037(4)
Mo1	P1	2.5279(8)
Mo2	C36[b]	2.057(4)
Mo2	C37[b]	2.040(4)
Mo2	C38[a]	2.025(3)
Mo2	C39[b]	2.066(4)
Mo2	C40[b]	2.066(4)
Mo2	P2	2.4982(8)

[a]Carbonyl *trans* to phosphorus
[b]Carbonyl *cis* to phosphorus

*Table 2. Bond angles (°) of **1** as compared to those of **2**.*

	Atom 1	Atom 2	Atom 3	Bond Angle (esd) (°)
Molecule 1	P1	Mo1	C1	90.80(10)
	P1	Mo1	C2	176.35(12)
	P1	Mo1	C18	97.46(9)
	P1	Mo1	C19	88.03(11)
	P1	Mo1	C20	90.63(10)
	O3	P1	Mo1	120.78(9)
	C12	P1	Mo1	113.10(10)
	C3	P1	Mo1	118.47(10)
	C2	Mo1	C18	86.18(15)
	C2	Mo1	C19	88.32(16)
Molecule 2	P2	Mo2	C36	89.86(10)
	P2	Mo2	C37	88.08(9)
	P2	Mo2	C38	173.97(11)
	P2	Mo2	C39	96.84(9)
	P2	Mo2	C40	86.53(10)
	O7	P2	Mo2	120.27(8)
	C27	P2	Mo2	112.83(10)
	C21	P2	Mo2	117.62(9)
	C38	Mo2	C39	88.79(14)
	C38	Mo2	C40	87.90(14)

	Atom 1	Atom 2	Atom 3	Atom 4	Torsion Angle (esd) (°)
Molecule 1	C18	Mo1	P1	O3	2.28(15)
	C18	Mo1	P1	C12	-111.65(15)
	C18	Mo1	P1	C3	131.18(15)
Molecule 2	C39	Mo2	P2	O7	3.32(13)
	C39	Mo2	P2	C27	-112.01(14)
	C39	Mo2	P2	C21	130.75(14)

Table 4. Bond lengths (Å) of **2**.

Atom 1	Atom 2	Bond length (esd) (Å)
Mo	C20[a]	1.995 (4)
Mo	C21[b]	2.034 (4)
Mo	C22[b]	2.032 (4)
Mo	C23[b]	2.061 (4)
Mo	C24[b]	2.050 (4)
Mo	P	2.5274 (9)

[a]Carbonyl *trans* to phosphorus

[b]Carbonyl *cis* to phosphorus

Table 5. Bond Angles (°) of **2**.

Atom 1	Atom 2	Atom 3	Bond Angle (esd) (°)
P	Mo	C20[a]	177.71 (10)
P	Mo	C21[b]	86.82 (10)
P	Mo	C22[b]	93.60 (10)
P	Mo	C23[b]	92.76 (9)
P	Mo	C24[b]	92.01 (10)
N	P	Mo	118.13 (9)
C1	P	Mo	113.41 (11)
C7	P	Mo	118.64 (10)

[a]Carbonyl *trans* to phosphorus
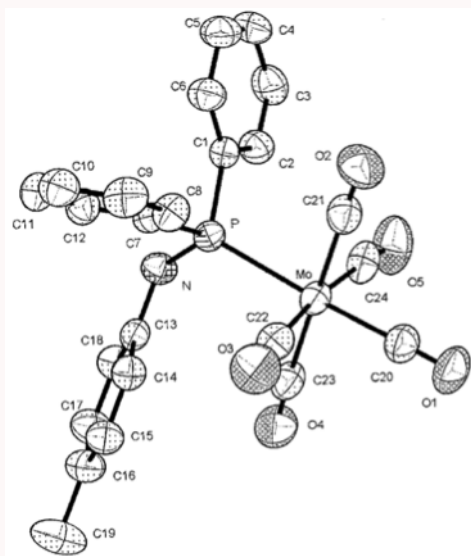
[b]Carbonyl *cis* to phosphorus

Figure 3. ORTEP drawing of the molecular structure of **2***. Thermal ellipsoids are drawn at 50% and hydrogen atoms are omitted for clarity.*

Unlike the crystal structure of **1**, the previously reported crystal structure of **2** (Fig. 3) has only one molecule in the asymmetric unit. Tables 4 and 5 contain important bond lengths and angles for **2**. This data allows the effects of the different phosphorus substituents in the two compounds to be compared.

Discussion

The crystal structure of **1** (Figure 2) has two molecules in the asymmetric unit. This allows for the comparison of conformations between the two molecules, as well as the identification of common structural features. The conformations of the two molecules are also compared to those of **2**.

The coordination geometry of the molybdenum in each molecule of **1** is a distorted octahedron due to the steric effects of the large phosphorus-donor group. The two molecules of **1** exhibit similar distortions with one of the P-Mo-C$_{cis}$ angles, defined by P1-Mo1-C18 and P2-Mo2-C39, respectively. Both of the aforementioned angles are significantly larger than the

expected angle of 90°, while the other three P-Mo-C$_{cis}$ angles in each molecule are slightly smaller than the ideal angle of 90°. The P-Mo-C$_{trans}$ angle is also significantly smaller than the expected angle of 180° (molecule 1: 176.35(12)°; molecule 2: 173.97(11)°).

To fully understand the distortions in the two molecules of **1**, the torsion angles from the carbonyl most closely aligned with one of the three phosphorus substituents were compared (Table 3). These are very similar for the two molecules and indicate that the isopropoxy group and the most distorted *cis* carbonyl group are eclipsed. The steric repulsion between these groups must be high and may give rise to the larger than expected P-Mo-C$_{cis}$ bond angles.

The steric interactions between the isopropoxy group and the most distorted *cis* carbonyl can result in other distortions. The C$_{cis}$-Mo-C$_{trans}$ angle is smaller than 90° (molecule 1: C2-Mo1-C18, 86.18(15)°; molecule 2: C38-Mo2-C39, 88.79(14)°), and the C$_{cis}$-Mo-C$_{trans}$ angle to the *cis* carbonyl opposite the most distorted *cis* carbonyl is also smaller than 90° (molecule

1: C2-Mo1-C19, 88.32(16)°; molecule 2: C38-Mo2-C40, 87.90(14)). This distortion can be envisioned as a tilting of the $Mo(CO)_5$ group away from the isopropoxy substituent of the phosphorus and a simultaneous compression of the *cis* carbonyls toward the *trans* carbonyl.

The distortion in coordination geometry in **1** is different from that in **2**. Three of the P-Mo-C_{cis} angles in **2** are significantly larger than 90°, while only one of these angles in **1** is significantly larger than 90°. However, the magnitudes of these distortions in **2** are not as large as those in **1**. This comparison suggests that the primary distortion in **2** is a compression of the *cis* carbonyls toward the *trans* carbonyl and that there is less tilting of the phosphorus ligand relative to the plane formed by the *cis* carbonyls.

The second interesting aspect of structures of the molecules of **1** is the correlation between the molybdenum-carbonyl ligand bonding and the Mo-C bond lengths. The Mo-C_{trans} bonds are shorter than all of the Mo-C_{cis} bonds (Table 1). More precisely, in molecule 1, the difference between the Mo-C_{trans} bond length (Mo1-C2, 2.011(4) Å) is significantly shorter than the average of the Mo-C_{cis} bonds (average Mo-C_{cis}, 2.053(8) Å), using equation 1. Likewise, the difference between the Mo-C_{trans} bond length in molecule 2 (Mo2-C38, 2.025(3)Å) the Mo-C_{cis} bonds (average Mo-C_{cis}, 2.049(7)Å) is also significant. This is consistent with bonding theories for $Mo(CO)_5$(phosphorus ligand) complexes, which predict that there should be more π-backbonding from the molybdenum to the *trans* carbonyl than from the molybdenum to the *cis* carbonyl,[7] resulting in a higher bond order and a shorter bond distance.[3]

A significant difference between the Mo-C_{trans} (Mo-C20, 1.995(4) Å) and the average of Mo-C_{cis} bonds (average Mo-C_{cis}, 2.044(8)Å) is also observed in **2**. However, both of these distances are shorter than those in either of the molecules in **1**. This suggests that there is more π-backbonding in **2** than in **1**. This is consistent with the isopropoxy substituent in **1** being more electron-withdrawing than is the *p*-tolylamido group in **2**, which makes the phosphorus ligand in **1** a poorer Lewis base than the ligand in **2**.

Conclusions
The comparison of the crystal structures of **1** and **2** has shown that the phosphorus ligands in these complexes have different electron-donor and steric properties. The ligand in **2** is a better electron donor, but does not appear to be as sterically demanding. Since both steric and electronic effects are important in determining the activity of catalysts containing such ligands, it might be expected that catalysts containing the two ligands might exhibit differences in activity and/or selectivity.

References
1. Kramer, P., van Leeuwen, P. (2012). *Phosphorus (III) ligands in homogeneous catalysis: Design and synthesis.* Hoboken, NJ: Wiley.

2. Butler, J. M., Knight, T. E., Sotoudehnia, S., Kadle, P. D., Green, S. L., Gray, G. M. (2004). *J. Chem. Crystallogr.* **34**, 111-118.

3. Atkins, P., Overton, T., Rourke, J., Weller, M., Armstrong, F. (1984). Chapter 4: Acids and bases. *Inorganic Chemistry* 5th ed. Oxford: Oxford UP, 2010. 116-19. Print.

4. Gray, G.M. (1984). Synthesis and multinuclear NMR and mass spectroscopic study of some Mo(CO)$_5$(PPh)$_2$XR) (X = O, S, NH; R = alkyl, aryl, Me$_3$Si) complexes. Chemical shift correlations with *cis*-Mo(CO)$_4$(PPh)$_2$XR)$_2$ chemical shifts. *Inorg. Chim. Acta.* **81**(2), 157-62.

5. Sheldrick, G.M. (2001). SHELXTL NT Version 6.12.

6. Glusker, J. P., Lewis, M., Rossi, M. (1994). *Crystal structure analysis for chemists and biologists.* (pp. 429-430). Hoboken, NJ: Wiley.

7. Gray, G. M., Fish, F. P., Srivastava, D. K., Varshney, A., van der Woerd, M. J., Ealick, S. E. (1990). X-ray crystallographic studies of three heterocyclic complexes of the type *cis*-Mo(CO)$_4${(R$_2$PO)$_2$Si(Me)R'} (R$_2$ = OCH$_2$CMe$_2$CH$_2$O; R' = Me, Bu^t or R$_2$ = Ph$_2$; R' = Bu^t). *J. Organomet. Chem.* **385**, 49-60.

The effect of speed of processing training on microsaccade amplitude

Stephen Layfield[1], Wesley Burge[2], William Mitchell[1], Lesley Ross[2], Christine Denning[2], Frank Amthor[2], Kristina Visscher[1]

[1] Department of Neurobiology, [2] Department of Psychology
University of Alabama at Birmingham

Abstract

Older adults experience cognitive deficits that lead to an increase in driving errors and result in a loss of mobility. Some of these cognitive deficits can be measured by the Useful Field of View (UFOV) test, and performance on the UFOV can be improved by Speed of Processing (SOP) training. Both involve simultaneous attention to a central and a peripheral stimulus. To date, the mechanisms behind Speed of Processing training remain unknown. We hypothesized that one mechanism underlying SOP training is a change in distribution of eye movements at different amplitudes. Microsaccades are small-amplitude eye movements made when fixating on a stimulus. They are thought to counteract the visual fading that occurs when static stimuli are presented. Due to retinal anatomy, larger microsaccadic eye movements are needed to move a peripheral stimulus between receptive fields and counteract visual fading. Alternatively, larger microsaccades may decrease performance due to neural suppression. Because larger microsaccades could aid or hinder peripheral vision, we examine the distribution of microsaccades during stimulus presentation. Our results indicate that there is no statistically significant change in microsaccade amplitude during a UFOV-like task before versus after training. Speed of Processing training does not result in changes in microsaccade amplitude in our limited size study, suggesting that the mechanism underlying SOP training is unlikely to rely on microsaccades.

Keywords: *microsaccade, peripheral, Speed of Processing, training, Useful Field of View*

Introduction

On average, 15 older adults are killed and 500 are injured in car accidents in the US every day.[1] One contributing factor leading to these accidents is a set of cognitive deficits that lead to an increase in driving errors[2] and declines in performance on other tests of everyday activities.[3] These cognitive declines result in a loss of mobility for the older adults,[4] which can increase their number of depressive symptoms.[5] Performance on these everyday activities is predicted by the Useful Field of View (UFOV) test, and deficits in everyday activities can be reduced by Speed of Processing (SOP) training.[6] Speed of Processing training improves participants' performance on tasks involving peripheral vision. The training involves presentation of increasingly complex central and peripheral

stimuli for continually reduced durations of time. Although SOP training has been shown to increase the processing speed of older adults, the mechanisms behind this training are still unknown. Understanding the mechanism of training is a first step toward developing optimized training paradigms. We hypothesized that microsaccades may be a link between SOP training and the observed benefits.

Microsaccades are small, high-velocity eye movements produced 1-2 times per second during fixation. They are the most important of the eye movements responsible for restoring visibility to fading targets during fixation.[7] Fading prevention may result from moving the target to a different receptive field and will also be observed in peripheral vision. Moving a stimulus from one receptive field to another requires larger microsaccadic eye movements in the visual periphery[8] and is associated with better performance on some visual tasks.[7,9] Changes in oculomotor activity are associated with a participant's task set; in other words, participants change their patterns of eye movements depending on the task they perform.[10] Microsaccades represent an easily modified eye movement that has the potential to strongly influence behavior. Microsaccade production is involuntary,[11] and so modifications of microsaccades may be one mechanism through which behaviors may be altered. We hypothesize that training in a task involving peripheral stimuli may increase the proportion of large microsaccades.

Alternatively, SOP training could result in a decrease in the number of larger saccadic eye movements, which have been shown to suppress neural activity.[12-13] Microsaccades are small eye movements which make smaller changes to visual perception, and as such, their effect on visual perception is more controversial. However, a recent study has shown that microsaccades suppress neural activity during stimulus presentation in primates.[14] We also hypothesize that SOP training will reduce the number of larger microsaccades to prevent suppression of neural activity and aid perception of the stimulus. Only larger microsaccades would be suppressed, as they have the most impact on peripheral stimuli.

The purpose of this experiment was to determine whether Speed of Processing training affects the magnitude and/or distribution of microsaccades. Larger microsaccades would

aid performance in peripheral vision due to visual fading or detract from performance due to neural suppression while the stimulus is present. Because microsaccades can also be affected by the anticipation of the stimulus, we focus on a particular time frame around the stimulus that includes 450 ms before and after the stimulus is presented. We define this time frame as *peristimulus*. It was determined that the training had no measureable significant effect on the distribution or amplitude of microsaccades.

Methods

Participants

Twenty-one volunteers ranging from 65 to 90 years old—with normal or correctable-to-normal vision and without dementia, a history of stroke, neurological problems, cataract surgery, or claustrophobia—were recruited for the study and compensated for their participation. The participants were a subset of a parent study and were required to attain a score of 65% on a task similar to the UFOV (Figure 1) performed in an fMRI scanner. Additionally, participants were not considered if they had steel implants or a pacemaker or if their weight and girth exceeded 300 pounds and 60 inches, respectively.

Eyetracking session

A UFOV-like task containing four stages similar to those of the UFOV (a central stimulus, a central and peripheral stimulus, a central and peripheral stimulus with triangle distractors, and a central and peripheral stimulus with car-like distractors; Figure 1) was created with Psychtoolbox.[15-17] The participants were seated, and their heads were stabilized with a chinrest approximately 93 cm from the monitor. The Eyelink 1000 eye tracker was calibrated, and the participants performed the 4 stages of the UFOV-like task.[18] Prior to the stimulus, a fixation cross was presented at the center of the screen. The stimulus in each trial was presented for 450 ms, and all task levels contained a central stimulus to ensure continued fixation in the center of the screen. After the stimulus presentation, white noise was presented for 500 ms. Then, the participants were presented with two options as to which central stimulus was presented and, when applicable, an additional question with eight options referring to where the peripheral stimulus was located. The participants responded using a mouse, which has been shown to be a reliable method.[19] Participants were instructed to remain focused on the center of the screen. The participants performed 25 trials at each task level, forming a block. The entire test consisted of 20 blocks, 5 at each task level, and the eye-tracker was recalibrated after each block. An identical test was given as a pre-test before and a post-test after each type of training. No participants made saccades greater than 2.5 degrees, and the peripheral stimulus had an eccentricity of approximately 6 degrees, so the participants performed as instructed.
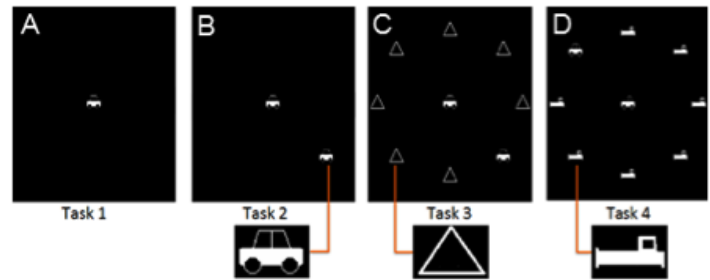

Figure 1. Eyetracking task. The Useful Field of View-like task consists of 4 task levels. (A) Task 1 presents a central stimulus as car or truck for fixation. (B) Task 2 includes a car (6° eccentricity) peripheral stimulus in one of eight spots near the edge of the screen. Task 3 and 4 are identical to task 2 aside from additional (C) triangle distractors in task 2 and (D) car-like distractors in task 4. Participants respond by clicking on a picture of the central stimulus and a box representing the location of the peripheral stimulus.

Training Overview

All participants underwent a screening session and a baseline behavioral session to acquire behavioral measures. Vision, mental status, UFOV performance, and performance on a UFOV-like task were assessed at the screening session. Participants were classified based on their performance on the first three subtests of the UFOV as either low-risk (with a score of 1 to 2) or high-risk (with a score of 3 or higher), as defined based on previous data.[20-21] The baseline behavioral session assessed the participants' performance on a range of neuropsychological tasks. After the baseline behavioral session, the participants underwent a pre-training eyetracking session. Participants were randomized to one of three training groups: a Speed of Processing training group (n=7), a social contact control group (n=6), or a no-contact control group (n=8). Both high-risk and low-risk participants were assigned to each group, and each trained for approximately 5 weeks. Following training, participants returned for a post-training behavioral session and a post-training eyetracking session.

Speed of Processing training involved five two-hour sessions. The training was customized for the participants based on their performance. Participants completed tasks that tested their ability to utilize processing speed, divided attention, and selective attention. The training was designed to improve the amount of visual information that an individual could process over brief periods of time. The specific protocol has been described in detail previously.[6,22]

Participants in the social contact control group attended five two-hour sessions over approximately five weeks during which they performed cognitively stimulating activities, e.g. crossword puzzles and brain teasers.

Measurement of Microsaccades

Raw gaze position data from the eye tracker output were

analyzed using MATLAB analyses described previously[23] to determine microsaccade amplitude and velocity during the 450 ms when the stimuli were displayed (post-stimulus) and 450 ms prior to stimulus presentation (pre-stimulus). Only trials from tasks 2 – 4 were analyzed because task 1 did not involve a peripheral stimulus and should not affect microsaccade amplitude. The distribution of microsaccades was normalized by the number of trials each participant performed. Paired t-tests were used to detect differences in the distribution with $\alpha = 0.05$. The microsaccade distributions of pre- and post-tests of each training group as well as the microsaccade distribution of pre-tests for high-risk and low-risk individuals were compared.
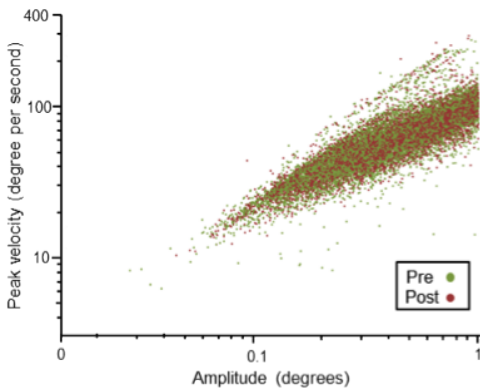
Results

Figure 2. Main sequence plot. Comparing amplitude and velocity of eye movements demonstrates main sequence-specific to saccadic eye movements.

Microsaccades were defined based on raw eye position data captured by the eyetracker. Therefore, an analysis was performed to ensure that the eye movements extracted truly represented saccades or microsaccades. Previous literature has shown that the magnitude and peak velocity of microsaccades and saccades are logarithmically related according to a main sequence.[10] This relationship (which appears linear on a log-log plot) was observed in our data, confirming that the algorithm did reasonably well isolating microsaccades and saccades from our dataset (Figure 2). In order to determine whether the distribution of microsaccades changed following training, microsaccades were grouped into bins according to their amplitude. The number of microsaccades per trial, averaged across all participants, is displayed on the x-axis of Figure 3. Error bars displayed on the graph show within-participant standard errors of the mean,[24-25] which are appropriate for assessing differences between pre- and post-tests. For each bin for each group, t-tests were performed. This version of testing may result in false positives because multiple significance tests are being performed on the same dataset. The method is unlikely to result in false negatives; that is, the test is relatively unlikely to miss an effect that is present in these data. Comparing pre- and post-tests for each training group showed only one

difference that met a threshold of $p < 0.05$ (as discussed, a relatively weak statistical threshold). This difference occurs for microsaccades between the amplitudes of 0.75 and 0.85 in the post-stimulus time frame (Figure 3B), where, consistent with the suppression hypothesis, pre-training shows slightly more microsaccades per trial than post-training (denoted by * in Figure 3). However, the p-value at this point was 0.0498, and does not meet a significant threshold after correction for multiple comparisons. For this reason, our data fail to reject the null hypothesis that the distribution of microsaccade amplitude do not change after training. Our data also fail to reject the microsaccade suppression hypothesis, as fewer large microsaccades were observed after training. Additionally, our data reject the hypothesis that training increases the proportion of large microsaccades.
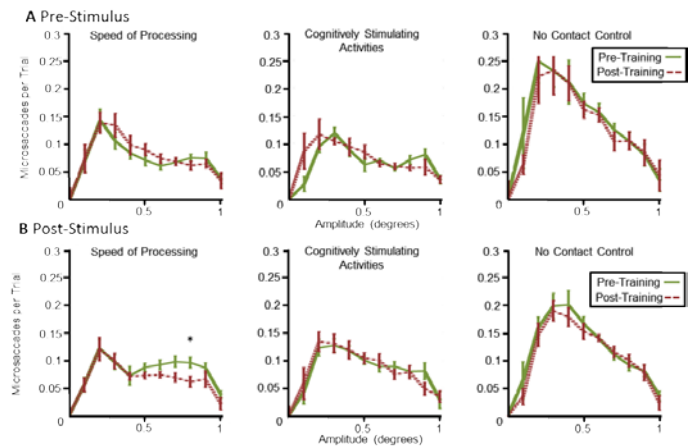
Figure 3. Comparison of training groups. Microsaccades were collected and sorted into bins for pre- and post-tests for each group. Error bars showing within-participant standard error of the mean are shown, and paired t-tests were used to analyze the distribution at each bin. (A) Pre-stimulus data show no significant difference between pre- and post-tests. (B) No significant difference in microsaccade amplitude was found except at 0.8 amplitude in the Speed of Processing group for post-stimulus data. This difference was only significant at $\alpha = 0.05$ prior to multiple comparisons correction, but it was consistent with the microsaccade suppression hypothesis.

To further detect any relationship between SOP and microsaccade amplitude, participants were separated into high-risk and low-risk groups based on their initial performance on the Useful Field of View test. Based on the visual fading hypothesis, we hypothesized that low-risk individuals would produce a greater number of microsaccades and larger microsaccades than the high-risk group because the high-risk group performed poorly. Based on the microsaccade suppression hypothesis, we expected low-risk individuals would produce a lesser number of microsaccades and larger microsaccades to reduce neural suppression and increase performance. The two groups displayed no statistically

significant difference for the post-stimulus timeframe, failing to disprove the null hypothesis (Figure 4B).

As described in the introduction, previous studies have shown that attention influences the rate of microsaccades.[8] In a further set of analyses, we addressed the question of whether training influences microsaccades during preparation for a visual stimulus. The same set of analyses were performed for data obtained in the 450-ms window prior to stimuli presentation (Figure 3A and Figure 4A). There were no significant changes in microsaccade amplitude distribution due to training and no significant differences in microsaccade amplitude between the high-risk and low-risk participants.
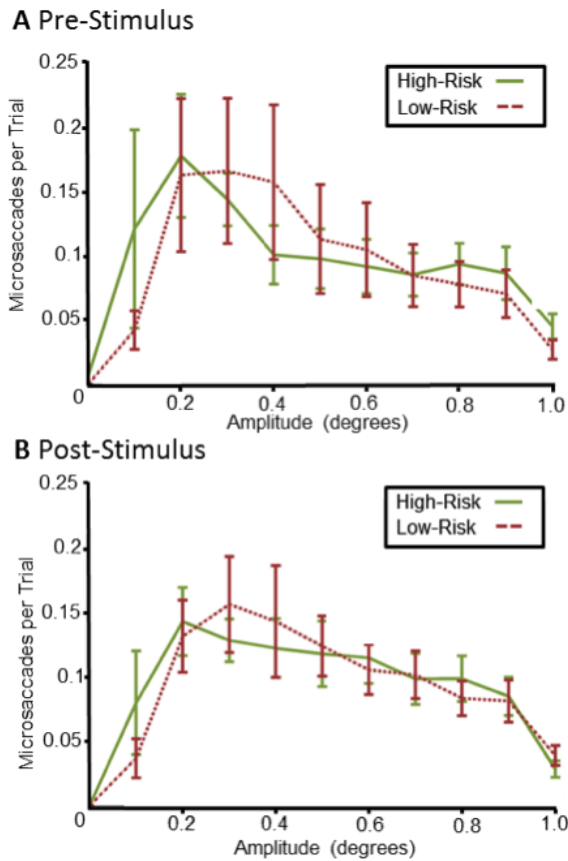

Figure 4. Microsaccades in high and low-risk groups. Participants were designated as high-risk or low-risk based on initial UFOV scores. Pre-test microsaccade distributions were compared for these groups, and no difference was observed in microsaccade distribution for both pre-stimulus data (A) and post-stimulus data (B). Error bars show standard error of the mean.

Discussion

We found that Speed of Processing training does not have a statistically significant effect on microsaccade magnitude as measured by distributions of amplitudes of microsaccades. The SOP training group was compared to a control group and a social contact group, both of which showed similar results. Prior to multiple comparisons correction, the only statistically significant difference observed was consistent with the microsaccade suppression hypothesis. However, our data fail to reject the null hypothesis that training does not influence microsaccade amplitude. Additionally, the same analysis was performed on data that included saccades over the one-degree-microsaccade cutoff point to avoid potential ceiling effects, and little difference was observed between pre- and post-tests.

One limitation of this study is that it was performed on a relatively small dataset (n = 7, n = 6, and n = 8 respectively) and thus has relatively weak statistical power. Additionally, receptive fields may be too small to affect the distribution of microsaccade amplitudes. It has been shown that the minimum angle of resolution for a six-degree peripheral stimulus is around 0.04 degrees.[26] This is significantly smaller than microsaccades measured using current techniques. Furthermore, the participants displayed a high percentage of correct responses on the UFOV-like task, which suggests that the task may have been too easy, reducing the effect of training. Finally, any effects found could be due to the speed of saccades rather than size, since they are tightly correlated.

Future research should target other possible mechanisms of Speed of Processing training. The time frame that the stimulus was presented (450 ms) may have been too short for visual fading to occur and the time interval may have been too long for saccadic neural suppression to impact perception. Microsaccade suppression may occur during stimulus presentation, but, due to the small sample size, may not be detectable. Additionally, the pre-stimulus time period did not show any statistically significant differences between pre- and post-test curves. This leads us to believe Speed of Processing training does not influence preparation for a stimulus through microsaccade amplitudes. Determining the mechanism behind Speed of Processing training is still important because if the mechanism can be discovered, we can develop more effective future therapies, potentially improving quality of life for many older adults.

Author Contributions

Conceived and designed the experiments: WKB KMV LAR. Performed the experiments: SJL WGM CRD WKB. Analyzed the data: SJL WGM. Contributed reagents/materials/analysis tools: KMV LAR. Wrote the paper: SJL. Critical revision for important intellectual content: KMV LAR.

References

1. Centers for Disease Control and Prevention. (2011). Older adult drivers data & statistics. Retrieved from http://www.cdc.gov/Motorvehiclesafety/Older_Adult_Drivers/

2. Anstey, K. J., Wood, J. (2011). Chronological age and age-related cognitive deficits are associated with an increase in multiple types of driving errors in late life. *Neuropsychology* **25**, 613.

3. Owsley, C., Sloane, M., McGwin Jr., G., Ball, K. (2002). Timed instrumental activities of daily living tasks: relationship to cognitive function and everyday performance assessments in older adults. *Gerontology* **48**, 254.

4. Owsley, C., McGwin Jr., G. (2004). Association between visual attention and mobility in older adults. *Journal of the American Geriatrics Society* **52**, 1901.

5. Fonda, S. J., Wallace, R. B., Herzog, A. R. (2001). Changes in driving patterns and worsening depressive symptoms among older adults. *The journals of Gerontology. Series B, Psychological Sciences and Social Sciences* **56**, S343.

6. Edwards, J. D. *et al.* (2005). The impact of speed of processing training on cognitive and everyday performance. *Aging & Mental Health* **9**, 262.

7. McCamy, M. B. *et al.* (2012). Microsaccadic efficacy and contribution to foveal and peripheral vision. *The Journal of Neuroscience: The Official Journal of the Society for Neuroscience* **32**, 9194.

8. Kandel, E. R., Schwartz, J. H., Jessell, T. M. (2000). *Principles of Neural Science, Vol. 4.* McGraw-Hill, New York.

9. Martinez-Conde, S., Macknik, S. L., Hubel, D. H. (2004). The role of fixational eye movements in visual perception. *Nature Reviews Neuroscience* **5**, 229.

10. Betta, E., Turatto, M. (2006). Are you ready? I can tell by looking at your microsaccades. *Neuroreport* **17**, 1001.

11. Martinez-Conde, S., Otero-Millan, J., Macknik, S. L. (2013). The impact of microsaccades on vision: towards a unified theory of saccadic function. *Nature Reviews Neuroscience* **14**, 83.

12. Ross, J., Morrone, M. C., Goldberg, M. E., Burr, D. C. (2001). Changes in visual perception at the time of saccades. *Trends in neurosciences* **24**, 113.

13. Wurtz, R. H. (1968). Visual cortex neurons: Response to stimuli during rapid eye movements. *Science* **162**(3858), 1148-1150.

14. Herrington, T. M. *et al.* (2009). The effect of microsaccades on the correlation between neural activity and behavior in middle temporal, ventral intraparietal, and lateral intraparietal areas. *The Journal of Neuroscience* **29**, 5793.

15. Brainard, D. H. (1997). The psychophysics toolbox. *Spatial vision* **10**, 433.

16. Kleiner, M. *et al.* (2007). What's new in Psychtoolbox-3. *Perception* **36**, 1.1.

17. Pelli, D. G. (1997). The VideoToolbox software for visual psychophysics: Transforming numbers into movies. *Spatial vision* **10**, 437.

18. Burge, W. K. *et al.* (2013). Processing speed training increases the efficiency of attentional resource allocation in young adults. *Frontiers in Human Neuroscience* **7**, 684.

19. Edwards, J. D. *et al.* (2005). Reliability and validity of useful field of view test scores as administered by personal computer. *Journal of clinical and experimental neuropsychology* **27**, 529.

20. Ball, K. K. *et al.* (2006). Can high-risk older drivers be identified through performance-based measures in a Department of Motor Vehicles setting? *J Am Geriatr Soc* **54**, 77.

21. Ross, L. A. *et al.* (2009). Do older drivers at-risk for crashes modify their driving over time? *The Journals of Gerontology Series B: Psychological Sciences and Social Sciences* **64**, 163.

22. Ball, K., Edwards, J. D., Ross, L. A. (2007). The impact of speed of processing training on cognitive and everyday functions. *The Journals of Gerontology Series B: Psychological Sciences and Social Sciences* **62**, 19.

23. Engbert, R., Mergenthaler, K. (2006). Microsaccades are triggered by low retinal image slip. *Proceedings of the National Academy of Sciences of the United States of America* **103**, 7192.

24. Cousineau, D. (2005). Confidence intervals in within-subject designs: A simpler solution to Loftus and Masson's method. *Tutorials in Quantitative Methods for Psychology* **1**, 42.

25. Loftus, G. R., Masson, M. E. (1994). Using confidence intervals in within-subject designs. *Psychonomic Bulletin & Review* **1**, 476.

26. Weymouth, F.W. (1958). Visual sensory units and the minimal angle of resolution. *American journal of ophthalmology* **46**, 102.

inquiro staff

Co-Editors

Miranda Collier

Miranda Collier is a senior in the University Honors and Chemistry Scholars programs. She is pursuing a degree in Chemistry with minors in Mathematics and Biology. Her research focuses on how lipids in the lens change with age with Dr. Janusz Kabarowski in the Department of Microbiology. In the fall, Miranda will begin graduate school at the University of Oxford for her Ph.D.

Chapin Cavender

Chapin Cavender is a junior in the University Honors Program majoring in Physics. He conducts research concerning the trafficking of proteins in secretory vesicles within astrocytes. After completing his undergraduate degree, he plans to pursue an M.D./Ph.D. to become a medical scientist. In his spare time, Chapin enjoys cats and playing the electric guitar.

Assistant Editor

John Decker

John Decker is a sophomore in the University Honors Program, with a major in Neuroscience and expected minors in Chemistry and Biology. His research is in the lab of Dr. Paul Gamlin and focuses on how the physical properties of images affect visual perception. After college, he intends to pursue a Ph.D. in Neuroscience. In his free time, he enjoys being in the outdoors, reading, listening to music, and spending time with family and friends.

Staff Writers

Amiya Ahmed

Amiya Ahmed is a senior in the University Honors Program majoring in Molecular Biology and Philosophy. Amiya has conducted research concerning heart failure and smoking with the Department of Medicine as well as breast cancer and epigenetics with the Department of Biology. He has also spent time teaching with UAB's Community OutReach Program. In his free time, he enjoys playing basketball and guitar.

Sadhvi Batra

Sadhvi Batra is a Neuroscience & Philosophy Major in the Science and Technology Honors Program. She is currently working towards a Masters in Public Health as well. Her undergraduate research is a qualitative assessment of self-perception in those living with Alzheimer's disease. This clinical project essentially aims to improve the quality of care for those suffering from dementia. After finishing her Masters, she plans on going to medical school and becoming an academic physician. Outside of academia, she likes to write and spend time with friends and family.

Bliss Chang

Bliss Chang is a junior majoring in Biochemistry and Biology. He currently works in two labs to provide an interdisciplinary approach to his research. In the lab of Dr. Elizabeth Sztul, he works on characterizing structure-function relationships of key proteins in the vesicular trafficking pathway. In the lab of Dr. Jamil Saad, he works as a Beckman Scholar on characterizing the structure of a protein involved in extrinsic apoptosis and its relationship to a ubiquitous calcium signaling messenger. He plans to pursue a Ph.D. or M.D./Ph.D., and his hobbies include table tennis and weight lifting.

Naveed Farrukh

Naveed Farrukh is a senior Neuroscience major who is also completing his Master's in Public Health with a concentration in Healthcare Organization and Policy. He will begin medical school in the fall, and hopes to one day work as a physician in the realm of healthcare policy.

Paul Lee

Paul Lee is a senior majoring in Biology. He research involves analyzing the biochemical properties of Cryptosporidium parvum pyruvate kinase. Pyruvate kinase is essential for the survival of C. parvum, a protozoan parasite that causes Human Cryptosporidiosis. He plans to attend medical school after graduation.

Roxanne Lockhart

Roxanne Lockhart is a junior in the University Honors Program with a major in Molecular Biology. She performs research under the mentorship of Dr. Farah Lubin through the Beckman Scholars Program. She is Vice President of Phi Sigma, UAB's Biology Honors Program. Roxanne plans on attending medical school after graduating UAB.

Susmita Murthy

Susmita Murthy is a sophomore double majoring in Biology and History. She works in Dr. Michael Miller's research lab in the Department of Cell Biology studying the effects of ALS in C. elegans. She plans on attending medical school at UAB after completing her undergraduate degree. In her free time, she is training for a marathon and enjoys reading.

Grace Nix

Grace Nix is a junior in the Neuroscience program at UAB. She works in Dr. Rita Cowell's lab in The Department of Behavioral Psychiatry and Neurobiology. Grace's research in the Cowell lab currently investigates different genetic predispositions and environmental factors that could potentially lead to Tourette's phenotypes in a mouse model. She plans to pursue a professional health degree.

Catherine Ritchey

Catherine Ritchey is a junior in the Science and Technology Honors Program, with a major in Biomedical Engineering. She conducts research with Dr. Lee Moradi developing a system for pediatric optical imaging that will reduce the fear and lack of focus that often impedes imaging children's eyes, while taking equivalent quality images to those of current technology. She plans to get a Masters in Biotechnology and dreams of starting her own biotechnology company and raising a family. Catherine also loves to sing and is a member of the UAB Concert Choir.

Ramya Singireddy

Ramya Singireddy is a senior majoring in Neuroscience. She plans to pursue medicine after graduating this spring. She performs research studying the effects of catalytic antioxidant drugs on spinal cord injury. She enjoys dancing and watching movies."

Harsh Shah

Harsh Shah is a senior in the University Honors Program majoring in Biology and working towards in a Masters in Public Health. Harsh is currently conducting research in the Department of Biology under the guidance of Dr. Trygve Tollefsbol. His research project focuses on natural alternative treatments against breast cancer. The alternative treatments consist of antioxidants found in grapes and blueberries. During his free time, Harsh likes to cook Indian food and choreograph dances.

Ambika Srivastava

Ambika Srivastava is a junior in Science and Technology Honors Program, majoring in Biomedical Engineering. She plans on attending dental school after graduating UAB. Currently, she performs research in Dr. Rita Cowell's lab on the biological effects of cerebral malaria. During her free time, Ambika likes to dance to Bollywood songs and watch Bollywood movies.

Amy Stewart

Amy Stewart is a sophomore Neuroscience major. She works in the Dr. Lori McMahon's research lab studying the neuroprotective effects of o-GlcNAC on epilepsy. She plans on getting a Ph.D. in Neuroscience and pursuing a career in research. Her hobbies include reading and playing the flute.

2014 *Inquiro* Submission Guidelines

Any UAB undergraduate student participating in scientific research and/or any undergraduate student participating in research at UAB is invited to submit a manuscript to be considered for publication in the 2014 issue of *Inquiro*. Papers will be subject to student and faculty review.

The deadline for submission is October 10, 2014; however, students participating in summer research at UAB or at another institution are encouraged to submit by September 1, 2014.

The journal accepts submissions in the following categories:

Short reports: A short report should give a concise overview of an original research project. Its content is comparable to that of science posters. The suggested length is 1000 – 2000 words.

Long papers: A long paper should give a substantial description of an original research project. It should include detailed discussions of the methods utilized and the results obtained. The suggested length is 2500 – 4000 words.

Research narratives: A research narrative is a personal piece written in editorial or narrative style. The content should relate to scientific research. The suggested length is 600 – 800 words.

Initial submissions should follow these guidelines:

1. All submissions should be submitted as Microsoft Word documents, double spaced and formatted in 12 pt Times New Roman font. Pages should be numbered with the first author's name appearing in a header on every page.

2. Research papers should be written in third person. Research narratives should be written in first person.

3. Research papers should include a title, the full name(s) and affiliation(s) of the author(s), and the following sections: Abstract, Introduction, Materials and Methods, Results, Discussion, Conclusion, and References. Please consult the Manuscript Guidelines for Authors on our website for more specific instructions on each section.

4. Figures, tables and graphs should be submitted in their original formats in the highest resolution possible. They may be submitted as separate files or embedded in the text of the document in the locations in which the author would like them to appear in a published version. If submitted separately, please indicate in the manuscript where the figures should appear.

Research papers can be submitted through the Submit page on our website. Before submitting, please ensure that your mentor has read and approved of your manuscript. Your mentor will automatically receive an email requesting his or her approval of your submission.

Research narratives can be submitted through email. Include the article title as well as your name, university, major, and class standing in the body of the email.

Please send any questions or comments to inquiro@uab.edu. Students who wish to join the *Inquiro* staff may also contact the editors at this address.

For more information or to view previous publications, visit our website at uab.edu/inquiro.

Authors retain all rights to their submitted work, except to publish in another undergraduate science journal. *Inquiro* is an internal document of the University of Alabama at Birmingham.

inquiro

acknowledgements